THE PHYSICAL NATURE OF THE CONTINUUM IN ACTIVE GALAXIES

Thesis by

Matthew Arnold Malkan

In Partial Fulfillment of the Requirements

for the Degree of

Doctor of Philosophy

California Institute of Technology

Pasadena, California

1983

(Submitted May 23, 1983)

To Mom and Dad

Acknowledgements

It is hard to imagine any modern astronomical paper to which the listed authors were the sole contributors. Below are some, but not all, of the people who added significantly to this thesis.

This work relied heavily on first-rate software created by Todd Boroson, William Sebok, Barbara Zimmermann, Abi Saha, Tim Pearson, and Mike Lesser. It would not have been possible without their unselfish dedication and programming expertise.

Tony Readhead, Ger deBruyn, Bev Oke, Gerry Neugebauer, and Tom Soiffer generously allowed me to explore their (not insubstantial) stores of unpublished data. Their open, enlightened attitude on exchanging information marks them as truly successful scientists.

The resident astronomers and telescope operators at IUE were always competent and helpful on my numerous trips to Greenbelt. I am indebted to the many people who keep Palomar Observatory the best in the world: Bob Thicksten, Larry Blakee, Earle Emery, Dave Tennant, Mike Doyle, Merle Sweet, and the indefatigatible 60 inch night assistants: Skip Staples, Bob Griffith, and Al Lilge. Bill Qualls got me there safely, and when I arrived, Wally, Ardith, Mary, Alicia, and Michael made me feel that I was coming home.

I received all sorts of help from the people who really keep the second floor of Robinson going: Marilynne Rice, Lilo Hauck, Bob Brucato, and Lorna Thayer. I am grateful to the Fannie and John Hertz Foundation for providing financial support for most of my

years at Caltech.

I am truly fortunate to have shared the fellowship and comraderie of a remarkable group of people--the Caltech astronomy grad students. Coming to know them has been one of the best things about being here, and it is nice to know that their friendship will be a source of enjoyment for the rest of my life. I owe much to Howard Yee, who contributed a great deal to my thinking on active galaxies. It was a special privilege and pleasure to know my first office-mate, Peter Young. I'll remember you, Peter, and I'll probably not meet your equal in this world.

The best luck I ever had in astronomy was having Wal Sargent for an advisor. For all the help and teaching he has given me, on astronomical and other matters, I will always be deeply grateful.

Finally and most importantly, my mother and father played active roles in every stage of this work, from detailed editing to guidance throughout my career as a professional student. They have always been far and away the greatest influences in every part of my life, and always will be. The opinions of committees, refer ees, pundits, and fellow students all have their place. But none of that counts as much as what Arnold and Audrey think. After all they have done for me, all that I owe them but can't begin to express in words, merely dedicating this thesis hardly seems adequate. Yet as long as it returns some little part of the love and happiness they have given me, I could never consider this work a failure.

Abstract

We have measured the intrinsic nonstellar continuum from the nuclei of a wide range of active galaxies. We find little or no continuum reddening (from the 2175Å absorption bump) above that expected from the interstellar medium of the Milky Way. Nor do optical and ultraviolet emission from permitted Fe II lines alter the overall appearance of the energy distribution very much. After accounting for hydrogen recombination radiation, we find the continuum consists of a power law ($f_\nu \propto \nu^{-1.1}$), closely related to the X-ray emission, and an optically thick thermal component. Some bright quasars produce as much or more thermal power as nonthermal. The thermal energy has an average characteristic temperature of 20—30,000 K. It is perfectly described by relativistic accretion disk models which include the gravitational redshifting and focusing of emerging light. These models are completely specified by two well-determined parameters: the mass of the central black hole and the accretion rate. The hole masses range from 0.2--0.5 billion $M_\odot$ in 3C 273 to 1--3 billion in the most luminous quasars, depending on the disk inclination and the angular momentum of the hole. All the bright quasars are shining at within a factor of two of their Eddington limits, while the Seyfert 1 galaxies are well below theirs.

Unlike most Seyfert 1 galaxies, those of type 2 have a large portion of their total power re-radiated in the infrared by warm dust grains. The intrinsic continuum in the Seyfert 2 galaxies may have a nonthermal power-law, but appears to lack the hot thermal component seen in quasars. The host galaxies around Seyfert nuclei of types 1 and 2, and those around low-redshift quasars are normal spirals of early to intermediate type.

We calculated the level populations for the O^+ and S^+ ions, to use the [O II] (7320+7330)/(3726+3729) and [S II] (4069+4076)/(6716+6730) line ratios as reddening indicators (accurate to $\pm$0.1 mag. in E_{B-V}). Seyfert 2 galaxies are typically reddened by 0.2--0.5 mag. Most Seyfert 1 galaxies have less than half as much reddening. The Hα/Hβ ratio in the broad-line region is often much larger than the Case B value, and it is significantly larger than 2.86 in some narrow-line regions. The intrinsic Balmer continuum/Hα ratio in the narrow-line region is 1.4, consistent with the Case B prediction. But in the broad-line region it is two to three times larger, because of the effects of high electron density and optical depth.

TABLE OF CONTENTS

Introduction

Probably the outstanding question about quasars, which has remained unanswered since their discovery, is the nature of their prodigious energy source. It is most directly addressed through observations of the continuous energy distribution itself. Yet much of the intensive observational and theoretical effort in this field has been devoted to understanding secondary phenomena, such as the broad emission lines and radio jets and lobes. Study of the continuum has been relatively underdeveloped, partly because of the difficulties in obtaining measurements over a sufficiently wide range of wavelengths, and a widespread feeling that the continuum was less observationally tractable. The increased sensitivity of infrared detectors and the opening of the ultraviolet and X-ray spectrum by several new orbiting telescopes have alleviated the first obstacle; this thesis attempts to eliminate the second.

The third, fifth, and sixth chapters of this thesis focus on two critical pieces of information which must be known before the intrinsic quasar continuum can even be analyzed: the amount by which it is reddened, and the extent to which it is contaminated by starlight from the host galaxy. Both effects are significant primarily in the least luminous active galactic nuclei. Yet even in these objects both can be corrected for, with the proper set of observations.

A unifying theme of this thesis is the similarity between active galactic nuclei of widely differing luminosities. Chapter 2 studies some of the brightest quasars known, while Chapter 5 analyzes one of the faintest classes of active galaxies, those of Seyfert type 2. They are distinguished from the brighter active galaxies by their lack of a broad emission-line region.

It is also useful to study the continuum light of the host galaxies themselves. This is done in Chapter 5 for Seyfert 2 galaxies, in Chapter 3 for Seyfert 1 galaxies, and in Chapter 4 for quasars.

Each chapter was or will be published in the Astrophysical Journal. The work was not done entirely on my own. Chapter 1 was co-authored by W. L. W. Sargent, Chapter 3 by A. V. Filippenko, Chapter 4 by B. Margon and G. Chanan, and Chapter 5 by J. B. Oke.

THE ASTROPHYSICAL JOURNAL, 254: 22-37, 1982 March 1

THE ULTRAVIOLET EXCESS OF SEYFERT 1 GALAXIES AND QUASARS

MATTHEW A. MALKAN AND WALLACE L. W. SARGENT
Palomar Observatory, California Institute of Technology
Received 1981 June 18; accepted 1981 September 1

ABSTRACT

We used published spectrophotometry to construct composite infrared-optical-ultraviolet spectra of eight Seyfert 1 galaxies and quasars. We subtracted a power-law determined in the red and infrared from each spectrum to measure the ultraviolet excess. The excess flux always has a sharp rise from 4000 to 3650 Å. It is produced by Balmer continuum emission, which, relative to Hα, is 1.5–2.5 times the prediction of Case B recombination.

We then fitted the spectra in detail with combinations of power-law and hydrogen recombination continua. At least five objects had an additional component present from 5000 Å to the far-ultraviolet. It is probably not produced by photoionization, since its luminosity can exceed the total ionizing energy available in the power law. This component is well described by a blackbody at a single temperature, which ranges from 20,000 to 30,000 K. The blackbody flux from 3C 273 requires a thermally emitting area of at least 3×10^{33} cm^2.

We were able to produce all of the observed spectra with combinations of power-law, recombination, and blackbody emission. Quasar spectra steepen at frequencies above 2×10^{15} Hz because of the exponential cutoff of the thermal component. The total ionizing flux is an order of magnitude less than would be predicted by simple extrapolation of the near-ultraviolet continuum. All of the objects in our sample have a power-law component with slope -1.1 ± 0.1. Extrapolations of the power-law to X-ray frequencies agree well with the observed 2 keV fluxes.

The ratio of thermal to power-law flux correlates with total luminosity. This may explain Baldwin's finding that the equivalent widths of ultraviolet emission lines in quasars decrease with ultraviolet luminosity.

Subject headings: galaxies: Seyfert — quasars — radiation mechanisms — spectrophotometry

I. INTRODUCTION

Oke and Sargent (1968) and other early studies demonstrated that the smooth continuum of quasars and Seyfert galaxy nuclei is largely nonstellar. From infrared to visual wavelengths it typically resembles a power law, $f_\nu \propto \nu^\alpha$, with a slope, α, which ranges around -1 (see Fig. 1 in Neugebauer *et al.* 1979). In the blue and ultraviolet, however, the continuum becomes essentially flat, resuming its fall around 2500 Å and steepening below 1200 Å. This excess of ultraviolet flux over the red power law has been referred to as the "3000 Å bump" (Richstone and Schmidt 1980) and is prominent in almost all quasar and Seyfert 1 spectra. It cannot be due to blended emission lines (see discussion in Grandi and Phillips 1980 and Neugebauer *et al.* 1979). The most promising explanation, Balmer continuum emission, has been rejected because the observed ultraviolet excess is too strong and too flat (e.g., Grandi and Phillips 1980). Shields (1978) and Ulrich *et al.* (1980) suggested that the ultraviolet excess is optically thick thermal emission, but neither Richstone and Schmidt nor Grandi and Phillips could obtain satisfactory fits with blackbody temperatures from 10,000 to 20,000 K.

We have combined recent spectrophotometric observations to study the spectra of eight active galactic nuclei from infrared to ultraviolet wavelengths. In § II we subtract power laws from the composite spectra to examine the ultraviolet excess. Balmer continuum emission is clearly present. In § III, we make detailed fits to the spectra, by adding Balmer continuum flux to a power law. This combination matches three spectra very well, but cannot reproduce the flat blue and ultraviolet continua of the other five. In § IV, we show that the addition of a third component, blackbody emission, can successfully fit all of the observations. We calculate the total fluxes in each of the components in § V, and discuss them in § VI.

II. MEASUREMENT OF THE ULTRAVIOLET EXCESS

a) The Data

Table 1 lists all eight active galactic nuclei with accurately measured fluxes from $\log \nu = 13$ to 15.5 (Hz) available before 1981. Optical spectrophotometry from $\log \nu = 14.98$ (3150 Å) to 14.45 (10,660 Å) was obtained by DeBruyn and Sargent (1978), using the multichannel spectrophotometer (Oke 1969) on the Hale telescope. The resolution was 20 Å in the blue ($\log \nu \geq 14.7$) and 40 Å in the red. Broad-band ($\Delta\nu/\nu \sim 0.15$) infrared photometry was taken from Rieke (1978) and Neugebauer *et al.* (1979). The ultraviolet spectra have been measured with the *International Ultraviolet Explorer* satellite (Oke and Zimmermann 1979; Oke and Goodrich 1981; Boksenberg *et al.* 1978; Boggess *et al.* 1979; and

TABLE 1

SEYFERT 1 GALAXIES AND QUASARS WITH ABSOLUTE SPECTROPHOTOMETRY

OBJECT	OBSERVATION DATES			E_{B-V} (mag)	
	Infrared	Optical	Ultraviolet	Foreground	Internal
MRK 9.....	76 May 2	75 Feb 17	78 Nov 21	0.12	0.00
MRK 10	76 May 2	75 Feb 17	80 Aug 2	0.04	0.07
MRK 79	76 Apr 30	75 Feb 17	78 Apr 15	0.05	0.17
MRK 335	75 Dec 3	74 Sep 23	78 July 7	0.02	0.00
MRK 509	76 May 30	77 Jun 20	79 Dec 6	0.04	0.00
NGC 4151	78 Apr 3	74 May 23	78 Feb 11	0.00	0.06
NGC 5548	79 Mar 7	79 Jun 11	79 Dec 8	0.00	0.02
3C 273	77 May	75 Feb 16	78 May	0.04	0.05

unpublished observations of Markarian 335, 509, and NGC 5548, released by the National Space Sciences Data Center). The continuum fluxes were measured by averaging the spectra over 100 Å regions devoid of strong emission lines.

The aperture sizes used were all quite similar: 8".5 in the infrared, 9".9 in the optical, and a 10" × 20" oval in the ultraviolet. Any aperture corrections to the composite spectra would be negligible, because the light of Seyfert 1 galaxies is highly concentrated in a pointlike nuclear source.

A larger uncertainty comes from the fact that the three spectral regions were not observed simultaneously. The measurements in the ultraviolet were typically made a year or two after those in the infrared, and two or three years after those in the optical. We have required that the composite spectra be continuous in the regions of overlap, 1.0–1.2 μm and 0.31–0.34 μm. In some objects this required small shifts ($\Delta \log f_\nu \leq 0.05$) in the absolute flux levels of the ultraviolet or infrared spectra, to match the optical data. No relative adjustments were made to the infrared and ultraviolet spectra themselves. When it was observed by DeBruyn and Sargent, NGC 5548 was near its minimum light, half a magnitude fainter than in 1979. Therefore, we have substituted a spectrum taken later with the same instrument at half the resolution, which matches the ultraviolet and infrared fluxes very well. All the data points were shifted to the rest frame using the appropriate emission-line redshifts from the literature.

b) Reddening

We estimated the reddening to each object, assuming it follows the ordinary interstellar law in our Galaxy, the van de Hulst curve 15 (Johnson 1966), with Seaton's (1979) ultraviolet extension. Foreground (zero redshift) absorption in our Galaxy was estimated with the Burstein and Heiles (1978) H I column density method. Since most of the objects were at high galactic latitudes, this correction was usually quite small. An additional internal nuclear reddening was added to match the observed strength of the 2175 Å absorption dip. The adopted reddenings were small because the 2175 Å dip was usually weak or absent. They are listed in Table 1.

Most Seyfert 1 galaxies and quasars probably do not have reddenings corresponding to visual extinctions, A_V, of more than a magnitude. In nearly all objects, the observed continuum from 3500 to 2800 Å is consistently rather flat (DeBruyn and Sargent 1978). If large reddening corrections were applied, the intrinsic ultraviolet spectra would increase rapidly with frequency.

We can rule out the suggestion of Netzer and Davidson (1979) that Seyfert 1 galaxies and quasars have enough reddening to bring their intrinsic hydrogen emission line ratios into agreement with the predictions of Case B recombination. Wu, Boggess, and Gull (1980), Lacy *et al.* (1982), and Puetter *et al.* (1981) showed that their Lyman-to-Balmer and Paschen-to-Balmer line ratios are usually inconsistent with Case B. If Case B applied, the hypothesized large reddenings would lead to a wide range of positive ultraviolet slopes to explain the wide range of observed Balmer decrements. Hα/Hβ ratios ranging from 2.8 to 5, if caused by reddening, would imply A_V's ranging from 0.0 to 1.6. After correction for this reddening, some intrinsic spectra would slope up into the ultraviolet as steeply as $f_\nu \propto \nu^2$, while some would be flat. Further, the widely ranging A_V's and ultraviolet slopes would have to be correlated in just the right way to produce ultraviolet spectra which are always observed to be nearly flat. Such coincidences would be highly unlikely. We conclude that the continuum reddening is usually small, as suggested by the weakness of the 2175 Å absorption. The intrinsic Balmer line ratios are not described by Case B: a more complex model will be needed before they can be used as reddening indicators.

Heavily reddened active galactic nuclei, were they common, would have been found by radio or objective prism surveys. Ultraviolet-excess searches, like those of Green (1976) and Markarian (Huchra 1977), should have been complete up to $A_V \sim 2.0$ mag. Our conclusion that few active galactic nuclei have continuum reddenings of $A_V > 1.5$ mag is therefore not a result of selection effects.

c) Dilution by Starlight

In preliminary analysis we attempted to estimate the stellar contribution to the spectra from the underlying galaxies. We combined power law and starlight spectra to match the observations. The "starlight" spectrum was that of an average elliptical galaxy, as in Yee and Oke (1978), extended with the infrared observations of Frogel *et al.* (1978) and Glass (1976), and the ultraviolet spectra

of M31 and M32 (Johnson 1979) and NGC 3379 and 4689 (Oke, Bertola, and Capaccioli 1981). The same exercise was made by Koski (1978) for Seyfert 2 galaxies, and by Yee and Oke (1978) for 3C radio galaxies. A strong starlight contribution makes the spectrum curve downward, with a distinctive kink at 1.6 μm, the wavelength of the peak stellar flux.

Markarian 10 was the only spectrum which clearly had a large proportion of starlight. From the infrared/optical spectrum shown in Figure 1, we estimated that the visual magnitude of the underlying galaxy in a 9".9 aperture was $V = 15.5 \pm 0.1$ mag. Williams, Morton, and Green (1981) fitted Mrk 10's surface brightness outside the nucleus with disk and bulge components. Using their derived disk scale length of 15", we calculated the disk magnitude in a 9".9 aperture. We integrated the bulge light assuming a seeing-limited core radius of 1", but the result was not affected by this choice. We then added the disk and bulge light to find the total galactic flux in a 9".9 aperture. It agrees with our spectroscopic result to within the 0.1 mag uncertainty.

Starlight appears to contribute less than 25% of the visual flux in the other spectra. We are certain that the nonstellar continuum from the nucleus dominates the starlight, at least in Markarian 335 and 509, since these low-redshift objects are almost pointlike, even in deep photographs. Wyckoff, Wehinger and Gehren (1981) estimated that the starlight contribution to the visual spectrum of 3C 273 was less than 5%.

Rieke (1978) suggested that most Seyfert 1 galaxies have hot (1500 K) dust grains a few tenths of a parsec from their nuclei which produce the bulk of their 2.2 μm flux. Since the high-frequency thermal emission spectrum of the dust falls exponentially, this would mean that much of the 1 μm flux would have to be starlight. This is probably not the case for Mrk 335, Mrk 509, and 3C 273, since their underlying galaxies are so faint. Fortunately, even if we underestimated the starlight contributions in NGC 4151, 5548, and Mrk 9 and 79, our measurement of the ultraviolet excess and subsequent deductions would not be seriously affected.

We will illustrate with NGC 4151, which is most likely to be contaminated by thermal emission from dust and has the least luminous nucleus. Rieke and Lebofsky (1981) assumed that 100% of the red light from 4151 came from stars during its minimum of 1979 March. This sets an upper limit on the starlight flux at 5500 Å of 15 mJy in our 9".9 aperture. (From similar considerations, Cutri *et al.* 1981 estimated it was 23 mJy in a 17" aperture.) Since our optical data were obtained when 4151 was bright, *at most* $\sim 30\%$ of the observed visual continuum could be starlight.

Rieke and Lebofsky (1981) fitted a composite spectrum of 4151 (in its bright state) which is essentially the same as ours. Even though they attributed most of the 2.2 μm flux to hot dust, they still found a nonthermal flux component with a fairly steep slope of $\alpha \sim -0.85$ from 10000 to 4500 Å. Adopting their hot dust model, rather than our power law, hardly changes the resulting strength or shape of the ultraviolet excess.

d) The Ultraviolet Excess

To measure the ultraviolet excess, we first subtracted power laws ($f_\nu = C\nu^\alpha$) from the spectra. We determined the power law slopes from the red and infrared data points, to an accuracy of ± 0.1. The procedure is illustrated for Mrk 9, Mrk 10, and 3C 273 in Figures 1 and 2. In Figure 1 the vertical bars represent observed fluxes. The solid lines are the power laws, reddened by the amounts in Table 1. The line for Mrk 10 also has a contribution from starlight, which produces 55% of the visual flux. All of the objects have a strong excess ultraviolet flux over the red power law.

Figure 2 shows the excess flux (observed minus power law), corrected for reddening, plotted on a linear intensity scale versus log rest frequency. This ultraviolet excess always has a rapid rise from about 4000 to 3500 Å. At shorter wavelengths it falls gradually, and then steepens beyond 1400 Å. In at least four objects, Mrk 79, Mrk 335, Mrk 509, and 3C 273, excess flux is present redward of 5000 A. The most extreme example, 3C 273, is included in Figure 2.

It is difficult to determine exactly where the ultraviolet excess begins, but it always has a clear change in slope around 4000 Å, except in 3C 273. We have estimated the frequency $\nu_{1/2}$, at which this 4000 Å jump rises to half of its final ultraviolet intensity. It is shown for Mrk 10 by the labeled arrow in Figure 2. Within the measuring uncertainties (typically $\sigma(\log \nu_{1/2}) \sim 0.01$), every object in our sample has the same value of $\nu_{1/2}$, 7.9×10^{14} Hz, or in wavelength, 3790 Å $\pm$ 40 Å (error in the mean).

This is the wavelength at which the overlap of the higher order Balmer line wings reaches half of the limiting intensity at 3646 Å. A simple calculation assuming Gaussian line profiles shows that $\nu_{1/2}$ for blended Balmer lines is 7.9×10^{14} Hz, if the full width at half-maximum is 3000 km s^{-1}. Some of the observed Balmer lines have smaller FWHMs. But in these objects $\nu_{1/2}$ is still near 8×10^{14}, since the line wings are broader and stronger than in a Gaussian. The observed increase in excess flux from 4000 to 3500 Å must be due to blended Balmer lines: no other mechanism could explain such a remarkable wavelength coincidence.

Several other observations support the contention that Balmer continuum emission contributes significantly to the observed 3500 Å flux:

1. The excess flux at 3500 Å correlates well with the Balmer emission line fluxes. We will demonstrate this for our sample below. Yee (1980) found a similar correlation for his large sample of quasars and Seyfert 1 nuclei. He showed that the total near-ultraviolet (3500–2800 Å) flux (which he called L_{NT}) correlated with the Hβ flux. No active galactic nucleus with very weak broad lines, such as NGC 1275 or a BL Lacertae object, has a "3000 Å bump."

2. When the Balmer line fluxes vary, so does the ultraviolet flux (Oke, Readhead, and Sargent 1980). When quasar lines fluxes are constant, even if the optical continuum varies, the "3000 Å bump" remains constant (Netzer *et al.* 1979).

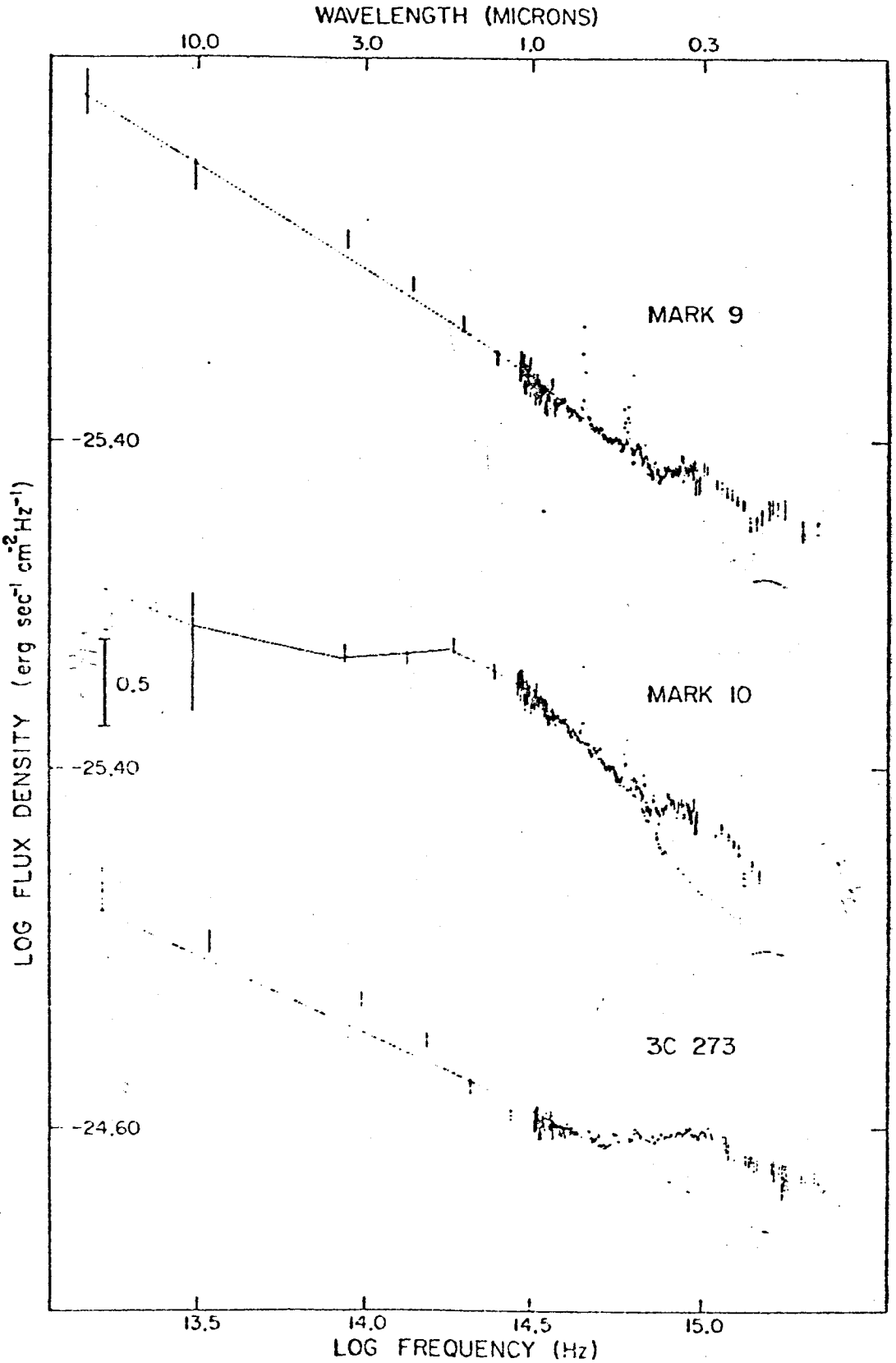

FIG. 1.—Power-law subtraction to measure the excess ultraviolet flux. The vertical bars represent observed flux densities, on a logarithmic scale, and their uncertainties. The lines are power laws with slopes $\alpha = -1.2$, -0.90, and -1.0 for Mrk 9, 10, and 3C 273, respectively. In Mrk 10, starlight, which contributes 55% of the visual flux ($\log \nu = 14.74$) produces a hump around 1.6 μm.

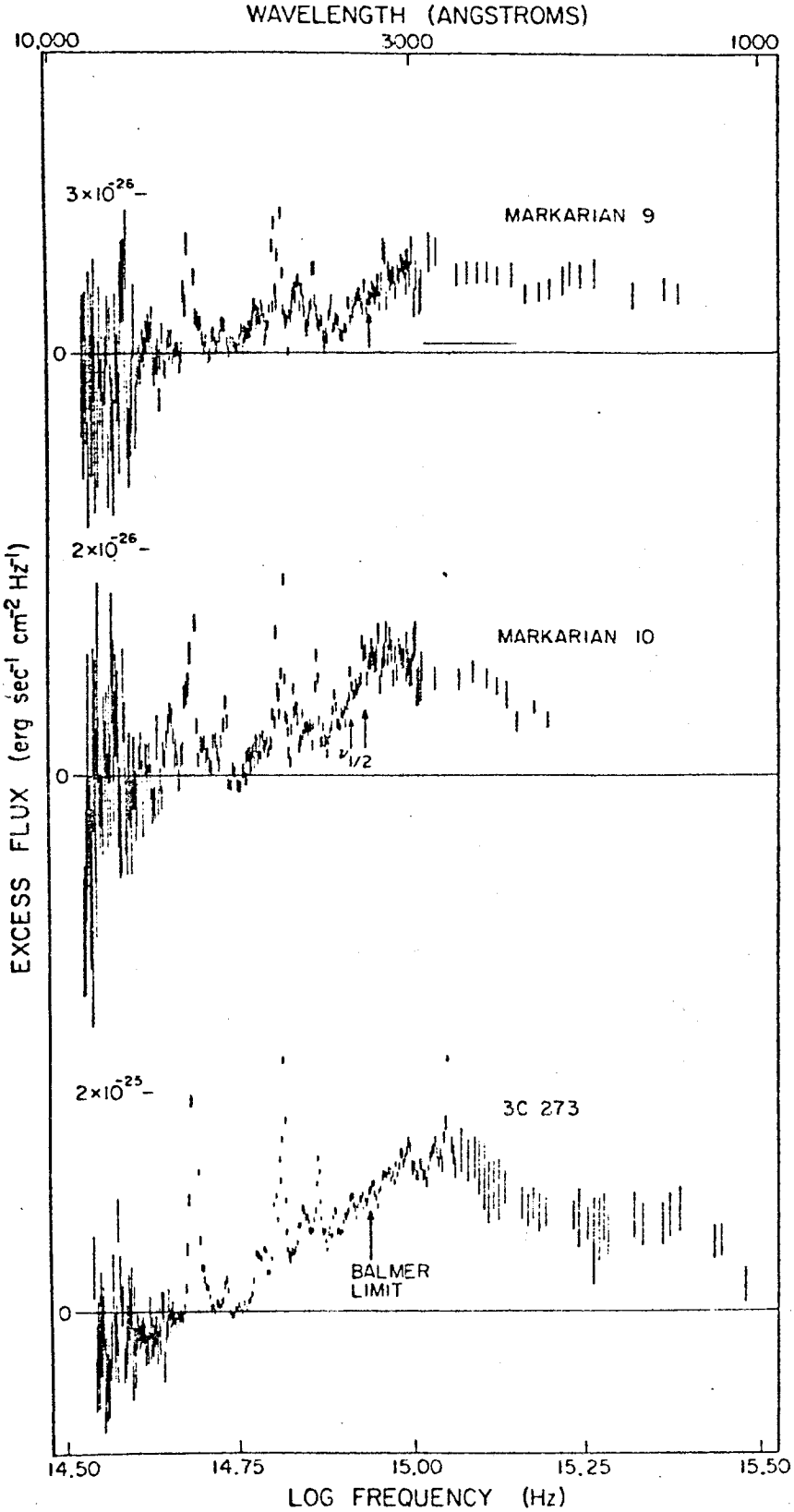

FIG. 2.—The excess flux, obtained by subtracting the power laws in Fig. 1 from the data, and converting to a linear flux scale. The points have been corrected for reddening. The ordinate is still log frequency, but the infrared points are not plotted. Arrows indicate the frequency of the Balmer limit (3646 Å) for the three objects and $\nu_{1/2}$ for Mrk 10.

3. DeBruyn (1980) found that the relative variability of Balmer line fluxes increases steadily from Hα to Hδ. For example, in NGC 7469, an increase of 30% in Hα corresponded to increases of 50, 80, and 160% in Hβ, Hγ, and Hδ, respectively. The near-ultraviolet flux almost doubled. The strong variability of the 3500 Å continuum is more closely linked to the Balmer lines higher than Hα.

4. The continuum polarization of NGC 4151 drops rapidly at wavelengths less than 4000 Å (Schmidt and Miller 1980). Their explanation, which we confirm, is that most of 4151's near-ultraviolet flux is produced by the Balmer continuum, which, like the broad Balmer lines, is unpolarized.

III. DETAILED SPECTRAL FITTING

We attempted to fit the spectra in the ultraviolet by adding a Balmer continuum (BaC) to the power laws discussed in § II. The $F_{BaC}/F_{H\alpha}$ ratio and the electron temperature were free parameters. A small amount of free-free emission was also added, scaled to the observed Hα flux, assuming Case B recombination. We added emission from the Balmer and Paschen lines up to $n = 40$, using their Case B ratios, as given by Brocklehurst (1971). We also added emission from the optical and ultraviolet complexes of permitted iron lines, using the strengths, relative to Hβ, given by Kwan and Krolik's (1981) "standard model." The line profiles were assumed Gaussian, with full widths at half-maximum given by Osterbrock (1977), smoothed by the instrumental resolution.

The spectra of the three intrinsically faintest galaxies, NGC 4151, NGC 5548, and Mrk 10, are well fitted by the addition of the Balmer continuum. The fit for NGC 4151 is illustrated in Figure 3: the parameters for the best fitting (*solid*) line are given in Table 2.

If most of the ultraviolet excess in these objects is in fact Balmer continuum emission, we draw several further conclusions:

1. The $F_{BaC}/F_{H\alpha}$ ratio is 50–150% larger than its Case B value (1.4 or 1.9, for $T = 10{,}000$ or 20,000 K). The relatively small dispersion in this ratio demonstrates that the Balmer line and continuum fluxes are well correlated, as claimed in § II. Columns (6) and (7) of Table 3 give the total fluxes. The dot-dash curve in Figure 3 illustrates the (less satisfactory) fit to NGC 4151, if the $F_{BaC}/F_{H\alpha}$ ratio is constrained to equal its Case B value. Our estimates of F_{BaC} are insensitive to the assumed strength of the blended iron line emission. They are unchanged, within the quoted uncertainties, when the Fe line fluxes are boosted by a factor of 3. Although this clearly overestimates the Fe line emission in several objects, it is still only a small fraction of the total observed ultraviolet excess.

2. The observations can be fitted satisfactorily with either an optically thin or an optically thick Balmer continuum. In the first case, the flux drops with $f_\nu \propto \exp(-h\nu/kT)$ (see the derivation of the Milne cross section relations in Osterbrock 1974; this is simply the Boltzmann factor reflecting the scarcity of more energetic electrons in a thermal gas). If, at the other extreme, τ_{3646} is larger than 10, the Balmer continuum should resemble a Planck function at the temperature of the emitting clouds, over the observed wavelength range. The flux would drop more gradually, as $\nu^3 \exp(-h\nu/kT)$. To fit the data, the Balmer continuum fluxes would have to be roughly doubled if the Balmer continuum were very optically thick. Best fits assuming the Balmer continuum is optically thin (*solid line*) or optically thick (*dashed line*) are shown for NGC 4151 in Figure 3.

3. The Balmer continuum is best fitted with a temperature of ~ 15,000 K if it is thin, or a few thousand kelvins less if it is thick.

IV. FLATTENING OF THE OPTICAL CONTINUUM

As mentioned in § II, the continua of 3C 273, Mrk 79, Mrk 335, and Mrk 509 begin to deviate from an $\alpha \sim -1$ power law well before 4000 Å. Stein, Burbidge, and Smith (1981) encountered this problem in attempting to fit the spectrum of 3C 273 with a power law plus strong Balmer continuum. Their fits are simply not flat enough in the

TABLE 2

SPECTRAL PARAMETERS FROM LEAST SQUARES FITTING

					BALMER CONTINUUM			
	POWER LAW		BLACKBODY		If Thin		If Thick	
OBJECT	f_{5500}[a]	α	f_{5500}[a]	Temp	f_{3646}[a]	Temp	f_{3646}[a]	Temp
Mrk 9	4.9	−1.2	.56	33,000	0.85	17,000	0.77	15,000
Mrk 10	2.1	−0.9	<0.7	...	1.6	...	1.4	...
Mrk 79	10.	−1.1	2.6	34,000	4.8	15,000	3.8	14,000
Mrk 335	9.0	−1.1	3.0	25,000	4.9	15,000	4.1	14,000
Mrk 509	12.	−1.0	4.0	21,000	6.4	15,000	5.6	15,000
NGC 4151	49.	−1.2	<1.0	...	16.	18,000	14.	14,000
NGC 5548	13.	−1.1	<0.8	...	3.4	15,000	3.0	14,000
3C 273	15.	−1.1	12.	26,000	6.0	15,000	4.7	13,000
Uncertainty	±10%	±0.1	$^{+10\%}_{-20\%}$	$^{+10000}_{-5000}$	±10%	±5000	±10%	±5000

[a] All fluxes in 10^{-26} ergs cm^{-2} s^{-1} Hz^{-1}.

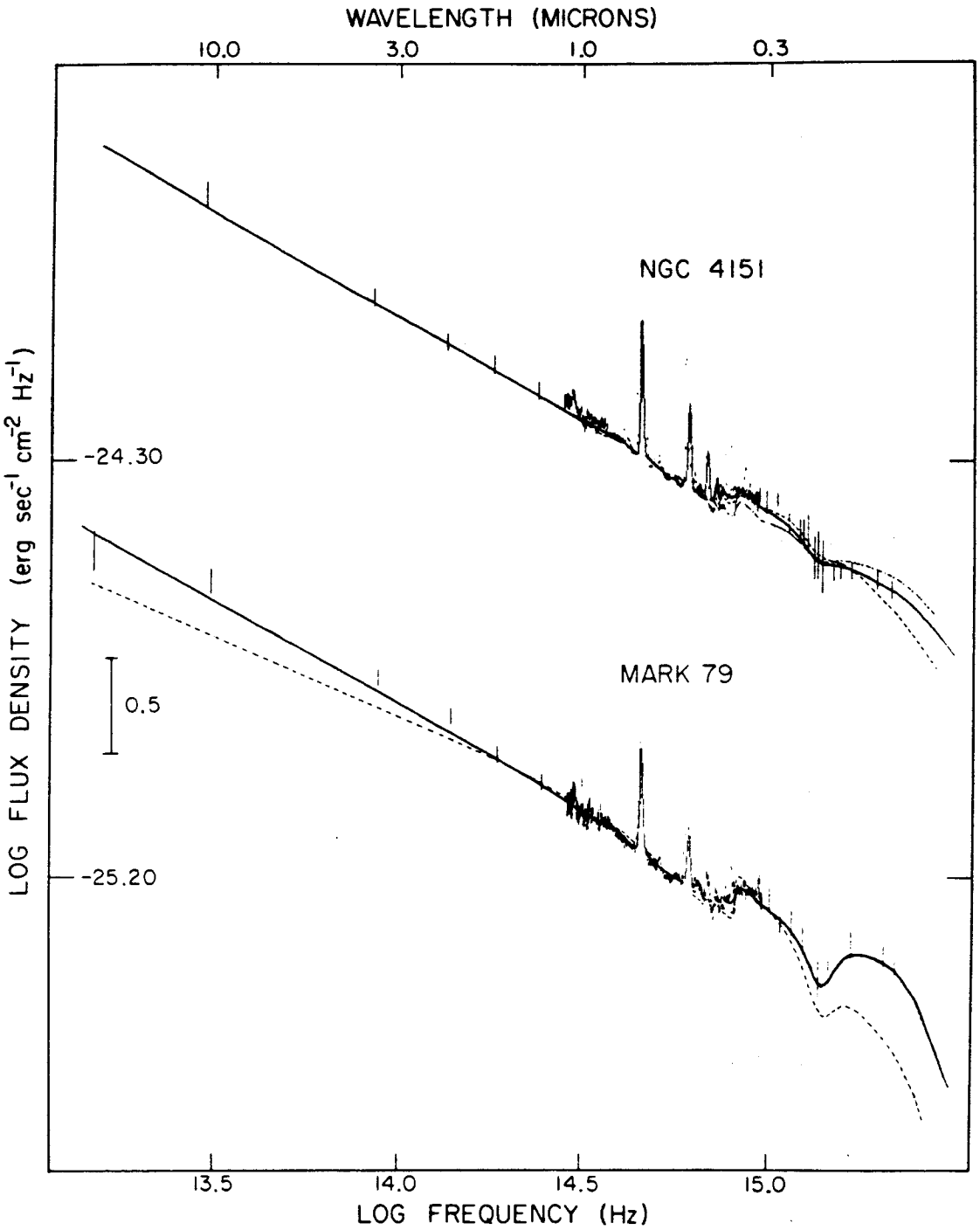

FIG. 3*a*.—Fits to the spectra of NGC 4151 and Mrk 79. The vertical bars represent observed flux densities and their uncertainties. The observed flux and frequency scale are logarithmic. The solid and dashed lines for 4151 are fits with an optically thin and optically thick Balmer continuum. They both match the observations very well. The dash-dot line, which does not fit the data so well, has the Balmer continuum reduced to its Case B value, relative to Hα. The solid and dashed lines for Mrk 79 are the best fits with and without a blackbody component. The lower branch of the solid line from 4000 to 3650 Å is the blackbody fit with the higher order Balmer lines removed. Parameters for the solid line fits are given in Table 3.

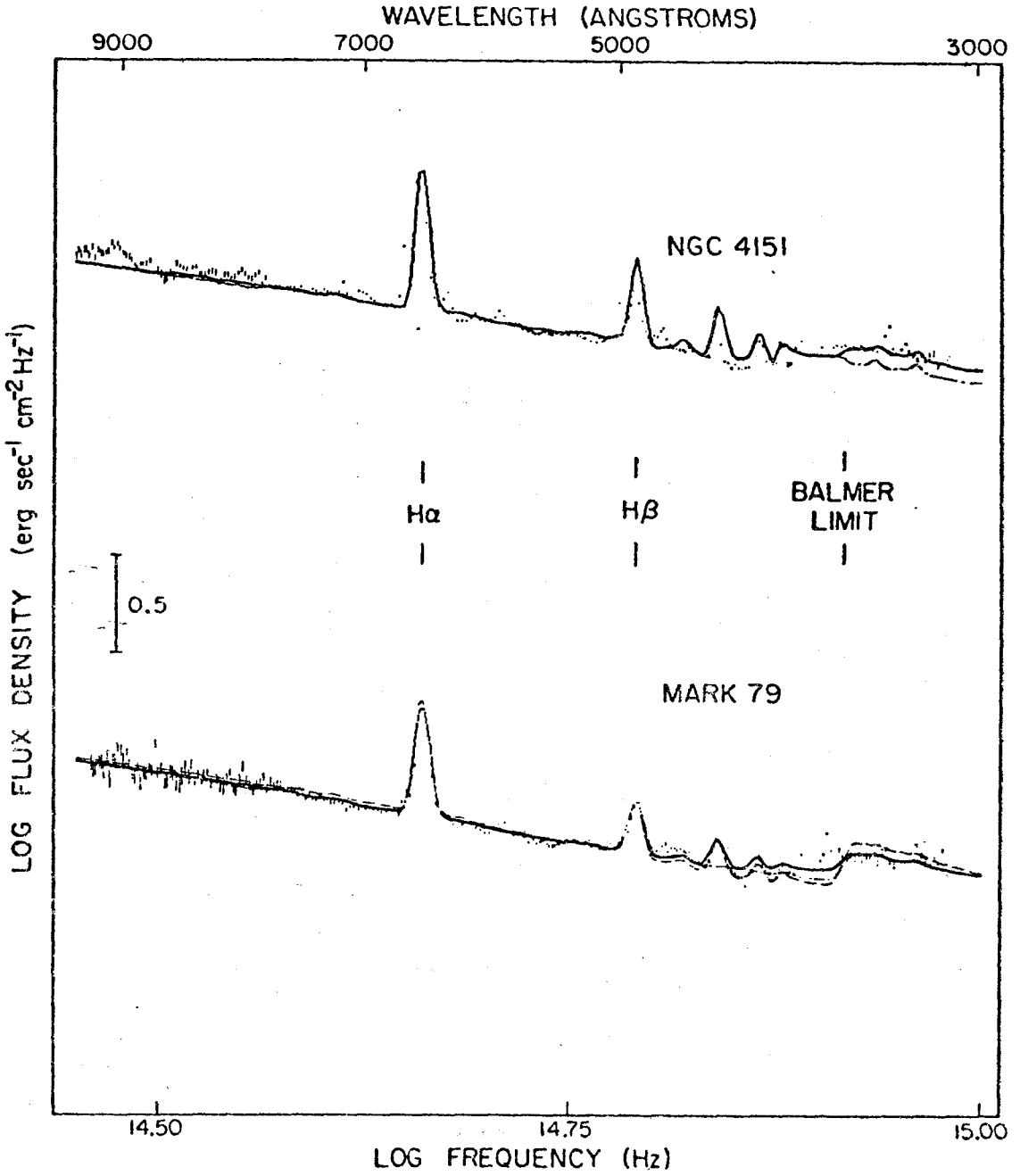

FIG. 3b.—Blowup of the optical portion of Fig. 3a. The fits to NGC 4151 with optically thin and thick Balmer continua cannot be distinguished in the wavelength range.

blue and ultraviolet to match their observations (compare their Figs. 3 and 5).

This optical flattening is a common feature of most quasar spectra (Neugebauer *et al.* 1979) and many of the high-luminosity Seyfert 1 nuclei observed by DeBruyn and Sargent (1978). The component which produces the flattening appears to extend well into the ultraviolet, since many objects have several times more flux at 1200 Å than would be expected simply from the Balmer continuum and extrapolated red power law.

We attempted to improve our spectral fits in the ultraviolet with the addition of several flatter components. The first two failed singly or in combination. The third succeeded.

A) We first added optically thin recombination emission from a hot plasma. The total flux and the plasma

temperature were free parameters, with temperature running from 70,000 to 3,000,000 K. Lower temperatures would not produce sufficient ultraviolet flux. Higher ones would produce too much X-ray emission. Most of the emission was free-free: $F_{ff}/F_{B,C} = 4.5$ or 30 for $T = 100{,}000$ or 500,000 K. The rather flat spectral distribution, $f_\nu \propto \exp(-h\nu/kT)$, did not have the upward curvature of the observed excess (see 3C 273 in Fig. 2). What was needed was a component which actually rises from the red to the violet, and then drops in the ultraviolet.

The best fit for 3C 273, with free-free, bound-free, and power-law emission, is shown by the dashed line in Figure 4. It has a free-free flux at 5500 Å of 1.8×10^{-25} ergs cm^{-2} s^{-1}. The enormous implied luminosity would require a volume integral of n_e^2 of almost 10^{71} cm^{-3}. This would be roughly twice that of the Hα-emitting region. If the electron density were 10^6, the total volume would be several thousand cubic parsecs, and the total mass would be $10^8\ M_\odot$.

B) If the escape probability for Lyα photons is less than $A_{Ly\alpha}/A_{2\gamma} = 5 \times 10^{-9}$, two-photon emission could become the dominant mechanism for de-exciting the $n = 2$ level. If $\tau_{Ly\alpha} \sim 10^4 \tau_{LyC} > 10^3$, and Lyα photons are not destroyed by dust, almost all of the $2 \rightarrow 1$ transitions can proceed by two-photon emission.

The distribution of emitted photons is symmetric about 2431 Å, twice the wavelength of Lyα. Two-photon flux is negligible in the red, but rises to a peak at 1621 Å, independent of temperature. If two-photon emission noticeably affected the blue fluxes, it would also produce a sharp spectral turnover from 1600 to its cutoff at 1216 Å. Only 3C 273 is sufficiently redshifted for *IUE* to observe its continuum below Lyα. Like the quasars observed by Green *et al.* (1980), 3C 273 has a steepening spectrum starting around 1300 Å, but the drop is too smooth to be produced by the two-photon cutoff. The dot-dash line in Figure 4 illustrates the fit with free-free, two-photon, bound-free, and power-law continua. The two-photon flux is 6×10^{-11} ergs cm^{-2} s^{-1}, and it produces a sharp kink below Lyα which is just barely consistent with the data. We consider this a safe upper limit; two-photon emission cannot produce the observed spectral flattening. Ground-based observations also demonstrate this for high-redshift quasars (Oke 1970, 1974; Osmer 1979; Soifer *et al.* 1981).

Two-photon emission is probably suppressed by collisions from the $n = 2$ level. Since the $2 \rightarrow 1$ collision rate is 1.2×10^{-8} cm^3 s^{-1} (from Krolik and McKee 1978), the electron density must exceed 10^9 cm^{-3}, if $\tau_{Ly\alpha} > 10^3$. A detailed study by Drake and Ulrich (1981), which explicitly solved the rate equations for the hydrogen atom for a range of densities, confirms our estimate. The strength of broad C III] lines in the spectra of active galactic nuclei sets an upper limit on n_e. Thus the electron density is constrained to lie between 10^9 and 10^{10} cm^{-3}.

In Kwan and Krolik's "standard model" ($n_e = 4 \times 10^9$), $F(2\gamma)/F_{B,C}$ was 0.07. Such a small two-photon contribution could not be detected, by even the best observations.

C) As suggested above (and, for example, by Ulrich *et al.*'s 1980 study of 3C 273), the excess flux may be thermal continuum from very optically thick gas. We assumed the simplest form for this emission: a Planck function at a single temperature. For objective estimates of a possible blackbody component, we used a nonlinear least squares routine to fit the continuum points. The free parameters were the strength and slope of the power law, the strength and temperature of the Balmer continuum, and the strength and temperature of the blackbody emission. By varying these parameters, we were able to fit every one of the eight spectra. The best fitting parameters, corrected for reddening, are listed in Table 3. Dashes in the tables indicate parameters which cannot be determined by the data. The quoted uncertainties were found by allowing all of the parameters to vary simultaneously. The fits to NGC 4151, Mrk 9, Mrk 79, and 3C 273 are illustrated by the solid lines in Figures 3–5.

In all cases these fits match the observations virtually as well as could any smooth curves. The blackbody

TABLE 3

ENERGY BUDGETS

	Line Fluxes				Balmer Continuum		Ionizing	Blackbody	
Object	Lyα	Hα	Hβ	Hγ	If Thin	If Thick	Flux	Flux	Area
Mrk 9	7.1	1.1	.40	.20	3.0	7.6	100	60	6
Mrk 10	3.2	.92	.38	.15	5.0	13.	120	<30	...
Mrk 79	15.	4.1	1.7	.70	15.	38.	330	300	8
Mrk 335	11.	2.8	1.3	.70	16.	36.	310	160	20
Mrk 509	16.	7.1	2.2	1.2	20.	55.	490	140	60
NGC 4151	48.	23.	7.0	3.2	60.	120.	1200	<80	...
NGC 5548	10.	3.7	.93	.27	12.	30.	430	<40	...
3C 273	16.	8.7	3.3	1.6	18.	38.	550	750	3000
Uncertainty ...	±10%				±10%		±30%	±30%	±50%

[a] All fluxes are in 10^{-12} ergs cm^{-2} s^{-1}.

[b] Areas (in 10^{30} cm^2) are lower limits, since an emissivity of 1 was assumed. They were calculated using a Hubble constant of 75 km s^{-1} Mpc^{-1}.

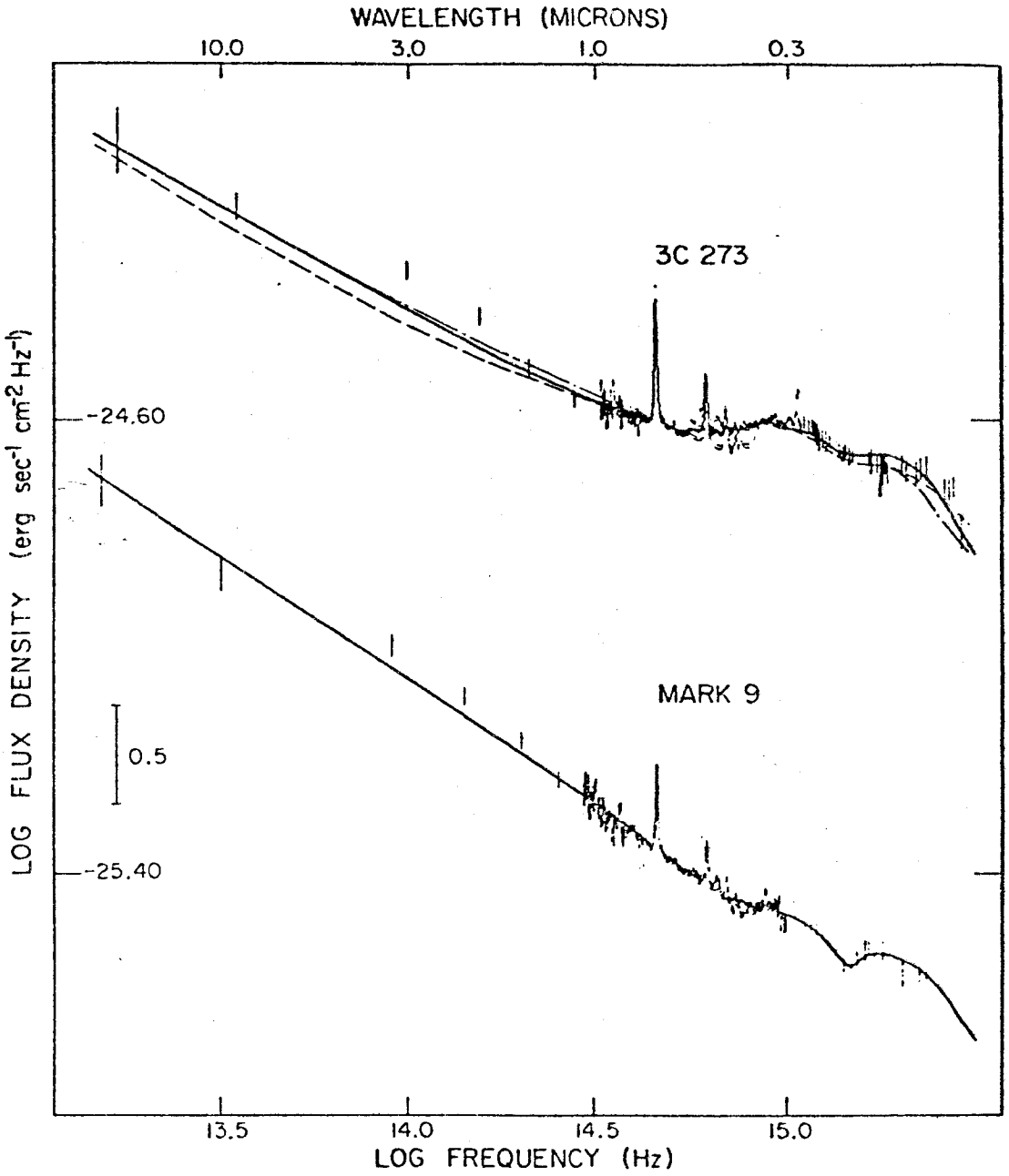

FIG. 4a —Fits to the spectra of 3C 273 and Mrk 9. The solid line, which fits the 3C 273 data well, has a power law, and optically thin Balmer continuum, and a 26,000 K blackbody. The two poorer fits have optically thin recombination emission from hot gas, but no blackbody. The short-long-short dashed line also has a contribution from two-photon emission. The solid line for Mrk 9 is the best fit with a power law, Balmer continuum, and 33,000 K blackbody. The lower branch from 4000 to 3650 Å has the highest order Balmer lines removed. Parameters for the solid curves are given in Table 3.

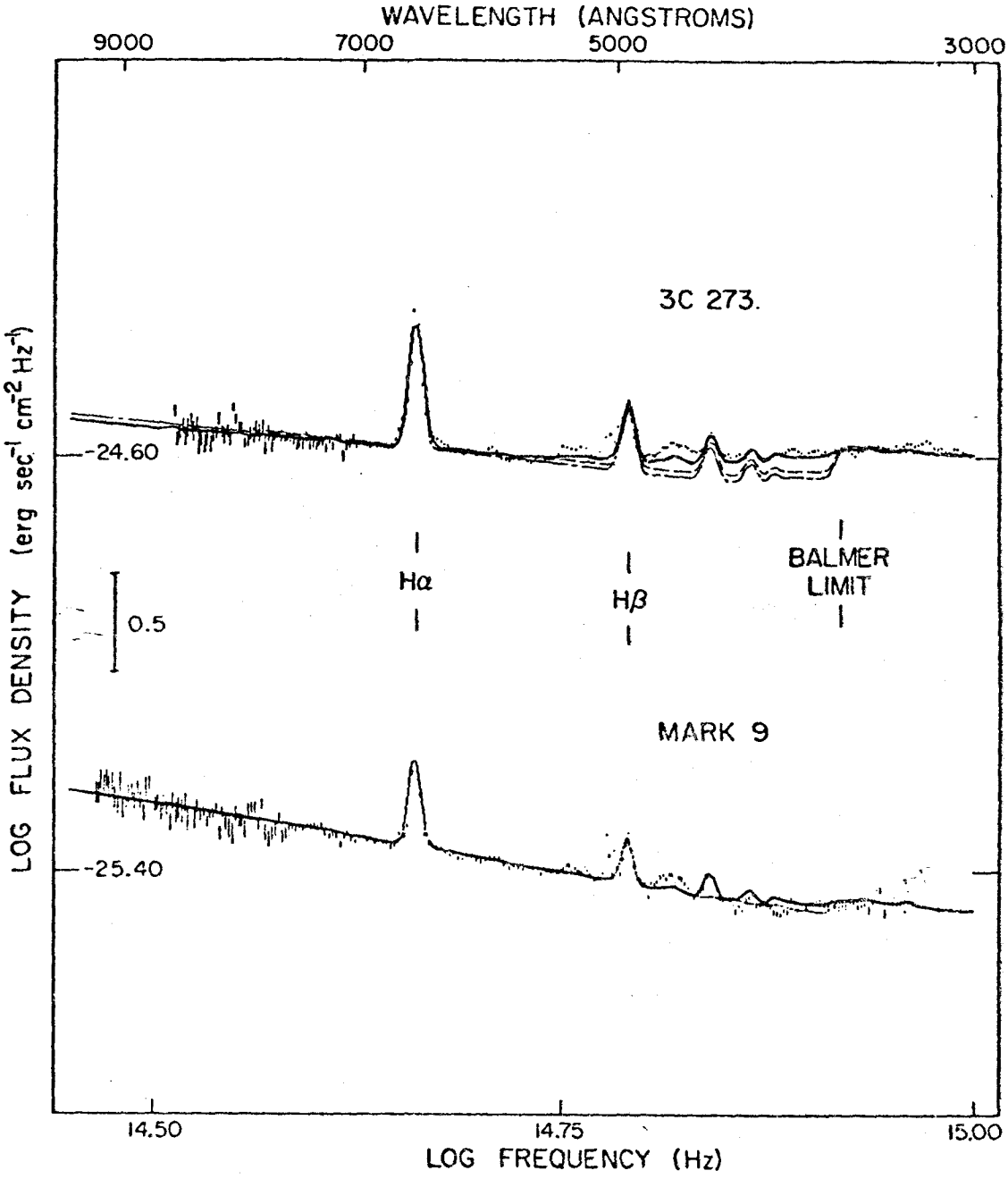

FIG. 4b.—Blowup of the optical portion of Fig. 4a. As in Figs. 1 and 3, the data in Figs. 4a and 4b have not been corrected for reddening. Instead, the fits were reddened to match them.

component is required for a good fit to five of the spectra. Figure 3 illustrates the fit (*solid line*) to the spectrum of Mrk 79. The best fit without a blackbody component is the dashed line. The data cannot be fitted with only a power law and Balmer continuum. As stated above, we could not conclusively measure the blackbody component in the other three, NGC 4151, NGC 5548, and Mrk 10, and can only set upper limits.

The estimated temperatures in all objects range from 20,000 to 30,000 K. There could be small thermal contributions present from hotter or cooler gas which would be difficult to detect. Cooler blackbodies are badly confused with the nonthermal power law. Observations to higher frequencies are needed to detect hotter thermal components. The sharp high-frequency cutoffs observed by Green *et al.*, however, indicate that there is little thermal

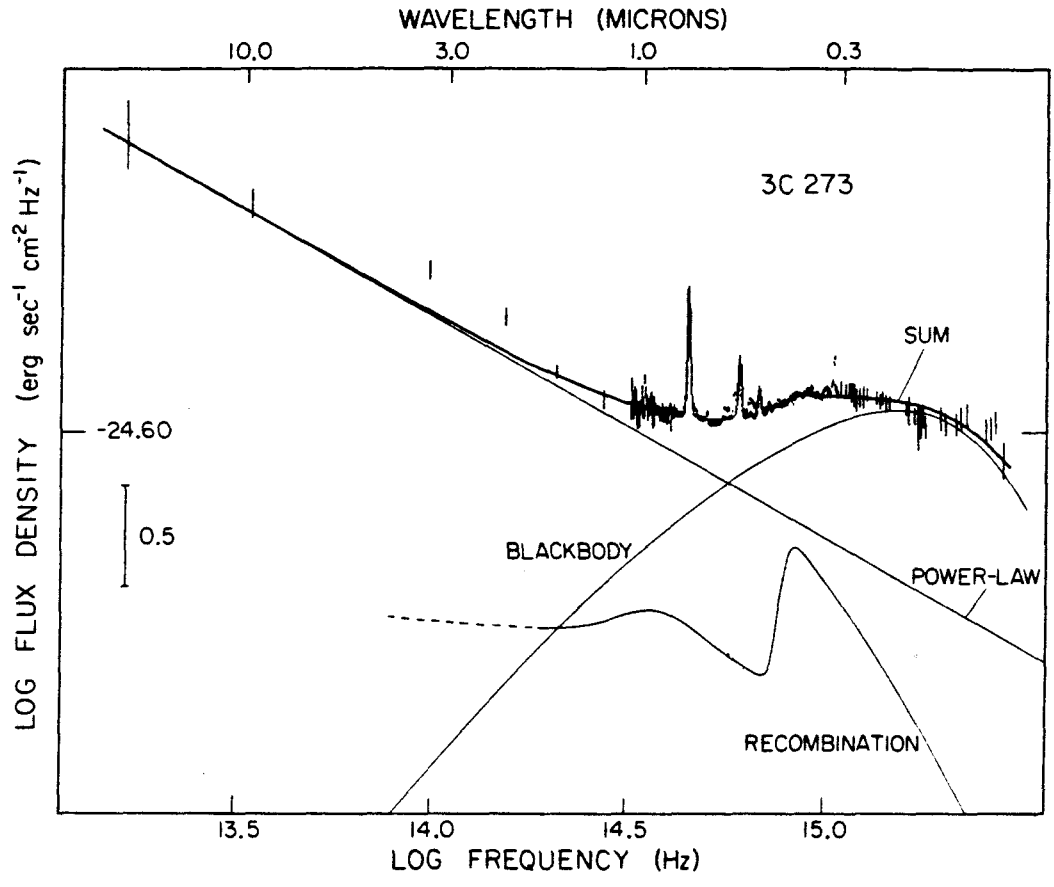

FIG. 5.—Decomposition of the best fit to 3C 273. In contrast to Figs. 1, 3, and 4, everything plotted here has been corrected for reddening. Three solid lines illustrate the power law, hydrogen recombinations, and blackbody components, as given in Table 2. Their sum fits the observed fluxes very well.

gas much hotter than 40,000 K. We stress that the thermal component need not be a single-temperature blackbody. This is just the simplest form which fits the data well. The thermal component must simply rise from the red to the ultraviolet, peak around 2000–3000 Å, and then fall rapidly at higher frequencies.

The final 3C 273 fit, and its decomposition into three components, are illustrated in Figure 5. All the curves and data in Figure 5 have been corrected for reddening, unlike those in Figures 1, 3, and 4. The power law dominates in the red, and probably in the (unobserved) extreme ultraviolet. The bright 26,000 K blackbody, peaking around 2000 Å, produces a slight increase in the total flux at wavelengths shorter than 3646 Å. Since most quasars and Seyfert galaxies have flat or falling spectra shortward of 3646 Å (DeBruyn and Sargent 1978; Neugebauer *et al.* 1979), 3C 273 may have an unusually high blackbody to power-law ratio.

Our results are not sensitive to the assumed form of the reddening law. The two most unusual observed reddening laws in Bless and Savage (1972) are for ν Ori and θ Ori (one of the Trapezium stars). They have the smallest known value of A_{2175}/A_{5500} in the Galaxy (i.e., the weakest relative strength of the 2175 Å dip). A_{2175}/A_{5500} for ν and θ Ori is only 2.0, half of the value in Seaton's (1979) standard reddening law. To take the most extreme case, had we used the ν Ori–θ Ori law for Mrk 79, we would have found $E_{B-V} = 0.44$ mag. Nonetheless, the best-fitting power law (and total ionizing flux) would be essentially the same as the ones in Tables 2 and 3. The total (dereddened) blackbody flux would also be unchanged, but its temperature would drop to 23,000 K. The total Balmer continuum flux would be tripled, while the Hβ flux would be doubled.

V. ENERGY BUDGETS

The average power-law slope in our eight objects is -1.1, with a very small dispersion, 0.1, only slightly larger than the observational uncertainties. This result disagrees with the fits made by many spectroscopists to their visual and ultraviolet spectra (e.g., for 3C 273, $\alpha = -0.48$ [Grandi and Phillips 1980] and $\alpha = -0.43$ [Boggess *et al.* 1979]; for Mrk 9 and Mrk 10, $\alpha = -0.6$ [Oke and Goodrich 1981]; for NGC 4151, $\alpha = -0.33$ [Schmidt and Miller 1980]). These flatter slopes result from the restricted wavelength range they considered. A flat power

law may fit a limited portion of the spectrum, but breaks down if extended to slightly lower or higher frequencies. As we showed in § IV, this is because a steeper power law ($\alpha = -1.1$) is diluted in the blue and ultraviolet by stronger, flatter thermal components.

Complete wavelength coverage, from the infrared to the far-ultraviolet, is essential for making quantitative conclusions about the ultraviolet excess. For example, if an arbitrary underlying continuum were drawn to fit only the spectral region from $\lambda_0 = 5500$ to 2700 Å, it might be possible to cut the deduced Balmer continuum flux in half. However, as we have seen, such a continuum would be meaningless, and the agreement of F_{BaC} with the Case B prediction would be misleading.

The thermal components (e.g., Balmer continuum, blackbody, free-free, or two-photon emission) provide few or no ionizing photons. Simple extrapolations of the optical continuum to high frequencies can overestimate the ionizing flux by a factor of 10–20.

In Table 3 we give the estimated total ionizing fluxes, up to 10^{18} Hz (0.25–34.6 rydbergs), obtained by integrating the extrapolated fluxes of the power laws listed in Table 2. To avoid underestimating the totals, we started the integrations at the Balmer limit, since the clouds may well have appreciable optical depth in the Balmer continuum (Kwan and Krolik 1981; Canfield and Puetter 1981). The results were insensitive to the choice of frequency limits. For example, if the integrations were cut off at 10^{17} Hz, the ionizing fluxes in Table 3 would be decreased only about 30%. This is comparable to the error produced by uncertain values of α, the power law slope. Columns (2)–(7) give the Balmer line and continuum and Lyα fluxes (the latter are from Wu, Boggess, and Gull 1980). The Hα and Hγ fluxes have been corrected for the small contamination from [N II] and [O III] lines, using line ratios from Osterbrock (1977). All quantities in Tables 2 and 3 have been corrected for reddening.

On the average, active galactic nuclei emit nearly as much energy in the Balmer continuum as they do in Lyα. If it is all supplied by photoionization from the power law continuum, the average covering factor must be at least 10%.

The total flux in 3C 273's optically thick thermal component exceeds the entire ionizing flux available from the nonthermal power law, even if the covering factor were 100%. This is true regardless of its assumed spectral shape. We conclude that this component is not powered by photoionization from the continuum, at least below 10 keV. This conclusion also applies to Mrk 9, 79, and 335, unless the thermal region absorbs more than half of the ionizing continuum. If we assume that the emissivity of the optically thick thermal gas is 1, we obtain the lower limits to the emitting surface area listed in Table 3. The strongest observed blackbody emission, from 3C 273, requires a surface area of 3×10^{33} cm^2.

VI. DISCUSSION

a) Balmer Continuum

In § III we concluded that the $F_{\text{BaC}}/F_{\text{H}\alpha}$ ratio in Seyfert 1 galaxies and quasars is 1.5–2.5 times its Case B value. If we had not included a blackbody component in the fits, or if we had substantially underestimated the reddening, the intrinsic $F_{\text{BaC}}/F_{\text{H}\alpha}$ ratios would be even larger. Our results prove that Case B recombination does not describe the Balmer emission of any of the active galactic nuclei in our sample, regardless of the assumed reddening corrections.

We must therefore consider more sophisticated models of quasar emission line clouds. Recently, Kwan and Krolik (1981) and Canfield and Puetter (1981) have calculated detailed optically thick models to explain the hydrogen line ratios in quasars and Seyfert 1 galaxies. In both sets of models, the Balmer emission comes from large optical depths, from which hardly any Lyα escapes. Here photon trapping produces large excited state populations, which are ionized by photons and collisions. In this "extended ionization region" Hα, which is optically thick, grows more slowly with τ than the Balmer continuum, until it too thickens, at $\tau_{\text{LyC}} \sim 10^5$. Kwan and Krolik found that the relative strength of the Balmer continuum is especially enhanced if the X-ray flux and electron density are high.

In attempting to explain the hydrogen line ratios, particularly the small value of Lyα/Hα, both studies came to conclusions consistent with our new observations. The required large optical depths and densities also lead them to predict an enhanced $F_{\text{BaC}}/F_{\text{H}\beta}$ ratio. Those models predicted that progressively thicker clouds (at least up to $\tau_{\text{BaC}} \sim 10$) should have increasing $F_{\text{BaC}}/F_{\text{H}\beta}$, $F_{\text{H}\alpha}/F_{\text{H}\beta}$, and $F_{\text{H}\beta}/F_{\text{Ly}\alpha}$ ratios. We have plotted BaC/Hβ against Hβ/Lyα and Hα/Hβ. Both plots are scatter diagrams, but each ratio varies over a relatively small range in this small sample. Incorrect reddening corrections would actually tend to produce an anticorrelation. More data are required to see if these ratios are correlated, as a simple interpretation of Kwan and Krolik and Canfield and Puetter's models might predict.

These models can explain why the Hα and Hβ fluxes vary less than proportionally with the 3500 Å flux (DeBruyn 1980; and Oke, Readhead, and Sargent). The 3500 Å flux, which is dominated by Balmer continuum flux, may be more variable because, like the higher Balmer lines, it is less optically thick than Hα and Hβ, and therefore more sensitive to changes in the amount of emitting gas.

b) Paschen Continuum

None of the 68 Seyfert galaxies and quasars observed by DeBruyn and Sargent show any evidence of excess emission around the wavelength of the Paschen limit, 8224 Å. Unfortunately, the upper limits we could set on $F_{\text{Paschen Continuum}}$ are high enough to be uninteresting, and we cannot think of any observations which could improve on them.

In our fits, the predicted strength of the Paschen jump is also small, due to the dilution by the power law flux. When the higher Paschen lines are included, appropriately broadened, as in Figure 4, the spectral inflection around 8224 Å is almost completely washed out. The predicted Paschen jump would still be very weak even if

its strength, relative to Hα, were enhanced several times over the Case B value.

In Kwan and Krolik and Canfield and Puetter's "standard models," the ratio of optical depths at the Balmer and Paschen edges is about 10:1. If the Paschen continuum were very thick at 3646 Å, the resulting recombination spectrum would resemble the source (Planck) function. There would be no Balmer jump, unless the Balmer and Paschen continuum excitation temperatures were sufficiently different. In § II we found a strong Balmer jump in emission in Seyfert 1 galaxies, at least in this sample. Thus most of the emission line clouds probably have Balmer continuum optical depths of less than 100.

c) *Blackbody Emission*

One possible interpretation of the optically thick thermal emission we described in § IV is that it comes from an accretion disk (see, for example, Shields's 1978 discussion of the optical spectrum of 3C 273). This hypothesis is supported by our result in § IV, that the thermal flux in 3C 273, and probably in three of the Seyfert galaxies, is too large to be powered by photoionization. Thermal emission from an accretion disk comes from the kinetic energy of accreting matter, transported outward by (as yet unknown) viscous torques in the disk.

The predicted accretion disk temperatures are insensitive to the luminosity of the disk. Our data show no trend of blackbody temperature with luminosity, but observations into the far-ultraviolet are needed to confirm this. There may well be a range of temperatures present in each object. As emphasized above, the temperatures in Table 2 should be considered the dominant temperatures of the optically thick region. It may never be possible to infer a unique distribution of temperatures from a single spectrum.

The continuum flux of quasars at the Lyman edge is still dominated by the thermal component. Yet observations of high-redshift quasars rarely reveal any drop in flux just shortward of 912 Å (Oke and Korycansky 1981). So the optically thick component probably has at most a weak Lyman jump, in contrast to typical stellar atmospheres.

The relative strength of the blackbody, compared to the power law, varies widely in our sample. However, the ratio of blackbody to power law flux correlates with total luminosity. The correlation is shown graphically in Figure 6. With the present limited sample, this correlation is, of course, poorly determined, especially at high luminosities.

The correlation may explain Baldwin *et al.*'s (1978) finding that the equivalent width of ultraviolet emission lines decreases with the square root of the ultraviolet luminosity (if $q_0 = 0$). The line fluxes are closely correlated with the ionizing power law. In the ultraviolet, however, the blackbody becomes increasingly dominant in the more luminous objects. Since the line emission is independent of this component, it becomes more and more diluted.

We can check our result against Baldwin's under the following simple assumptions: (*a*) the 1550 Å continuum is the sum of a power law of slope −1.1 and a 26,000 K

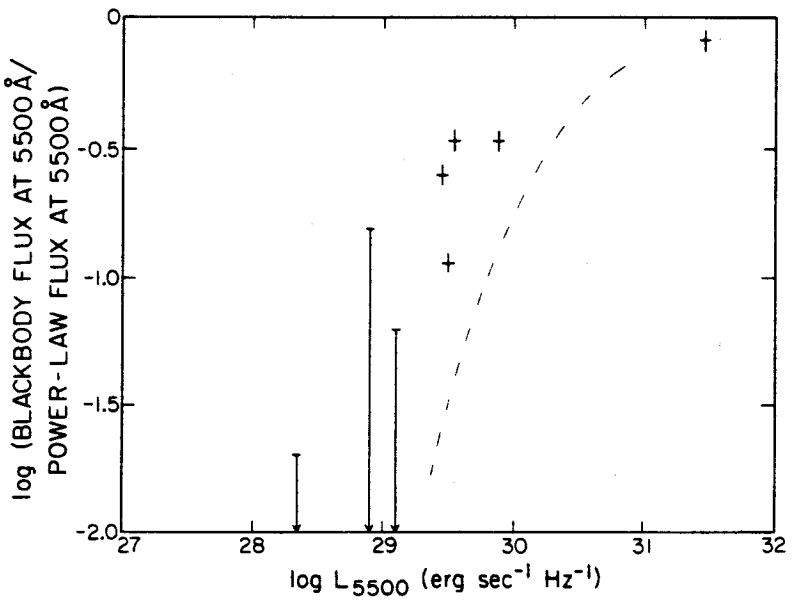

FIG. 6.—The correlation between the ratio of blackbody to power-law flux at 5500 Å (*ordinate*) and the total luminosity at 5500 Å (*abscissa*). Both scales are logarithmic. The three upper limits to the blackbody component are for the three faintest Seyfert galaxies, NGC 4151, 5548, and Mrk 10. The point in the upper right-hand corner represents the bright quasar 3C 273. Observational uncertainties in both coordinates are at most ±0.04 dex. Thus most of the scatter in this diagram is real. The dashed line represents the prediction from Baldwin *et al.*'s (1978) correlation between luminosity and equivalent width of the C IV line, under the simple assumptions listed in the text.

blackbody, (*b*) the C IV flux is a constant multiple of the power law flux, and (*c*) the reddening varies little from object to object. Baldwin *et al.*'s correlation (assuming $q_0 = 0$) is then equivalent to the dashed line in Figure 6.

There is evidence that the thermal emission can be strongly variable. By differencing Seyfert 1 spectra taken a year apart, DeBruyn found a variable component with a relatively flat optical spectrum. We believe that much, if not all, of this visual variability is due to changes in the intensity and spectral shape of the thermal component discussed above. Note however, that they do not account for the variability sometimes observed in the infrared. One corollary is that variations in the blue-to-ultraviolet continuum need not correspond to changes in the total ionizing flux.

d) Nonthermal Power Law

i) *Near-Infrared Emission*

The narrow range of power law slopes we found in the red and infrared ($\alpha = 1.1 \pm 0.1$) suggests that much of the near-infrared emission is produced by a nonthermal spectrum with a similar shape in many active galactic nuclei. Most of the quasars in Neugebauer *et al.* (1979) have simple power-law spectra from the infrared to the red, with slopes between -1.0 and -1.4. As discussed in § II, most of their 1 μm flux is probably nonthermal, since any underlying galaxy would be very faint, and thermal emission from hot dust would have an exponential cutoff at wavelengths shorter than 2 μm. Neugebauer *et al.*'s discovery of 2 μm variability in some quasars supports this conclusion.

The majority of the Seyfert 1 galaxies observed by Rieke (1978) also have near-infrared spectra with slopes between -0.9 and -1.4. Most of the others (such as Mrk 10) have obvious inflections around 1.6 μm, indicating substantial starlight contamination. We suspect that most of the apparent power law spectra with slopes flatter than -1.4 are dominated by nonthermal emission, as in quasars. Rieke and Lebofsky's (1979) discovery of rapid infrared variability in the Seyfert 1 galaxy III Zwicky 2 confirms that most of its 1 μm emission, at least, is nonthermal.

ii) *X-Ray Emission*

The observed continuum should curve downward sharply in the far-ultraviolet as the thermal components cut off exponentially. The only available far-ultraviolet observations with *IUE* (Green *et al.* 1980) do in fact show that quasar spectra steepen rapidly at $\log \nu > 15.4$–15.5. By $\log \nu = 16$, only the $\alpha \sim -1.1$ power law should remain. We have extrapolated the fitted power laws in Table 2 to $\log \nu = 17.68$ (2 keV). The extrapolated power-law flux agrees well with the observed X-ray flux from Kriss, Canizares, and Ricker (1980): $\log (L_{\text{X extrapolated power law}}/L_{\text{X observed}}) = 0.23 \pm 0.29$. The individual scatter, a factor of 2, is fully explained by the uncertainties in our measurements of α and the variability of the X-ray flux. To within a factor of 2, the X-ray flux in active galactic nuclei appears to be a simple extrapolation of the optical/infrared power law.

The blue and ultraviolet portions of the spectra do not extrapolate simply to the X-ray portion because they include strong fluxes from additional components, discussed above. The [3.5 μm] is correlated with the X-ray flux (Kriss, Canizares, and Ricker 1980) since both lie near a power law with a slope consistently around -1.1. The X-ray flux, which is proportional to the total ionizing flux, correlates with the Hβ flux since the latter two are closely correlated.

The power law slope we derive, $\alpha = -1.1 \pm 0.1$, is flatter than typical values of α_{ox}, which range from -1.2 to -1.6. This is because α_{ox} is usually calculated from the *total* ultraviolet flux—at 2500 Å, for example (Zamorani *et al.* 1981). As we have shown, the power law component is only a fraction of the total observed ultraviolet flux. If only the power law portion of the ultraviolet fluxes (typically $\sim 30\%$ of the total) is considered, the average α_{oxNT} found by Zamorani *et al.* is also -1.1.

The average α_{oxTOT} (uncorrected for contamination from thermal ultraviolet emission) is larger (more negative) for the more luminous quasars. This may be a consequence of the correlation we found between f_{BB}/f_{NT} and L_{TOT}. The ultraviolet fluxes of the more luminous quasars are more contaminated by thermal emission. Thus α_{oxTOT} becomes more negative, while α_{oxNT} is still -1.1 for these objects.

Zamorani *et al.* (1981) and Ku, Helfland, and Lucy (1980) found that radio-loud quasars, particularly the violently variable ones, have smaller values of α_{oxTOT} than radi-quiet quasars. We suggest this is because, at a given luminosity, radio-loud quasars have smaller f_{BB}/f_{NT} ratios than radio-quiet quasars.

BL Lacertae objects and highly polarized quasars appear to be extreme cases where $f_{NT} \gg f_{BB}$. Thus they usually have smooth, straight power law spectra. Nearly half have optical slopes between -0.9 and -1.3; only one of 40 has a flatter slope than $\alpha = -0.9$ (Angel and Stockman 1980). There is a tail of steeper slopes not present in our sample, which could be due to large starlight contributions or interstellar reddening.

The nine highly polarized quasars measured by the *Einstein* Observatory have $\alpha_{oxTOT} = -1.16 \pm 17$ (± 0.06 in the mean) (Moore and Stockman 1981). The nine BL Lacertae objects in Schwartz *et al.* (1979) have $\alpha_{oxTOT} = -1.03 \pm 0.14$ (± 0.05 in the mean). As we would expect, these objects have $\alpha_{oxTOT} \sim \alpha_{oxNT} \sim -1.1$, since the thermal contamination is negligible.

We have not proven that the optical/infrared power law extends continuously up to the X-rays. But the extrapolated power law proves to be an excellent predictor of the flux around 2 keV. At the least, the optical/infrared power law and the X-ray emission must be intimately related in most active galactic nuclei.

VII. SUMMARY

1. The bend in the spectra of Seyfert 1 galaxies and quasars from 4000 to 3600 Å is Balmer continuum emission, which is enhanced, relative to Hα, 50–150% over its Case B value.

2. In at least the five more luminous objects, there is an

additional component which flattens the spectra starting around 5500 Å, and dominates in the far-ultraviolet. Its total flux is too large to be produced by photoionization, in 3C 273 and probably Mrk 9, Mrk 79, and Mrk 335. This component is well described by a blackbody at 20,000–30,000 K.

3. All of our spectra have red/infrared power laws with slopes near −1.1. The X-ray fluxes lie near the high-frequency extrapolations of these power laws, for the objects in our sample, and for most quasars and BL Lacertae objects.

4. The ratio of blackbody to power law flux correlates with the total luminosity. This may explain why the equivalent widths of the ultraviolet, but not the optical, emission lines are anticorrelated with luminosity.

We are grateful to Drs. J. Baldwin, A. G. DeBruyn, W. Ku, J. B. Oke, R. Puetter, G. Shields, D. Weedman, and T. Williams for helpful discussions. We thank G. Rieke for supplying the dates of his infrared observations.

M. M. is supported by a Fannie and John Hertz Fellowship. W. L. W. S. thanks the National Science Foundation for support under grant AST 80-22279, and the National Aeronautics and Space Administration for support under grant NAG 5-4.

Note added in manuscript.—A recent preprint by Grandi discusses the "3000 Å bump" in quasars. He constructs "synthetic spectra" with a power law ($\alpha = -0.6$ to -0.9), Balmer and Paschen lines and continua, and Fe II lines. Although Grandi does not make a direct comparison with observations, he does show eight quasar spectra. Unfortunately, they only run from Mg II λ2798 up to Hβ or Hα. Two of his spectra (like three of our eight) appear to be fitted with just a power law and Balmer continuum. The remaining six have far more flux around 2500–3000 Å than this combination would predict. We agree with Grandi that this excess is not two-photon emission. And we agree that it is not a blackbody at a temperature of 15,000 K or less. As Grandi states, this would not produce sufficient ultraviolet flux. Grandi does not discuss the possibility that the temperature might be 20,000 or 30,000 K, and there is nothing in his paper to contradict it.

REFERENCES

Angel, J. R. P., and Stockman, H. S. 1980, *Ann. Rev. Astr. Ap.*, **18**, 321.
Baldwin, J. A., *et al.* 1978, *Nature*, **273**, 431.
Bless, R. C., and Savage, B. D. 1972, *Ap. J.*, **171**, 293.
Boggess, A., *et al.* 1979, *Ap. J. (Letters)*, **230**, L131.
Boksenberg, A., *et al.* 1978, *Nature*, **275**, 404.
Brocklehurst, M. 1971, *M.N.R.A.S.*, **153**, 471.
Burstein, D., and Heiles, C. 1978, *Ap. J.*, **225**, 40.
Canfield, R. C., and Puetter, R. 1981, *Ap. J.*, **243**, 390.
Cutri, R. M., *et al.* 1981, *Ap. J.*, **245**, 818.
DeBruyn, A. G. 1980, *Highlights of Astronomy*, **5**, 631.
DeBruyn, A. G., and Sargent, W. L. W. 1978, *A. J.*, **83**, 1257.
Drake, S. A., and Ulrich, R. K. 1980, *Ap. J. Suppl.*, **42**, 351.
Frogel, J. A., Persson, S. E., Aaronson, M., and Matthews, K. 1978, *Ap. J.*, **220**, 75.
Glass, I. 1976, *M.N.R.A.S.*, **175**, 191.
Grandi, S. A., and Phillips, M. M. 1980, *Ap. J.*, **239**, 475.
Green, R. F. 1976, *Pub. A.S.P.*, **88**, 665.
Green, R. F., Pier, J. R., Schmidt, M., Estabrook, F. B., Lane, A. L., and Wahlquist, H. D. 1980, *Ap. J.*, **239**, 483.
Huchra, J. 1977, *Ap. J. Suppl.*, **35**, 171.
Johnson, H. L. 1966, *Ann. Rev. Astr. Ap.*, **4**, 192.
Johnson, H. M. 1979, *Ap. J. (Letters)*, **230**, L137.
Koski, A. T. 1978, *Ap. J.*, **223**, 56.
Kriss, G. A., Canizares, C. R., and Ricker, G. R. 1980, *Ap. J.*, **242**, 492.
Krolik, J. H., and McKee, C. F. 1978, *Ap. J. Suppl.*, **37**, 459.
Ku, W., Helfland, D., and Lucy, L. 1980, *Nature*, **288**, 323.
Kwan, J., and Krolik, J. H. 1981, *Ap. J.*, **250**, 478.
Lacy, J., *et al.* 1982, *Ap. J.*, in press.
Moore, R. L., and Stockman, H. S. 1981, *Ap. J.*, **243**, 60.
Netzer, H., and Davidson, K. 1979, *M.N.R.A.S.*, **187**, 871.
Netzer, H., Wills, B. J., Uomoto, A. K., Rybski, P. M., and Tull, R. G. 1979, *Ap. J. (Letters)*, **232**, L155.
Neugebauer, G., Oke, J. B., Becklin, E. E., and Matthews, K. 1979, *Ap. J.*, **230**, 79.
Oke, J. B. 1969, *Pub. A.S.P.*, **81**, 11.
Oke, J. B. 1970, *Ap. J. (Letters)*, **161**, L17.
———. 1974, *Ap. J. (Letters)*, **189**, L47.
Oke, J. B., Bertola, F., and Capaccioli, M. 1981, *Ap. J.*, **243**, 453.
Oke, J. B., and Goodrich, R. 1981, *Ap. J.*, **243**, 445.
Oke, J. B., and Korycansky, D. 1981, preprint.
Oke, J. B., Readhead, A. C., and Sargent, W. L. W. 1980, *Pub. A.S.P.*, **92**, 758.
Oke, J. B., and Sargent, W. L. W. 1968, *Ap. J.*, **151**, 807.
Oke, J. B., and Zimmermann, B. A. 1979, *Ap. J. (Letters)*, **231**, L13.
Osmer, P. 1979, *Ap. J.*, **227**, 18.
Osterbrock, D. E. 1974, *Astrophysics of Gaseous Nebulae* (San Francisco: Freeman).
———. 1977, *Ap. J.*, **215**, 733.
Puetter, R. C., Smith, H. E., Willner, S. P., and Pipher, J. L. 1981, *Ap. J.*, **243**, 345.
Richstone, D. O., and Schmidt, M. 1980, *Ap. J.*, **235**, 361.
Rieke, G. H. 1978, *Ap. J.*, **226**, 550.
Rieke, G. H., and Lebofsky, M. J. 1979, *Ap. J.*, **227**, 710.
———. 1981, *Ap. J.*, **250**, 87.
Schmidt, G. D., and Miller, J. S. 1980, *Ap. J.*, **240**, 759.
Schwartz, D. A., Doxsey, R. E., Griffiths, R. E., Johnston, M. D., and Schwarz, J. 1979, *Ap. J. (Letters)*, **229**, L53.
Seaton, M. 1979, *M.N.R.A.S.*, **187**, 73P.
Shields, G. 1978, *Nature*, **272**, 706.
Soifer, B. T., Neugebauer, G., Oke, J. B., and Matthews, K. 1981, *Ap. J.*, **243**, 369.
Stein, W., Burbidge, E. M., and Smith, H. E. 1982, *Ap. J.*, in press.
Ulrich, M.-H., *et al.* 1980, *M.N.R.A.S.*, **192**, 561.
Williams, T., Morton, D., and Green, R. 1981, *A.J.*, **86**, 178.
Wu, C., Boggess, A., and Gull, T. 1980, *Ap. J.*, **242**, 14.
Wyckoff, S., Wehinger, P. A., and Gehren, T. 1981, *Ap. J.*, **247**, 750.
Yee, H. 1980, *Ap. J.*, **241**, 894.
Yee, H., and Oke, J. B. 1978, *Ap. J.*, **226**, 753.
Zamorani, G., *et al.* 1981, *Ap. J.*, **245**, 357.

MATTHEW A. MALKAN and WALLACE L. W. SARGENT: Astronomy Department, 105-24, California Institute of Technology, Pasadena, CA 91125

The Ultraviolet Excess of Luminous Quasars: II. Evidence for Massive Accretion Disks

Matthew A. Malkan

Palomar Observatory; California Institute of Technology

Received 1982 September 13

Abstract

This paper presents new infrared, optical, and ultraviolet spectra of three high-redshift quasars. They are analyzed along with three published quasar spectra. After accounting for other sources of radiation, the continua are fitted with spectra predicted for optically thick steady-state accretion disks which include the effects of general relativity. The two fitting parameters, the mass of the accreting black hole and the accretion rate, are determined by the data with a formal accuracy of 20%. The masses range from 0.2—0.5 billion $M_\odot$ for 3C 273 and PKS 0405-123, to 1—3 billion $M_\odot$ for the high-redshift quasars. The values depend on the assumed disk inclination and the angular momentum of the hole. The high luminosities of these six quasars are all within a factor of two of their Eddington limits, and this conclusion is not extremely sensitive to the modelling assumptions.

I. Introduction

Malkan and Sargent (1982, Paper I) showed that the ultraviolet excess in Seyfert 1 galaxies and quasars can be fitted by a blackbody with a temperature of 23—30,000 °K. They argued that it is optically thick thermal emission (see also Shields 1978 and Ulrich 1981). Since the total thermal flux can exceed the available ionizing flux, it is probably produced by accreting optically thick gas, perhaps in a disk.

The best observed object in Paper I was 3C 273. Its International Ultraviolet Explorer (IUE) spectrum goes down to a rest wavelength of 1100Å. Since this is not much bluer than the maximum in the thermal component, its high-frequency spectrum was not well-determined. In this work three high-redshift quasars were observed with the I.U.E. to measure their spectra down to a rest wavelength of 800Å. These observations determine the high-frequency portion of the thermal emission more accurately, for a comparison with the expected emission from optically thick accretion disks.

II. Observations

Table 1 summarizes the observations used in this paper. Three quasars were observed with the LWR camera of the I.U.E. for about seven hours each in June 1981. The two dimensional data were geometrically corrected at Goddard Space Flight Center.

One-dimensional spectra were then extracted by summing the five diagonal lines parallel to the dispersion, which include essentially all of the signal.

Absolute optical spectrophotometry was obtained with the multi-channel spectrometer on the Hale 5 meter telescope and the SIT spectrograph on the 1.5 meter telescope at Palomar. The quasars were each observed three times from the ground, from May--Nov 1981. There was no evidence that any of the optical spectra varied by more than 10% during this period. Table 2 lists the absolute fluxes for bins approximately 200Å wide. The uncertainties are generally 4 or 5%, but twice as large for the ultraviolet points. The emission line fluxes listed in Table 2 are less accurate, because of the uncertainty in separating the broad line wings from the continuum.

Near-infrared photometry was obtained for 1421+330 (z_{em}=1.90) on the Hooker 2.5 meter telescope, and for 1435+638 (z_{em}=2.06) by Neugebauer and Soiffer (private communication) on the 5 meter telescope in July 1981. Neugebauer et al.'s (1983) infrared magnitudes for 0302-223 (z_{em}=1.41) in February 1980 were too faint to be consistent with the optical observations, and there is no obvious explanation for the discrepancy. In the fits to the spectrum these infrared points were raised by 0.25 dex and assigned low weights.

In February 1981 the Einstein Observatory IPC detector observed 1435+638 for 4400 seconds. The 3 Kev X-ray flux was .065±.010 μJy. QSO 0302-223, first discovered by its X-ray emission, has the same IPC count rate, and therefore about the same flux (Chanan et al. 1981). The following analysis includes published observations of the quasars PKS 0405-123 (z_{em}=0.57) (Green et al. 1980, Allen and Hyland 1982, Neugebauer et al. 1979) and Ton 490=QSO 1011+250 (z_{em}=1.64) (Gondhalekar and Wilson 1980, Capps et al. 1982, Oke private communication) and 3C 273, from Paper I, with the new infrared photometry of Cutri et al. (1981).

The absence of a strong continuum dip around 2175Å$(1+z_{em})$ indicated quite small reddenings at the quasar redshifts, and the adopted E_{B-V}'s listed in Table 1 are almost negligible. There should not be significant reddening at zero-redshift from the Milky Way, since all six quasars are at high galactic latitudes.

All the continuum fluxes below the Lyα emission line were statistically corrected for blanketing from the weak unresolved absorption lines, mostly due to Lyα (Sargent et al. 1980). The total rest frame absorption measured by Young et al. (1982) from all lines above their detection threshold of 0.32Å is 17Å per Δz=1 at z_{abs}=1.8. This corresponds to a blanketing correction of about 3%, which has been applied to all continuum points in Table 1 below a rest wavelength of 1216Å.

All three spectra are cut off at the shortest wavelengths by optically thick Lyman continuum absorptions, with redshifts given in Table 1. These systems have Lyman absorption lines which are strong enough (~5Å equivalent width) to be seen in the IUE data. In some cases the C IV doublet has been detected in the optical spectrum. The absorption systems will be discussed in another paper.

Between $(1+z_{em})912$Å and the wavelength of the optically thick Lyman edge there may be weak Lyman limit absorptions from HI systems with optical depths around a tenth. They would not be detectable in the low signal-to-noise IUE spectra, but they would depress the apparent continuum level. 1421+330 should have three or four absorption systems with Lyα rest equivalent widths greater than 0.6Å and Lyman limits between 2650 and 2180 Å. Their inferred HI column densities depend critically on the velocity dispersion parameter σ ($f(v)=\exp(-(v-v_0)^2/2\sigma^2)$). A Lyα equivalent width of 0.6Å is produced, for example, by an HI column of 4×10^{14} cm^{-2} with σ=35 km/sec or an HI column of 4×10^{15} cm^{-2} with σ=23. If σ is as low as 19, the Lyman limit optical depth is 0.1. The following analysis treats continuum points below the Lyman edge as lower limits, since the flux may have been depressed by these weak continuum absorptions.

III. The Thermal Continuum

(a) Single-temperature blackbody

All the spectra show the same broad downward curvature over rest wavelengths of 7000 to 912 Å, sometimes referred to as the "3000 Å bump". This feature is seen in the spectra of virtually all bright Seyfert 1 galaxies and quasars (Soiffer et al. 1983) and constitutes the evidence for optically thick thermal emission. It can be fitted as in Paper I. As before, a power-law drawn through the red and infrared points is extrapolated to higher frequencies. Since its slope is always near -1.1, it makes a negligible contribution to the blue and ultraviolet regions of the spectrum. The thermal ultraviolet flux is described by a hot blackbody, whose size and temperature are free parameters. Hydrogen Balmer and Fe II emission lines and bound-free and free-free continua are also included in the fits, since the observations did not resolve them. The Fe II and H fluxes were scaled to the Hα flux using Grandi's (1981) empirical line ratios. The estimation of Hα fluxes is discussed below.

The power-law + single-temperature blackbody fits are shown by the dashed lines in Figure 1. The parameters for each fit are given in Table 2. The average blackbody temperature is $27{,}000 \pm 1000$, as in Paper I. The high-redshift quasars have the same ratio of thermal to non-thermal flux as the Seyfert 1

galaxies Mrk 335 and 509 (Paper I). 3C 273 has a significantly larger ratio than any of the other active galactic nuclei studied so far. The correlation of this ratio with luminosity suggested in Paper I does not extend to the high luminosity quasars studied here.

If the red continuum at wavelengths much beyond Hα is not observed (as in 1421+330 and 1435+638), it is possible to fit the spectra with a power-law as flat as $\alpha=-0.7$, and a weaker thermal component. But in all cases where the flux is observed at a rest wavelength of 1μm, it is too large to be consistent with such a flat power-law. There is no reason to suspect that the near-infrared continua of 1421+330 and 1435+638 are dramatically different from the observed ones in lower redshift quasars. So we have assumed their power-law slopes are also around -1.0. This can be confirmed by sensitive observations at 10μm.

The fits to all six quasar spectra were improved significantly by the inclusion of Balmer continuum emission. As its shape was not well-determined, we assumed it was optically thin at 15,000 K (Paper I). The Balmer continuum fluxes for the high-redshift quasars could be substantially less than the estimates listed in Table 2, but cannot exceed them by more than 25%. If we assume the Hα flux is two thirds the observed Lyα flux or 2.5 times the C IV λ1549 emission (Lacy et al. 1982; Baldwin 1977), the estimated Balmer continuum/Hα ratios are

around 3, comparable to those in Paper I.

(b) Accretion disk spectra

The single-temperature blackbody fits tend to have too little flux at the highest and lowest frequencies. In other words, the ultraviolet excess flux actually has a broader spectral distribution than a single Planck function. The discrepancy between observation and fit is even larger when the possible absorption below the Lyman limit is considered.

To improve the fits, the Planck function was replaced with a thermal component containing a range of temperatures. The thermal emission was described by a physical model, viz: an optically thick steady-state accretion disk. The radial structure equations of Novikov and Thorne (1973) and Page and Thorne (1974) for relativistic accretion disks were used. The disk is assumed to be sufficiently geometrically thin and optically thick that its surface flux is emitted as a blackbody. The local temperature is simply $(F(r)/\sigma)^{1/4}$, where σ is Stefan's constant.

Spectra for accretion disks around non-rotating (Schwarzschild) black holes, and rapidly rotating (Kerr) holes with a dimensionless angular momentum-to-mass ratio of 0.998 were calculated. The latter case is more realistic, since the accreting matter quickly spins a black hole up to this value

(Thorne 1974). The disk around a Schwarzschild hole extends in to a radius of 6 r_* ($r_* \equiv GM_{bh}/c^2$), yielding a luminosity efficiency ε ($L_{emitted} = \varepsilon \dot{M} c^2$) of 0.057. Since the disk around the Kerr hole extends in to 1.23 r_*, it is about five times more efficient.

Like the single-temperature blackbody, the optically thick accretion disk spectrum has only two fitting parameters: the mass of the central accreting object, and the mass accretion rate. These two parameters specify the run of temperature with radius. The resulting thermal spectrum has an exponential high-frequency turnover not quite as sharp as that of a Planck function. However, at low frequencies it has $f_\nu \propto \nu^{1/3}$, and there is a broad transition region of two octaves in frequency where the spectrum is flat.

The light emitted locally from the inner regions of the disk is modified by general relativistic redshift and focusing. Especially for the Kerr hole disk, the predicted emergent spectrum is much redder than the one emitted at the disk surface. We included these effects using the calculations of Cunningham (1975). The disk spectrum was numerically integrated out to 800 times the inner radius, which included more than 99.9% of the total disk luminosity.

The model accretion disks have the same temperature distributions as those given in Thorne's (1974) Figures 1 and 2. It was also confirmed that the total observed disk luminosities, after corrections for general relativistic redshift and focusing agreed with those given by Cunningham in his Figure 9.

The accretion disk fits to the data are shown by the solid lines in Figures 1a and 1b. Each line actually represents two fits—one for a Schwarzschild hole and one for a Kerr hole--which are indistinguishable over this wavelength range. (This happens because the spectrum of a disk around a Schwarzshild hole looks very similar to that of a disk around a Kerr hole with two or three times the mass). The broader accretion-disk spectra fit the data significantly better than a single-temperature blackbody, although the number of fitting parameters is still the same. For a given set of assumptions, both M and $\dot{M}$ are independently determined to within 20%. The uncertainties for the two low-redshift quasars, which were not observed to such high rest frequencies, are twice as large.

The results are not sensitive to small errors in the data. They are more sensitive to some of the modelling assumptions:

1) When the luminosity distance of a quasar was increased by 70%, the derived $\dot{M}$ almost tripled, to produce the larger luminosity. But the hole mass also more than doubled, to

maintain nearly the same temperature distribution in the disk, scaled to three times larger radii.

2) The spectrum of a disk around a Schwarschild hole depends little on the observer's inclination angle θ(Cunningham 1975). If the disk is not pointed directly at the Earth, the effect is the same as increasing the luminosity distance: both M and $\dot{M}$ increase by $\sim 1/\cos\theta$. For the rapidly rotating hole the observed spectrum becomes harder as the disk is seen at a higher inclinations. If the disk were highly inclined, the fits to the data would have given up to 100% larger hole masses. However, in this case the total flux from the disk is insensitive to inclination, so the accretion rates would hardly change.

3) In the inner regions of the disk the locally emitted spectrum may deviate from the assumed blackbody shape. Exact calculation of these deviations requires knowledge of the vertical structure of the disk, which depends on the viscosity. In the "α-disks" described by Shakura and Sunyaev (1973) and others, α is the constant of proportionality between viscosity and total pressure. At small radii, the electron-scattering opacity dominates the free-free opacity. Especially when α is near its maximum value of 1, emerging photons are redistributed to higher frequencies (Shakura and Sunyaev 1973).

Also the electron-scattering optical depth of a disk with α=1 may drop below 1, and its inner regions may be geometrically thick. The minimum optically thick radius is around 10 to 100 r_*/α at the critical mass accretion rate (Novikov and Thorne 1973). If the disk emission which must escape locally is not thermalized, much of it leaves at high frequencies, producing a stronger high-frequency tail in the disk spectrum than the optically thick model predicts.

In either case, the local spectrum is harder than the Planck spectrum for the given effective temperature. This is equivalent to tilting the Kerr disks: the estimated mass of the black hole would increase, without any change in the accretion rate. The effects of inclination and electron-scattering opacity may have caused us to systematically underestimate the black hole masses. They are most likely to be important at radii less than 10 or 20 r_*. The illustration of the Kerr accretion disk fit to 0405-123 in Figure 2 shows that the "inner" region of the disk ($r<20r_*$) only contributes at the highest observed frequencies. Thus a more realistic disk model could perhaps double the estimates of M_{bh} in Table 2, without changing $\dot{M}$.

If the accretion disk hypothesis is correct, the estimated mass accretion rates should not greatly exceed the Eddington limit: $L/L_{Edd} = 4.5 \times 10^8 \, \varepsilon \, \dot{M}/M_{bh} \leq 1$ for pure hydrogen gas with $\dot{M}$ and M_{bh} in solar units. The L/L_{Edd} ratios estimated from the

spectroscopic fitting are listed in the final columns of Table 2. It is probably not a coincidence that the six high-luminosity quasars in this study are emitting energy at approximately their Eddington limits. Evidently the luminosity of a bright quasar is set by the mass of its black hole. Radiation pressure then regulates the accretion rate to keep the luminosity near the Eddington limit. Like many previous studies, this one found no difference between the radio-quiet quasars (1E 0302-223 and Mrk 679) and the radio-loud ones.

(c) Other Observational Tests

The spectroscopic evidence discussed above argues strongly that the ultraviolet excess in quasars, which accounts for roughly half their total luminosity, is thermal emission from gas in a disk accreting onto a massive central object. Three other independent observations also support this conclusion:

a) Time Variability. Figure 2 shows that little near-ultraviolet flux in 0405-123 comes from within 3×10^{15} cm of the hole. The usual light-travel time argument implies that this quasar should not change its ultraviolet brightness in less than a day. However, gas at this radius takes more than a month to complete one orbit. Since the radial drift velocity must be less than the orbital velocity, the thermal emission hypothesis could not explain ultraviolet variability with a time-scale less than half a year. For a given local disk temperature, the

orbital time is proportional to the square root of the accretion rate. This variability restriction would apply to all bright quasars.

The most recent literature search (Moore 1983) lists 15 high-redshift quasars with blue luminosities exceeding 3×10^{31} erg $sec^{-1}Hz^{-1}$ which have been carefully monitored for optical variability. (This disregards BL Lac objects, since their steep, polarized continua are predominantly non-thermal). The measurements were made photographically, with standard errors of 0.08--0.15 mag. To this accuracy, none of these 15 quasars showed any significant optical variability on time-scales of weeks to many years. For disks with an α viscosity law, detection of long-term variability in the ultraviolet continuum would set a lower limit on α.

b) Polarization. The optical continuum in luminous high-redshift quasars is always observed to have a very low linear polarization. The polarizations in 25 high-luminosity quasars measured by Stockman (1978) range from 0 to 0.5%, and could be produced entirely by aligned interstellar dust grains in the Milky Way and the host galaxy in which the quasar resides. The thermal accretion disk spectrum is not expected to have significant intrinsic polarization, a prediction entirely consistent with the large body of high-quality observations presently available.

c) Lyman Jump. Most of the 912Å flux comes from the portion of the disk at T~40,000 K. In this region of an α-disk, the electron-scattering opacity dominates the Lyman continuum (bound-free) opacity (Novikov and Thorne 1973). The typical surface gravity is log g~1--3, as in extreme B supergiants. Stellar atmosphere calculations (Kurucz 1979) suggest there will be little neutral hydrogen to produce a Lyman jump in absorption. And the large range of gravitational and Doppler redshifts will smear out the weak one which might be present. Thus one would not expect to see much of a Lyman jump in emission or absorption from the accretion disk, and none is observed (Oke and Korycansky 1982; Smith et al 1981).

The accretion disk must have an outer radius which will cause the spectrum to steepen into a Jeans law ($f_\nu \propto \nu^2$) below $\nu_{Jeans} \sim kT_{outer}/h \sim 8 \times 10^{13}\ M_9^{1/2}\ (r_{outer}/1000\ r_*)^{-3/4}$ Hz. This is why the disk spectrum in Figure 2 is extrapolated into the infrared with a dashed line. The surface gravity in the disk drops with the cube of the radius. At radii larger than a few thousand r_*, the disk surface can be significantly heated by reabsorption of the external radiation field produced at smaller radii (Shakura and Sunyaev 1973). Thus the outermost parts of the disk are probably unstable. This probably occurs around $r \sim 10^{3--4}\ r_*$, which is also the characteristic radius of the broad-emission-line region in quasars.

IV. Ionizing Continuum

The power-law flux densities at 5500Å are 2000 to 3000 times those at 2 Kev. This is the same ratio found in Paper I, and corresponds to an extrapolation from optical to X-ray frequencies with $f_\nu \propto \nu^{-1.1}$ to -1.2. This confirms the suggestion of Paper I that the X-ray emission is closely related to the non-thermal power-law, but not necessarily to the thermal ultraviolet component.

Beyond the Lyman limit, the blackbody used in Paper I falls significantly below the accretion disk spectrum. Thus the accretion disk, rather than the non-thermal power-law, is the dominant source of ionizing photons with energies between 13.6 and 50 ev. If the power-law extends with the same slope from optical wavlengths into the soft X-ray region, it would re-emerge (become as bright as the accretion disk) around 250—350Å. But the "power-law" need not extend much above optical frequencies. It already shows some mild downward curvature around 1--3μm in the spectra of 3C 273, and most of the Seyfert 1 galaxies in Paper I. If this curvature of the non-thermal continuum continues to higher frequencies, as it does in many BL Lac objects for example, its total energy could be relatively minor. Until the <u>intrinsic</u> quasar continuum has been observed at 200--300Å, substantial uncertainty about the shape of the ionizing continuum will remain. And the ionizing spectrum in a

single quasar is probably softer for emission-line clouds above the disk poles than for gas near the disk equator.

Paper I showed that the thermal ultraviolet component is much weaker (and may not be present at all) in the fainter Seyfert 1 galaxies. Yet they may still have substantial thermal emission from accretion disks which are smaller and hotter than those discussed above. If the faint Seyfert 1's also accrete at nearly their Eddington limits, most of their thermal emission would emerge in the unobserved far-ultraviolet to soft X-ray region. Alternatively, they could be accreting at well below the Eddington limit if their accretion disks were too optically thin to emit as blackbodies. As discussed above, the flux would again be shifted to higher frequencies. In either case the accretion rate would be two orders of magnitude less than those in Table 2, so that the thermal emission could vary in weeks to months. The harder ionizing spectrum in the Seyfert 1 galaxies could also lead to spectroscopic differences from quasars, such as their larger C IV/C III] emission-line ratios, although there are other possible explanations (Wu et al. 1982).

V. Conclusions

This paper presented spectrophotometric data with sufficient wavelength coverage to make an accurate measure of the thermal ultraviolet continuum in bright quasars. In all six cases it is

very well described by simple optically thick accretion disk models. The black hole masses were measured spectroscopically, on the simplifying assumption that the disks are optically thick and geometrically thin. The mass accretion rates in bright quasars are always near their Eddington limits, regardless of the accretion disk details.

It is a pleasure to thank Skip Staples, Bob Griffith, Juan Carrasco, Dan Harris, and the I.U.E. staff for help with observations, Bohdan Pacyzinski and W.L.W. Sargent for helpful discussions, G. Neugebauer and T. Soiffer for communication of unpublished infrared photometry, and the Fannie and John Hertz Foundation for financial support. W.L.W.S. and M.M. acknowledge support from NASA grants NG 5-4 and NG 8406.

TABLE 1

JOURNAL OF OBSERVATIONS

Quasar	0302-223	0405-123	1011+250	1226+023	1421+330	1435+638
UV	10 Jun 81	7 Dec 78	20 Nov 78	Aug 78	9 Jun 81	10 Jun 81
Optical						
1.5m+SIT	31 Oct 81				4 Jul 81	28 May 81
1.5m+SIT	23 Nov 81				27 Jul 81	28 Jul 81
5m+MCSP	22 Aug 81	Dec 76	1 Jun 79	16 Feb 75	22 Aug 81	22 Aug 81
IR	Feb 81	Feb 77	5 Mar 81	Mar77-Dec78	7 May 81	Jun 81
X-ray						Feb 81
E_{B-V}	.05	.03	.03	.03	.02	.03

TABLE 2

LINE AND CONTINUUM DATA

LOG CONTINUUM FLUX DENSITIES (mJy=10^{-26} erg $cm^{-2}sec^{-1}Hz^{-1}$)

Log ν (Hz)	0302-223	1421+330	1435+638
15.122	-0.45	-0.69	
15.110	-0.47	-0.59	
15.100	-0.46	-0.50	
15.089	-0.41	-0.45	
15.073	-0.33	-0.46	
15.062	-0.28	-0.38	
15.050	-0.23	-0.32	-0.65
15.036	-0.19	-0.29	-0.53
15.024	-0.16	-0.26	-0.41
15.010		-0.23	-0.40
14.993		-0.20	-0.37
14.985	-0.13	-0.14	
14.974		-0.12	
14.965	-0.11	-0.13	-0.33
14.949	-0.10	-0.14	-0.33
14.933	-0.09		-0.29
14.924	-0.09		
14.900		-0.08	
14.880		-0.07	-0.22
14.869	-0.08		-0.21

14.856		-0.06	-0.21
14.843	-0.06	-0.05	
14.831	-0.04		-0.19
14.820			-0.18
14.794	-0.04		
14.781			-0.13
14.772	-0.03	0.03	
14.762	-0.04	0.04	-0.13
14.748	-0.03	0.03	-0.14
14.735	0.00		-0.13
14.720	0.01	0.04	-0.13
14.710	0.04	0.06	
14.699	0.06	0.07	-0.14
14.686	0.08	0.08	-0.14
14.677		0.09	-0.12
14.669	0.10	0.10	-0.11
14.660		0.10	-0.12
14.647	0.12	0.12	-0.12
14.638		0.15	-0.08
14.626		0.15	-0.10
14.615	0.13	0.16	-0.10
14.597	0.14	0.19	
14.582		0.17	
14.574	0.14	0.21	0.00
14.552	0.15	0.19	0.00

14.535	0.09	0.16	
14.518	0.16	0.18	
14.502	0.16		
14.490	0.11	0.18	0.02
14.473		0.20	
14.455	0.20	0.20	
14.380	0.08	0.24	0.03
14.260	0.39	0.22	0.06
14.130	0.32	0.29	0.13

Line	Flux/10^{-14} erg $cm^{-2}sec^{-1}$		
Lyα	30	23	
C IV	9	7	6
C III]	6	4	2.5
Mg II			6
z_{em}	1.41	1.90	2.06
z_{abs}	1.29	1.46	1.92

TABLE 3

MODEL-FITTING RESULTS

QSO	z	Balmer Cont.	Power-Law[a]		Blackbody	M_{bh}	$\dot{M}$	$\frac{L}{L_{Edd}}$
		Hα	α	fy_o[b]	fy_o[b]	Temp.	$10^9 M_\odot$	$M_\odot$/yr	
1435+638	2.06	2.5	-1.0	.28	.06	28,000	0.9	53.	1.5
							2.1	19.	1.2
1421+330	1.90	3.2	-0.9	.41	.09	25,000	1.5	54.	0.9
							3.6	21.	0.8
1011+250	1.64	3.3	-1.1	.27	.07	28,000	1.2	21.	0.45
							2.4	8.	0.45
0302-223	1.41	2.9	-1.0	.57	.16	27,000	0.75	35.	1.2
							1.8	14.	1.0
0405-123	0.57	3.0	-1.1	1.6	.54	30,000	0.18	19.	2.7
							0.50	7.	1.9
1226+023	0.16	3.4	-1.1	13.	10.	26,000	0.17	12.	1.8
							0.51	4.	1.1
Uncertainty		±25%	±0.2	±10%	±1000	±20%	±15%		

[a] These are the power-laws found in the blackbody fits. When the blackbody was replaced with an accretion disk spectrum, the best-fitting power-law slopes were 0.1 to 0.2 steeper, and the power-law fluxes dropped 20 to 40%, to compensate for the additional red flux from the outer regions of the disk.

[b] All Flux Densities in MilliJanskies (10^{-26} erg $cm^{-2}sec^{-2}Hz^{-2}$)

REFERENCES

Allen, D. A. and Hyland, A. R. 1982, M. N. R. A. S. 199,

Baldwin, J. A. 1977, M. N. R. A. S, 178, 67P.

Capps, R. W., Sitko, M. L., and Stein, W. A. 1982, Ap. J. 255, 413.

Chanan, G. A., Margon, B., Downes, R. A. 1981, Ap. J. Lett. 243, L5.

Cunningham, C. T. 1975, Ap. J. 202, 788.

Cutri, R. M. et al. 1981, Ap. J. 245, 818.

Gondhalekar, P. M. and Wilson, R. 1980, Proc. of Second European IUE Conference (ESA SP-157), p. 176.

Grandi, S. A. 1981, Ap. J. 251, 451.

Green, R. F. et al. 1980, Ap. J. 239, 483.

Kurucz, R. L. 1979, Ap. J. Suppl. 40, 1.

Lacy, J. H. et al. 1982, Ap. J. 256, 75.

Malkan, M. A. and Sargent, W. L. W. 1982, Ap. J., 254, 22. (Paper I)

Moore, R. L. 1983, Ap. J., in press.

Neugebauer, G., Oke, J. B., Becklin, E. E. and Matthews, K. 1979, Ap. J. 230, 79.

Neugebauer, G. et al. 1983, A. J., in press.

Novikov, I. D. and Thorne, K. S. 1973, in Black Holes, eds. C. DeWitt and B. DeWitt (New York: Gordon β Breach), p. 343-450.

Oke, J. B. and Korycansky, 1982, Ap. J. 255, 11.

Page, D. N. and Thorne, K. S. 1974, Ap. J. 191, 499.

Sargent, W. L. W., Young, P. J., Boksenberg, A., Tytler, D. 1980, Ap. J. Suppl. 42, 41.

Shakura, N. I. and Sunyaev, R. A. 1973, Astr. and Ap. 24, 337.

Shields, G. A. 1978, Nature, 272, 706.

Smith, M. G. et al., 1981, M. N. R. A. S. 195, 437.

Soiffer, T. B. et al., 1983, Ap. J., in press.

Stockman, H. S. 1978, Proc. Pittsburgh Conf. on BL Lac Objects, ed. A Wolfe, Univ. Pittsburgh Press, p. 149.

Thorne, K. S., 1974, Ap. J. 191, 507.

Ulrich, M. H. 1981, Space Science Reviews 28, 89.

Wu, C. C., Boggess, A., Gull, T. R. 1982, Ap. J., in press.

Young, P. J., Sargent, W. L., Boksenberg, A. 1982, Ap. J. 252, 10.

Figure 1. The spectra of the three newly observed quasars. The vertical error bars represent the flux densities in Table 1. The dashed lines are the fits with a power-law and a blackbody. The solid lines, which match the data better, are the fits with an accretion disk spectrum replacing the blackbody. Each solid line represents two indistinguishable disk models--one around a Schwarzschild hole and one around a Kerr hole. When the mass of the Kerr hole is reduced by 25%, the resulting accretion disk fit for 0302-223 is represented by the long-dash line. It has too much flux at high frequencies to agree with the observations.

Figure 1b. Previously published quasar spectra, and their fits are plotted, as in Figure 1a. As before, the large vertical bar on the left represents $\Delta \log f_\nu = 0.5$.

Figure 2. The spectrum of PKS 0405-123 ($z_{em}=0.57$) is re-plotted, along with the model of an accretion disk around a rapidly rotating black hole. The "inner" portion of the disk runs from the inner radius of $1.23\ r_* = 8 \times 10^{13}$ cm, to $20\ r_* = 1.3 \times 10^{15}$ cm. The "middle" portion runs from $20\ r_*$ to $100\ r_*$, and the "outer" portion extends to $1000\ r_*$. The "inner" region is the most likely part of the disk to have a local spectrum which is harder than that of a blackbody. Fortunately it only contributes to the observed flux at the highest frequencies. The low-frequency portion of the disk spectrum must steepen to a Jeans law ($\alpha=+2$) beyond the peak frequency of the emission from the outer edge of the disk.

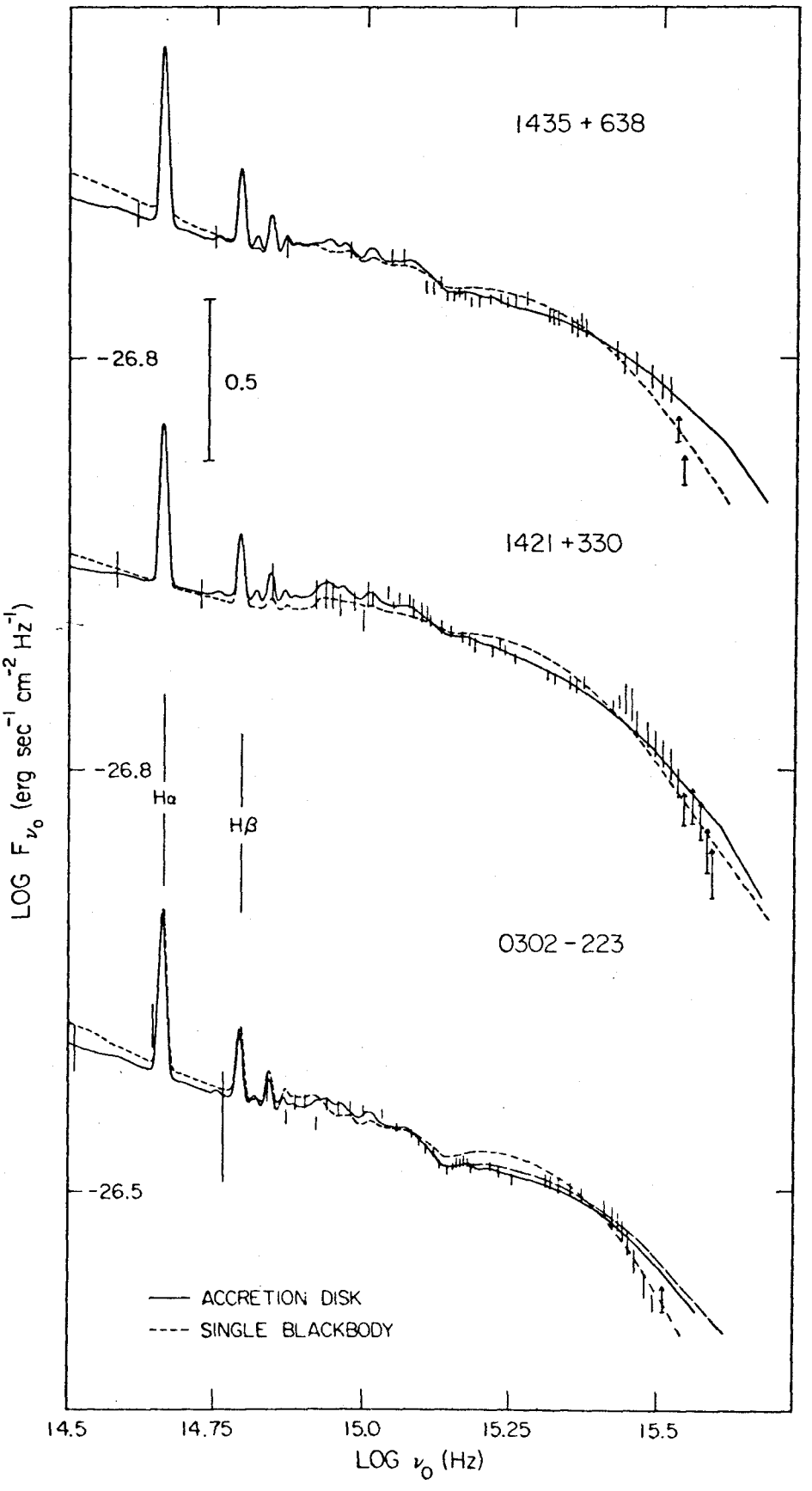
1435 + 638
-26.8
0.5
1421 +330
-26.8
Hα
Hβ
0302 - 223
-26.5
ACCRETION DISK
SINGLE BLACKBODY
LOG F_{ν_0} (erg sec^{-1} cm^{-2} Hz^{-1})
14.5
14.75
15.0
15.25
15.5
LOG ν_0 (Hz)

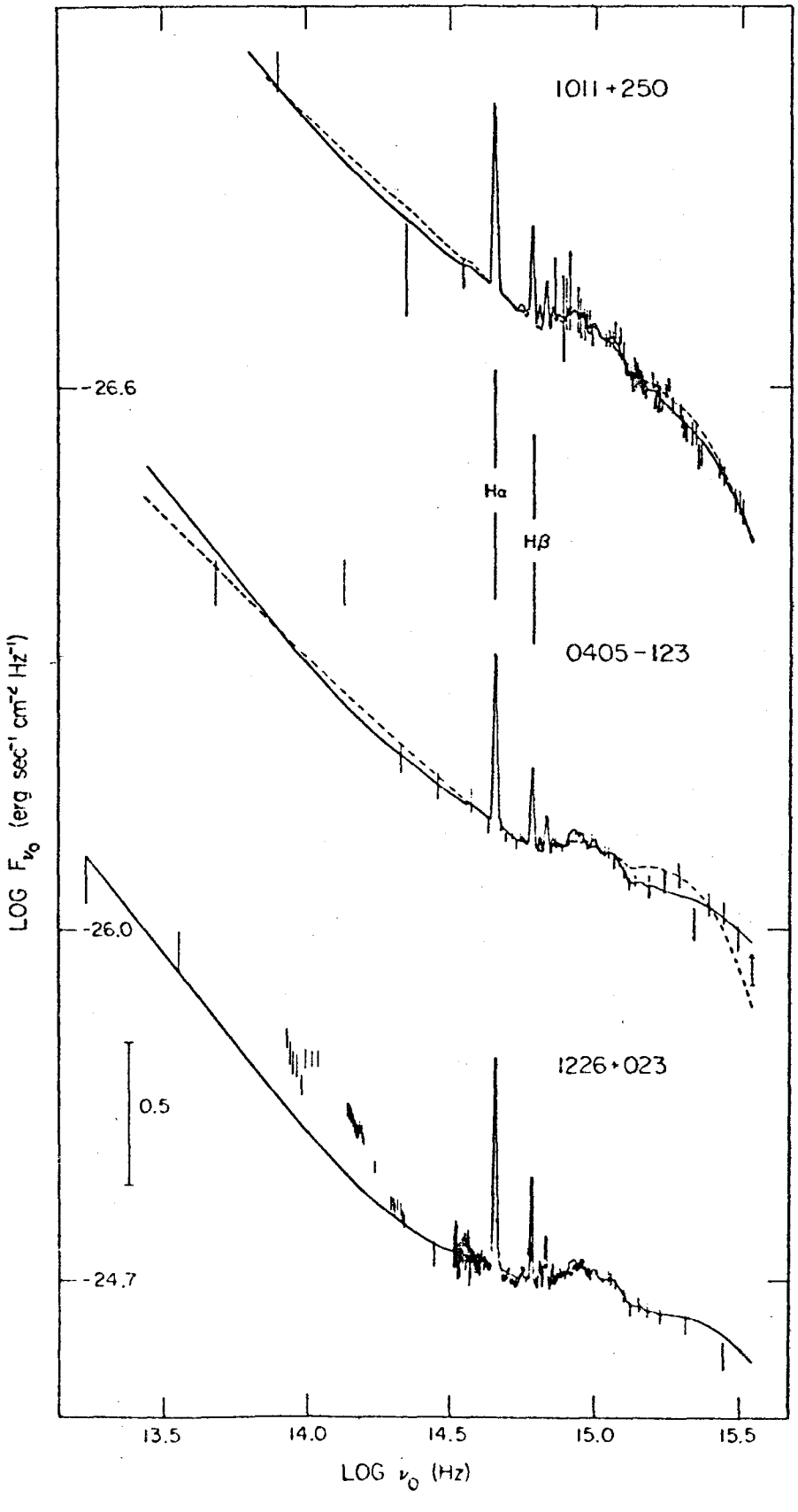
1011+250
-26.6
Hα
Hβ
0405-123
-26.0
1226+023
0.5
-24.7
13.5
14.0
14.5
15.0
15.5
LOG ν_0 (Hz)
LOG F_{ν_0} (erg sec^{-1} cm^{-2} Hz^{-1})

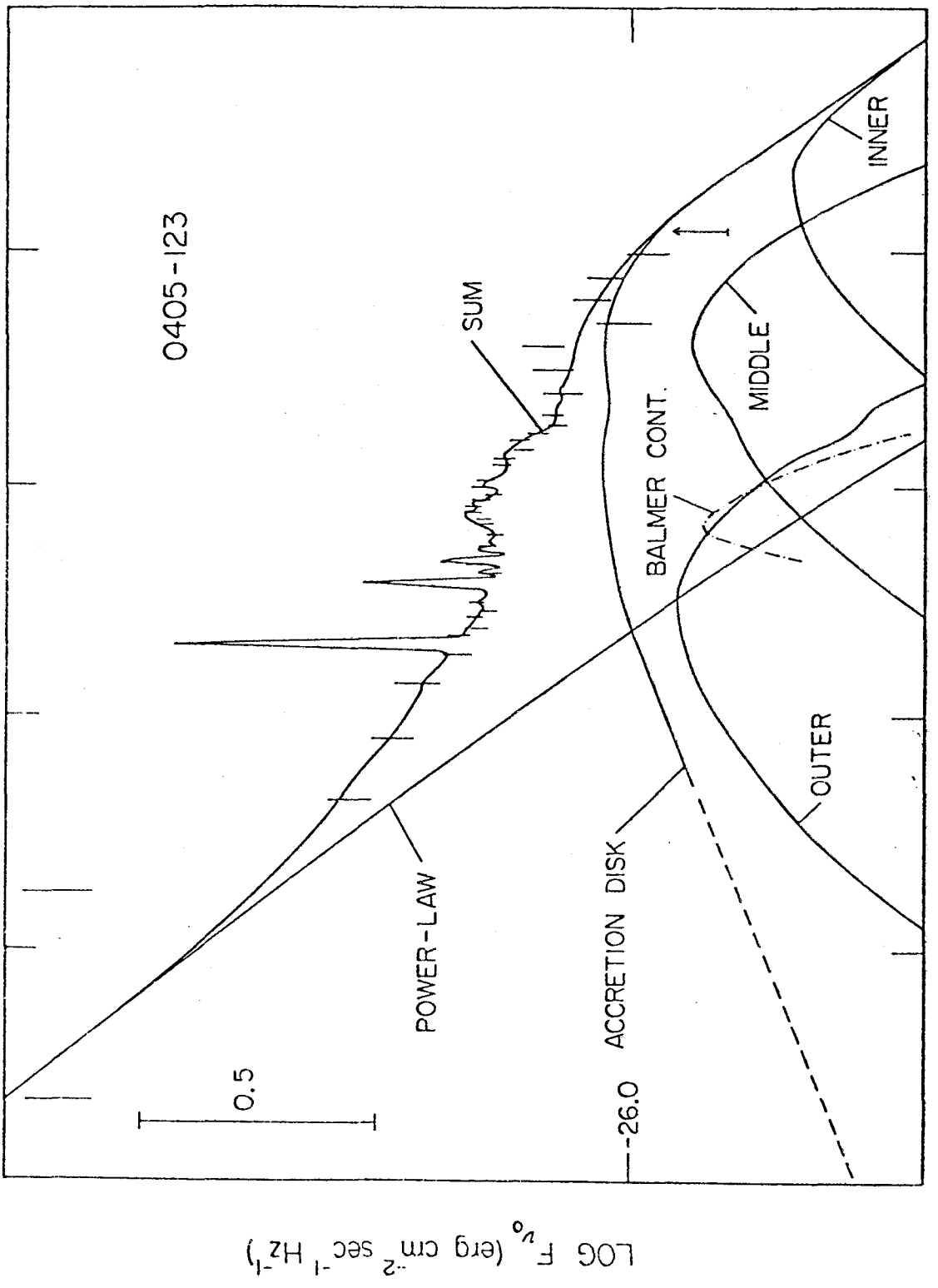
0405-123
SUM
POWER-LAW
ACCRETION DISK
BALMER CONT.
MIDDLE
INNER
OUTER
0.5
-26.0
13.5
14.0
14.5
15.0
15.5
LOG ν_0 (Hz)
LOG F_{ν_0} (erg cm^{-2} sec^{-1} Hz^{-1})

THE STELLAR AND NONSTELLAR CONTINUA OF SEYFERT GALAXIES: NONTHERMAL EMISSION IN THE NEAR-INFRARED

Matthew A. Malkan and Alexei V. Filippenko

Palomar Observatory, California Institute of Technology

Running title: Stellar and Nonstellar Continua of AGN

Submitted to The Astrophysical Journal

Received: 1983 March 24

ABSTRACT

Spectra having high resolution and excellent signal-to-noise ratios have been obtained for the nuclei of 9 Seyfert galaxies. In Seyfert 1 nuclei the Mg I 5175 Å, Na I D 5892 Å, and Ca II 8542 Å stellar absorption lines are extremely weak, indicating that galactic starlight does not contribute a significant fraction of the observed continuum. The relative amount of light (in a given aperture) due to the unresolved nucleus of each galaxy has been measured from direct images of these galaxies with a Silicon Intensified Target (SIT). Knowing the fraction of nuclear light which comes from stars, we deduced the total stellar and nonstellar continuum fluxes in the spectral range $\lambda\lambda$ 5000 -- 8600 Å. Within a 10" aperture stars contribute a sixth or less of the visual continuum in Mkn 335 and Mkn 509, a quarter to two-fifths of that in NGC 4151, 5548, and 7469, and three-fifths of that in NGC 1275, 3227, and 4051. These fractions are accurate to 10 -- 15%. The starlight has colors which are typical of those in the disks of normal spiral galaxies. The nonstellar continuum is similar to that of quasars -- it drops from the near-infrared to the visual like a power-law with slope $\alpha \sim -1.1$ to -1.2, and in the brighter spectra it flattens in the blue. Even at minimum brightness, the nonstellar flux has no short-wavelength cutoff near 1 μm, eliminating the possibility that the near-infrared flux is dominated by thermal emission from hot dust grains.

In an appendix, we report several weak emission lines that have not been previously seen in the spectra of active galactic nuclei. Some interesting characteristics of the broad permitted lines, as well as differences in the widths of various forbidden lines, are also mentioned.

Subject headings: galaxies:nuclei -- galaxies:Seyfert --
galaxies:stellar content -- spectrophotometry

I. Introduction

Nearby Seyfert galaxies have been extensively investigated because they are bright and easy to observe. Their relatively faint nonstellar continuum is more difficult to study, however, due to substantial contamination from starlight. In particular, the spectral shape of the nonstellar continuum has not been unambiguously measured in any low-luminosity Seyfert galaxy; rather, many workers have simply assumed that it is similar to that of luminous quasars.

Direct imaging cannot in itself determine the galactic contribution, since much of the starlight may lie within the seeing disk and is inseparable from the point-like (unresolved) nonstellar light. Nor is low-resolution spectrophotometry of the continuum adequate, as it cannot distinguish a large stellar component with a weak blue nonstellar continuum from a smaller stellar component with a strong red nonstellar continuum (Malkan and Oke 1983). The most effective spectroscopic indicators of a stellar population are prominent absorption lines such as the G band (λ4304 Å), the Mg I b triplet (λ5167, λ5173, λ5184 Å), and the Ca II near-infrared triplet (λ8498, λ8542, λ8662 Å). These lines are presumably absent in any nonstellar continuum, and their strengths in normal galaxies are well known. The strong Na I D (λ5890, λ5896 Å) and Ca II H (λ3968 Å) and K (λ3934 Å) lines can also be useful, but they may be contaminated by interstellar absorption in the host galaxy

(Osterbrock 1978, 1983).

Osterbrock (1978, 1983) gave estimates or upper limits to the starlight components of many Seyfert 1 spectra from the strength of the Ca II K line. However, the slit size was small (2."7 x 4."0), so these measurements refer only to the nucleus. Direct imaging is required to estimate the starlight contribution seen in large apertures. In addition, the nonstellar light in Seyfert 1 galaxies is much bluer than that of stars, and it is therefore essential to measure the stellar flux at longer wavelengths, where its relative strength is greater. Finally, since the nonstellar continuum often varies by more than a magnitude on timescales of a month (Penston et al. 1974), images and spectra should be obtained contemporaneously. Malkan and Oke (1983) used this combination of slit spectroscopy and direct imaging of the Seyfert galaxies Mkn 3, Mkn 6, and NGC 1068. Their spectra had reasonably good signal-to-noise ratios, but only 7 Å resolution, and it is not easy to separate weak absorption lines from adjacent emission lines.

In this paper, digital images of 9 Seyfert galaxies are combined with Coude spectra having excellent signal-to-noise ratios and high resolution in order to more precisely estimate the stellar flux and to determine the nature of the remaining continuum. The observations are presented in Section II, and the methods used to analyze them are outlined in Section III. Section IV discusses the host galaxies, whereas Section V examines properties of the

nonstellar continuum. A brief summary of our main conclusions is given in Section VI.

II. OBSERVATIONS

Direct images were obtained with the SIT Area Photometer (Kent 1979) on the Palomar 1.5 m telescope, as listed in Table 1. The data come in the form of a 256 x 256 array of square pixels, each 0."7 on a side, giving a 3' x 3' field of view. To maximize the dynamic range, the image tube was run at a relatively low gain, corresponding to a saturation level of 10000 photons per pixel. The required integration times for our bright objects were still only 10 -- 600 s, and two or three consecutive exposures of each galaxy were usually taken. The light passed through square filters selected to exclude significant contamination from emission lines. Most images were obtained through either a Gunn violet (v) filter (Thuan and Gunn 1976), with $\lambda_0 = 4000$ Å and $\Delta\lambda = 400$ Å, or a Wratten 88A filter, which gives $\lambda_0 = 7900$ Å, $\Delta\lambda = 1200$ Å, corresponding approximately to the i magnitude defined by Wade et al. (1980). A few images were obtained through narrow-band ($\Delta\lambda = 100$ Å) filters centered on either 6615 Å or 6760 Å, which were kindly loaned by Dr. H. C. Arp. For each galaxy, the filter was selected to avoid the strong Hα + [NII] emission lines; thus the 6760 Å filter was used for low-redshift galaxies, and the 6615 Å filter for objects of higher redshift. Comparison with the absolute spectrophotometric scans of deBruyn and Sargent (1978) shows that contamination from line emission in all these filters was negligible.

An average zero-level picture was removed from each frame, and pixel-to-pixel sensitivity variations were eliminated by flattening with a lengthy exposure of the illuminated dome ceiling. The sky measured in a large (typically $\geq 1'$) annulus centered on the galaxy was subtracted from each exposure. Since this correction was well-determined, and generally less than 10% of the central brightness of the galaxy, it is a small source of uncertainty in the derived surface brightness profiles. The photometric zero-points were set by several measurements of defocused standard stars, and are accurate to 10%. Spatial distortions in the SIT frames were negligible in the regions of interest.

Spectra having ~ 1.6 Å resolution were obtained with a photon-counting Varo-reticon detector (Shectman and Hiltner 1976) at the Coude focus of the Mt. Wilson 2.5 m Hooker telescope. A small aperture ($\sim 1.''6 \times 3.''7$) isolated light from the nuclear seeing disk. An image derotator was not used because of the unacceptably large light losses it would have caused. The sky was measured in an identical aperture displaced by $\sim 6''$, and appropriate corrections were applied when light from the galactic disk contaminated the sky spectrum. Owing to the very steep surface brightness profiles in Seyfert galaxies, these corrections were generally very small, but in several cases (e.g. NGC 1068) we obtained additional sky spectra a few arc minutes away from the object to achieve greater accuracy. Standard stars (Oke and Gunn 1983) were used to calibrate the

instrumental response, and all observations were divided by the spectrum of an intrinsically featureless continuum from a tungsten lamp to remove local variations in the detector sensitivity. Wavelengths were calculated from Fe-Ar arcs taken several times throughout the night. There were gradual drifts in the wavelength scale, but the calibration should be accurate to ~ 0.3 Å. Atmospheric absorption lines were removed by comparison with the spectra of early B-type stars.

III. Analysis

(a) Direct Images

The radial surface brightness profiles for each object were derived by azimuthally averaging the signal as a function of distance from the image center. Repeated measurements on different nights show that these curves are accurate to 0.1 magnitude for radii up to 15". The same information is also available as the integrated fluxes within a series of concentric circles centered on the peak brightness of the galaxy. A typical example of these two forms (differential and integral) of displaying the data is shown for NGC 5548 in Figures 1 and 2. The following analysis does not assume the galaxies are azimuthally symmetric: we simply refer all measurements to circular apertures for convenient comparison with other observations.

The galaxy profiles were then compared with those of field stars on the same frames to determine the resolved fraction of galaxy light. That is, a stellar (unresolved) seeing profile was scaled to match the galaxy profile in the central few arc seconds. Any remaining galaxy light above this profile is resolved and presumed to arise from stars, as shown in Figures 1 and 2. The scaled seeing profiles match the inner parts of the galaxy profiles with high precision: the residuals are only 2 -- 3%, smaller than the width of the lines in Figure 1.

The limiting source of error in this procedure was the accuracy with which the seeing profile could be determined at the time each Seyfert nucleus was measured. When a single frame had more than one bright stellar image, their surface brightness profiles were always very similar, with full widths at half maximum (FWHM) ~ 1."4 -- 1."9. On average, the seeing profile was independent of wavelength. However, there were small but detectable changes in the profile of a single star observed in two consecutive exposures, and gradual changes in the seeing occurred throughout the course of a night. Roughly half of the program galaxies did not have a bright field star in the same frame, so we compared these to stellar images observed either immediately before or after the galaxy. Owing to the seeing fluctuations, our estimates of the unresolved fractions are only accurate to 10 -- 15%. That is, two stellar images obtained in the same part of a night were often not identical. Compared to the sharper image, the poorer one had up to 10 -- 15% of its light "resolved." This dominant source of error was reduced by averaging the results of several frames. Possible errors in the photometric zero-points would not alter the fractions of resolved light we found by this procedure.

Our estimates of the fraction of resolved light in NGC 5548 and NGC 7469 agree with those obtained by deBruyn (1982, private communication) in June 1978. In several cases, galaxies were imaged on more than one night. Even when their nuclear brightness varied,

we found the same amount of starlight present, to within 0.10 — 0.20 mag. This is a reasonable measure of the total uncertainties associated with the estimates of starlight fluxes, which are listed in Table 4. The errors for NGC 3227 are somewhat larger since it was imaged on only one night.

(b) Spectra

The unresolved continuum comes from the point-like nonstellar nucleus and the starlight of the central part of the galaxy which falls within the seeing disk. Our spectra were used to estimate the ratio of unresolved stellar to nonstellar flux, under the assumption that the fraction of light in the nucleus due to stars is simply the ratio of the observed equivalent width of a stellar absorption line to its average value in the spectrum of an ordinary galaxy.

Figures 3 — 5 illustrate all of the spectra included in our analysis, with the exception of some repeat observations. The relative flux per unit frequency interval is plotted as a function of wavelength, and both scales are linear. Wavelengths have been reduced to the rest system of the observed galaxy. Since small apertures and long integration times were used, in some cases atmospheric dispersion produced substantially unequal light losses in different portions of a spectrum (Filippenko 1982). Therefore, to flatten the continuum for accurate measurements of absorption lines, every spectrum was normalized by fitting a cubic spline

through the continuum and dividing the flux in each bin by the local value of the spline. This technique artificially removes any broad intrinsic spectral shape, so the true relative intensities of regions separated by more than ~ 100 Å are not displayed exactly. Note that in most spectra the relative scale is adjusted to emphasize the continuum, so very low or high flux levels are not plotted.

Although they are potentially useful indicators of starlight, the G band and the Ca II H and K lines were not observed because of the increasing proportion of nonstellar light and, in particular, the decreasing detector sensitivity at short wavelengths. Similarly, the Ca II near-infrared triplet could be measured in only the brightest nearby galaxies NGC 1068 and NGC 4151, as the efficiency of the system plummets redward of ~ 8000 Å.

Prominent emission and absorption lines (or the expected positions of absorption lines) are marked on the spectra. The equivalent widths of absorption features were measured in the standard manner, but some difficulties were encountered with Mg b and Na D. For example, galaxies such as NGC 1068, 3227, 4051, and 4151 exhibit strong forbidden lines of nitrogen and highly ionized iron which contaminate the Mg b absorption, as well as narrow He I λ5876 near the Na D doublet. These emission lines could be removed to first order because the high spectral resolution adequately isolated them from the absorption lines. Permitted lines

of Fe II presented an additional problem near Mg b, as can be seen in Mkn 335, NGC 5548, and NGC 7469. The spectra were compared with those published by Phillips (1977, 1978), and once again our high spectral resolution was necessary for accurate measurement of the absorption lines. Finally, a suitable correction was made to the equivalent width of Na D in objects which show broad He I λ5876 emission, and in spectra from which broad Na D emission (due to high-pressure sodium vapor lamps) could not be completely subtracted.

Our assumption that the spectra measure only unresolved nuclear light is conservative, since light from the galactic disk entered near the ends of the long (3."7) aperture. Furthermore, if some off-nuclear light entered the aperture due to guiding errors or atmospheric dispersion, the strengths of absorption lines would be overestimated. Despite these effects, the absorption lines in most of the spectra are extremely weak, indicating that the unresolved light is almost entirely nonstellar.

Since some Na D absorption may arise from the interstellar medium of the host galaxy, the true equivalent width of the stellar absorption could be even smaller than the values listed in Table 3. NGC 3227 has extremely strong, narrow Na D absorption (Figure 4), which seems inconsistent with its very weak Mg b lines. NGC 4051 also exhibits an easily resolved Na D doublet, in contrast to the stellar Na D absorption in the bulge of NGC 1068 (Figure 3). The

nucleus of NGC 3227 is obscured by $A_V \sim 1.4$ magnitudes, and NGC 4051 could have half as much extinction (Malkan 1983a). We suspect that most of the Na D absorption in these two objects (and possibly in others as well) is interstellar. Na D absorption due to our Galaxy did not present any difficulties, since $cz \geq 1000$ km s^{-1} for all of the Seyferts observed.

The equivalent widths of stellar absorption lines in the spectra of Seyfert nuclei are given in Table 3. Our measurements may be somewhat generous: the true widths could be less, but certainly do not exceed the ones listed by more than ~ 25%, so it is unlikely that the contribution due to stars has been significantly underestimated. Since the absorption lines are very weak in most of the objects, we were concerned primarily with the danger of underestimating the starlight contribution; such an error would have an important impact on our conclusions. The small equivalent widths listed for the Mg b lines are in good agreement with the Ca K widths measured by Osterbrock (1978) in these objects.

(c) Stellar and Nonstellar Fluxes

In order to determine the amount by which galactic absorption lines have been diluted by a nonstellar featureless continuum, we must know the intrinsic strengths of the lines. The spectra measured light from roughly the central kiloparsec of the galaxies, where the bulge dominates the contribution from the disk component

in early- and intermediate-type spirals. Since the integrated spectra of galactic bulges are dominated by red giants, the strengths of stellar absorption lines do not vary greatly from galaxy to galaxy. Cohen (1978) found that the near-infrared Ca II triplet lines have relatively constant equivalent widths in different galaxies, and exhibit no spatial variations in a given object. The equivalent widths of Mg b and Na D in Table 3, taken from Hartwick and Cowley (1980) and Stauffer (1983), are averages over all types of spiral galaxies. The larger variations seen in the b and D lines are due to metallicity differences and dilution from the blue continuum of hot young stars.

Although these variations in equivalent width are a non-negligible source of error in our analysis, it is likely that the stellar population in the nuclei of Seyfert galaxies more closely resembles that of ellipticals or early-type spirals than that of late-type spirals. Thus, the <u>effective</u> scatter in the width of a line is probably smaller than indicated in Table 3. For example, late-type spirals exhibit relatively weak Mg b absorption, but their stellar population is probably not representative of Seyfert 1 nuclei since features such as Fe I λ5269, whose strengths should be comparable to that of Mg b (Osterbrock 1983), are not visible (except weakly in NGC 1068 and NGC 3227).

The direct imaging gives R, the ratio of resolved to total light within a 10" aperture (as illustrated in Figure 2). To compare estimates made at different wavelengths, we assume that the starlight spectrum is that of the "standard galaxy" of Yee and Oke (1978), in which the ratios of flux at 4000, 5200, 6600, and 8000 Å are 0.33:1.0:1.5:2.3. As illustrated by Malkan and Oke (1983), it is a good match to the integrated spectra of early-type galaxies and to the central regions of later-type spirals, which are dominated by bulge light from red giants.

The starlight flux at 5200 Å in a 10" aperture is given by

$$F_*(5200) = C_*(\lambda)F(\lambda)\left[R + (1 - R)\ (EW_{obs}/EW_*)\right] \ ,$$

where the measurements of <u>total</u> flux ($F(\lambda)$), R, and absorption equivalent width (EW_{obs}) are made at a wavelength λ. $C_*(\lambda)$ is the standard galaxy color $F_*(5200)/F_*(\lambda)$, and EW_* is the equivalent width of the absorption line in the case of pure starlight. The first term, $C_*(\lambda)F(\lambda)R$, is the resolved (extended) flux, which is by assumption entirely stellar. The second term is the portion of the unresolved nucleus which is starlight, as manifested by absorption lines in our spectra. In all objects the first term is larger than the second, since (EW_{obs}/EW_*) is typically 0.05 — 0.20 and tends to be smallest when R is small (e.g. in Mkn 335 and Mkn 509).

Errors in the photometric zero points (leading to incorrect $F(\lambda)$) and those in the galaxy color $C_*(\lambda)$ propagate linearly as errors in the estimated stellar flux. We confirm in Section IV that the galaxy colors are indeed very similar to those of our standard galaxy, so the second source of error is negligible. For the values listed in Tables 3 and 4, it is evident that the dominant source of error comes from 10 — 15% uncertainties in R, although the second term tends to offset errors in the first. As long as a portion of the seeing disk is contaminated by starlight (i.e., as long as EW_{obs}/EW_* exceeds zero), the resolved flux ratio (R) tends to increase as the seeing improves, but this improvement in the seeing also decreases EW_{obs}/EW_*. If the seeing is <u>identical</u> during the direct and spectroscopic observations, its effects cancel. On the other hand, if it is much <u>worse</u> during the direct observations, the starlight flux is underestimated. It is probable that any differences in our observations were actually in the opposite sense: the direct images were generally obtained under slightly better seeing conditions than the spectra (if we include guiding errors in the effective "seeing"). In the next section we confirm that seeing did <u>not</u> lead to an underestimate of the stellar flux.

The additional photometric errors and uncertainties in EW_* lead to estimates of stellar and nonstellar flux in Table 4 that are accurate to 15 — 20%. Aperture growth curves were used to calculate the total amount of visual continuum flux from stars in

10" — 30" apertures (Table 4).

IV. THE HOST GALAXIES

Having separated the stellar and nonstellar continuum in each Seyfert nucleus, we can now compare the host galaxies to others which lack active nuclei. As Yee (1983) concluded for 11 Seyfert 1 galaxies, the nuclear colors (dominated by nonstellar light) are much bluer than those of starlight. But it is relatively easy to measure the colors at radii larger than 5", where contamination from the unresolved nucleus is negligible. The starlight colors measured 5" to 30" from the nuclei of NGC 4051, 4151, 5548, and Mkn 335 are approximately the same as those of the standard galaxy. Colors were not measured in NGC 3227 and Mkn 509.

The type 2 Seyfert galaxy in our sample, NGC 1068, shows little color change from the nucleus to a radius of ~ 7". At larger radii (8" -- 17"), the color becomes bluer than that of a standard galaxy by 0.2 magnitude in $\underline{v} - \underline{r}$. This is due to the contribution from bright rings of HII regions and their associated young stars which are evident on photographs having short exposure times (Alloin *et al.* 1981). The FWHM of the Na D and Ca II near-infrared lines is 570 ± 40 km s^{-1}, and the corresponding velocity dispersion (240 ± 20 km s^{-1}) is at the high end of observed values in bulges of spiral galaxies (cf. Kormendy and Illingworth 1982).

We checked our estimates of the stellar flux in the nucleus at several different wavelengths to see if they are consistent with the light from a standard galaxy. In all cases except NGC 1275, the inferred galaxy colors are the same as those of the standard galaxy to within 0.1 — 0.2 mag. NGC 1275 is unusual in that $v - g$ does not change by more than 5% from the nucleus out to a radius of 15". Thus, its nucleus and the nearby starlight both have roughly the same blue color, $v - g \sim 0.25$, which is several tenths of a magnitude bluer than the standard galaxy. The additional blue light around the nucleus of NGC 1275 probably comes from a population of young stars, as has already been revealed by previous observations of Balmer absorption lines in off-nuclear spectra (Minkowski 1968).

We agree with Yee (1983) that the starlight in most Seyfert galaxies has the colors of typical spiral disks. That is, it is only slightly bluer than an elliptical galaxy. Malkan et al. (1983) found the same result from imaging quasars of low-redshift selected from X-ray surveys.

The surface brightness profiles allow one critical check for consistency with the spectroscopy. As illustrated in Figures 6 and 7 for NGC 1068 and NGC 4151, we can use the images to estimate the total stellar flux by a method which is completely independent of the spectroscopy. Guided by the portion of the profile outside $r = 3"$, which is entirely starlight, we smoothly extrapolate (as indicated by the thin dashed line) the galaxy flux to $r = 0"$, much

as Yee (1983) did in his analysis. We then compare the inferred central surface brightness of the stars to the observed central surface brightness to find what fraction of the nuclear light is stellar. Approximately a third of the *v* light in the nucleus of NGC 1068 is predicted to be stellar, and in NGC 4151 stars should contibute a tenth of the *v* light and a third of the *i* light. These predictions are in excellent agreement with the observed absorption line strengths, confirming our assumptions that the seeing was similar during the direct and spectroscopic observations, and that the intrinsic strengths of absorption lines in the stars were normal.

V. THE NONSTELLAR CONTINUUM

The estimates of starlight flux in the preceeding section allow us to isolate the spectra of the nonstellar continuum. Several of the galaxies in this program have been observed nearly simultaneously at infrared and optical wavelengths. The observing dates are given in Table 1. Optical spectrophotometry was obtained through a 10" aperture by deBruyn, Sargent, and Readhead (1982, private communication) with the multichannel spectrometer (Oke 1969) on the Hale 5 m telescope. Near-infrared photometry (1.2 -- 3.5 μm) was obtained with the Las Campanas duPont 2.5 m and Mt. Wilson 1.5 m reflectors, or taken from previous studies by Rieke (1978), McAlary et al. (1983), Cutri et al. (1981), Rudy et al. (1982), McAlary et al. (1979), and Balzano and Weedman (1981). Our new infrared photometry is presented in Table 2. Most of the measurements were made with 8" -- 12" apertures, so that only very minor corrections were required before combining the infrared with the optical observations, as has been done in Figure 8. The data are plotted as vertical bars. We also include measurements made at 10 μm, although generally these were not simultaneous with the other observations. If there is significant variability at 10 μm in any of these galaxies, this portion of the composite spectra should be considered more uncertain.

In Mkn 335 and Mkn 509, the correction for starlight included in a 10" aperture is 15% or less, and can almost be ignored completely. The corrected nonstellar continua look very similar to the multichannel spectra published by deBruyn and Sargent (1978). However, starlight produces a significant fraction of the light within 5" of the nucleus in all of the other Seyfert galaxies. Figure 8 shows the infrared and optical spectra of NGC 4051, 4151, 5548 and 7469 obtained through a 10" aperture. Channels containing strong emission lines were excised. The dashed line shows the estimated flux due to stars (from Table 4), and the solid line is the remaining nonstellar light (which is the difference between the bars and the dashed line). Although optical and infrared photometry is available for NGC 1275, we did not attempt a subtraction because, as discussed above, we suspect its starlight is bluer than that of the standard galaxy. For two galaxies, NGC 4151 and NGC 7469, combined infrared and optical data are available for two epochs -- one in which the nuclei were near their maximum brightness, and one when they were near minimum. NGC 4051 has never shown optical variations greater than ~ 0.3 mag.

All of the nonstellar spectra exhibit a decrease in slope near 4000Å (log ν = 14.875), and then level off at ~ 3650 Å (log ν = 14.915). Malkan and Sargent (1982; hereinafter MS) have already seen this feature in six Seyfert galaxies. The exact wavelength coincidence lead them to attribute it to blended Balmer

lines and strong emission in the Balmer continuum. Our results strengthen their view that it is always present in the spectra of Seyfert galaxies.

In Figure 9 we have shifted the nonstellar spectra on top of each other, in two distinct groups. The "faint" group includes NGC 4151 and NGC 7469 near minimum, and NGC 4051. These spectra are slightly steeper, and show no indication of any flattening before the Balmer jump which could be attributed to thermal emission (MS). The "bright" group includes NGC 4151 and NGC 7469 near maximum, and NGC 5548. Their nonstellar spectra are almost identical to the spectrum of Mkn 509, which is plotted for comparison. They show a small but significant flattening in the visual, considerably before the blending of Balmer lines merges into the Balmer continuum. This characterstic "ultraviolet excess" (or "blue bump") is present in nearly all luminous Seyfert 1 galaxies and quasars. It has been analyzed in detail by MS and by Malkan (1983b), who found that it is best interpreted as thermal emission from optically thick accreting gas. The two least luminous Seyferts studied by MS were NGC 4151 and NGC 5548, for which only an upper limit on the strength of the thermal ultraviolet emission could be established. The present measurements of starlight in NGC 4151 and NGC 5548 provide a more precise estimate of their nonstellar spectra, and it is now evident that when they are bright they also flatten around 5500 Å (Figure 9). Thus, the less luminous Seyfert nuclei can show the

same signature of optically thick thermal ultraviolet emission that MS concluded was present in all brighter objects.

All the nonstellar spectra slope down from 10 μm to the visual roughly like power-laws ($f_\nu \propto \nu^\alpha$). with slopes (α) of -1.1 or -1.2. This characteristic shape is commonly seen in most broad emission-line objects, as discussed by MS. A closer look reveals that the spectra are not exactly described by power-laws, but usually have a slight downward curvature, as mentioned by Malkan (1983b) and others. The logarithmic slope from 0.8 μm to 2.5 μm is one or two tenths steeper than the slope from 2.5 μm to 10 μm. It seems reasonable to expect this curvature to continue to longer and shorter wavelengths. The 10 -- 100 μm spectra of Seyfert 1 nuclei should show noticeable curvature and an overall slope which is flatter than -1.0. Note that on the scale of Figure 9, even a 10% error in the relative calibration of optical and infrared fluxes would still have no discernible effect on our results.

Our estimate of stellar flux in NGC 1068 is slightly higher than that obtained by Malkan and Oke (1983). Since it is based on better observations, it supercedes the previous value. The estimate of starlight flux in NGC 4151 is lower than that of Schmidt and Miller (1980), probably because they assumed the nonstellar light was a flat power-law ($f_\nu \propto \nu^{-0.33}$).

Rieke (1978, 1981) has made estimates of the starlight flux in NGC 4151 and in several other low-luminosity Seyfert nuclei to examine their nonstellar infrared spectra. In NGC 4151, he assumed that the red spectrum at minimum light is entirely due to stars. Our spectra of the nucleus of NGC 4151 at minimum do not confirm this, since all of its absorption lines are far too weak to arise from pure undiluted starlight. Thus, Rieke's estimate of the stellar flux in 4151 is ~ 50% too high. Consequently, the nonstellar spectrum of NGC 4151 at minimum is not qualitatively different from that at maximum brightness: both fall smoothly from 2 -- 3 μm to the visual, roughly with a power-law slope of -1.1 to -1.2. There is no short-wavelength break around 1 μm. If the bulk of the 2 μm flux came from hot dust grains, such a thermal Boltzmann cut-off in the nonstellar spectrum should be observable. Since it is not seen in any of the Seyfert 1 spectra in our sample and has an approximately power-law shape (as in quasars), we conclude that the bulk of their 2 μm flux is not thermal.

Careful photometric monitoring by Lebofsky and Rieke (1980) shows that the blue and infrared variations in NGC 4151 and in the low-redshift quasar III Zwicky 2 are sometimes not instantaneously correlated. If (as MS argue) the blue light is predominantly thermal, while the red is nonthermal, they may not always vary synchronously. Rieke's measurements also show that the nonstellar infrared continuum may steepen slightly when it fades.

Although our results severely restrict the role that thermal dust emission could play in contributing to the near-infrared flux, they do not conclusively rule out the possibility that thermal emission may become important at longer wavelengths in many Seyfert 1 nuclei. For example, the "power-law" seen at shorter wavelengths could turn over beyond 3 μm if the right amount of thermal emission from dust at T ~ 500 K were present to preserve the linearity of the resulting spectrum. Yet it seems implausible that the thermal and nonthermal fluxes would always be so well-balanced: one should expect to see some spectra with a sharp (exponential) increase to longer wavelengths, as well as some with a turnover at 10 μm. This conflicts with the great uniformity of most infrared spectra of Seyfert 1 nuclei and quasars.

The starlight fluxes derived for NGC 1068 in the blue and red agree fairly well with those estimated by Malkan and Oke (1983). However, our high-quality

near-infrared spectrum shows that the Ca II lines are probably seen at full strength in the nucleus of NGC 1068. At most 10% of the near-infrared continuum within a 10" aperture is nonstellar, indicating that the "power-law" seen by Malkan and Oke (1983) at shorter wavelengths has flattened by 8000 Å. Since the nonstellar light is bluer than the starlight, the increase in polarization at shorter wavelengths is probably due to the nonstellar component (cf. Visvanathan and Oke 1968, Miller 1983). Our failure to detect

dilution from nonstellar light at 8500 Å in NGC 1068 indicates that at least some Seyfert 2 galaxies do not have the same red power-law that is generally present in type 1 Seyferts. It is not possible to ascertain whether the nonthermal component extends into the infrared in Seyfert 2 nuclei because this portion of their spectra is dominated by thermal emission from dust with a maximum temperature of 300 — 800 K (Malkan and Oke 1983). The same complication arises in the unusually red spectra of a few heavily reddened Seyfert 1 galaxies such as Mkn 231, which have very steep infrared spectra that are predominantly thermal (Rieke 1976).

VI. SUMMARY

Coude spectroscopy and direct imaging have been combined to estimate the starlight fluxes in the nuclei of 9 nearby Seyfert galaxies. The starlight colors agree with those expected from early-type spiral galaxies. The nonstellar continuum in low-luminosity Seyfert 1 nuclei is similar to that of very luminous Seyferts and quasars. It falls from the infrared to the visual roughly as a power-law with a slope of -1.1 to -1.2. Except in the least luminous Seyfert nuclei studied, there is also a flattening before the Balmer limit which has been attributed to optically thick thermal emission. Even at minimum brightness, there is no spectral steepening at wavelengths less than 1 μm, ruling out a thermal origin for the bulk of the 2 μm emission.

During the many nights required to obtain the data, expert assistance was provided by Howard Lanning and Jim Frazer at Mt. Wilson, Skip Staples and Bob Griffith at Palomar, and Oscar Duhalde, Fernando Peralta and Angel Guerra at Las Campanas. We are grateful to A. G. deBruyn, A. C. S. Readhead, and W. L. W. Sargent for private communication of unpublished data, as well as Abi Saha and James Fillmore for some of the computer programs used in the analysis. Informative discussions with J. B. Oke, G. Rieke, W. L. W. Sargent and D. P. Schneider are appreciated, and we thank H. K. C. Yee for particularly illuminating conversations. This work was supported by the Fannie and John Hertz Foundation through two graduate fellowships, and by NASA through grant NG 8406 to W. L. W. Sargent.

APPENDIX

LINE PROFILES AND NEW EMISSION LINES

The data obtained for this investigation have also been used in a study of the emission lines in Seyfert galaxies. Although a detailed analysis will be presented elsewhere (Filippenko and Malkan 1983), a few conclusions are briefly discussed here.

Several new emission lines have been identified in the Coude spectra. One is He II λ8237 Å, in NGC 4151 (Figure 3). Careful examination of Figure 1 in Grandi (1978) reveals that the feature may also be present in NGC 1068, NGC 4051, and Mkn 335, but this must be confirmed with spectra of higher quality. In principle, He II λ8237 can be used together with He II λ4686 as a reddening indicator; the signal-to-noise ratio in our data, however, is not sufficiently large.

A stronger and more puzzling line in NGC 4151 is at $\lambda \sim 8617$ Å. It is narrow, and therefore probably corresponds to a forbidden transition. Several spectra obtained by J. B. Oke (1983, private communication) confirm the presence of this line. The most likely identification is [FeII] λ8617, which is also visible in the Eta Carinae nebula (Thackeray 1953) and in the Orion nebula (Grandi 1975; Danziger and Aaronson 1974). A considerably broader feature appears at approximately the same wavelength in NGC 1068 (Figure 3), but the width is consistent with that of other forbidden lines in

this object.

Still another line which (to our knowledge) has not been previously reported in Seyfert galaxies appears at $\lambda \sim 5120$ Å in NGC 4051, 4151, 7469, and possibly 1068. Although its exact identification is unknown, it is probably a forbidden line from a highly ionized species, since [FeVII] emission is strong in these galaxies. The feature also appears in NGC 6741 and IC 418 (Aller and Walker 1970), two planetary nebulae which exhibit lines from multiply-ionized elements, but surprisingly it may be absent in other high-excitation planetaries (Kaler 1976).

With high spectral resolution, we can investigate line profiles and small differences in the width and redshift of lines which represent a wide range of excitation. Such studies will provide information concerning the kinematics and geometry of the gas and dust in Seyfert nuclei. For example, the width of the [FeVII] + [CaV] λ6087 line in NGC 1068 and NGC 7469 is considerably greater than that of [OI] λ6300, and in Mkn 335 the widths differ by a factor of 2 to 3. A similar increase in line width with increasing ionization potential of the corresponding ion has been noticed in several other Seyfert galaxies (Osterbrock 1981, Pelat, Alloin, and Fosbury 1981), and indicates that the cloud velocity dispersion is greatest near the central source of ionizing radiation. Moreover, the difference between the redshift of emission and absorption lines in NGC 1068, which was first noticed

by Burbidge, Burbidge, and Prendergast (1959), is confirmed, and slight discrepancies are evident in other objects as well.

A search for broad wings in the emission lines has also been conducted. For example, NGC 1068 may have a very faint, broad component of Hβ which qualitatively resembles that of Seyfert 1 galaxies. Similarly, the Hβ profile in NGC 5548 has three distinct components: one corresponds to the narrow forbidden lines, another has a width which is typical of that in type 1 Seyferts, whereas the third may extend redward of [OIII] λ5007 and is reminiscent of the extremely broad wings seen in broad-line radio galaxies (Osterbrock, Koski, and Phillips 1976). Finally, it is possible that very weak wings are present in the [OIII] λ4959, 5007 lines of NGC 4151, but this must be confirmed in future investigations.

Table 1. Journal of Observations (UT)

Galaxy	Coude Spectroscopy	Direct Imaging	Optical Spectrophotometry	Infrared Photometry
NGC 1068	4 Jan 82 (Mg)	16 Oct 81		
	14 Nov 82 (Na)	7 Mar 82		
	24 Oct 81 (Ca)			
1275	22,23 Oct 81 (Mg)	9,10,14,16 Oct 81		
3227	29 Mar 81 (Mg)	1 Apr 81		
	14,15 Nov 82 (Mg)			
	10 Jan 81 (Na)			
4051	28 Mar 81 (Mg)	1 Apr 81	12 Jun 79	22 Feb 78
	22 May 82 (Mg)	20 May 82		25 Mar 80
	19 Apr 82 (Na)			30 Mar 80
	21 May 82 (Na)			
4151	29 Mar 81 (Mg)	1 Apr 81	9 Mar 80	11 Feb 80
	22 May 82 (Mg)	7 Mar 82	16 Apr 79	30 Mar 80
	19 Apr 82 (Na)	20 May 82		13 Apr 79
	20 Apr 82 (Ca)			6 May 79
5548	30 Mar 81 (Mg)	1 Apr 81	9 Mar 80	30 Mar 80
	22 May 82 (Mg)	7 Mar 82		15 Apr 80
	21 May 82 (Na)	21 May 82		
7469	22 Oct 81 (Mg)	9 Aug 81	30 Sep 80	25 Oct 80
	14 Nov 82 (Na)	10,15,17 Oct 81	12 Jun 79	29 Jun 79
Mkn 335	23 Oct 81 (Mg)	9 Aug 81		
	15,16 Nov 82 (Na)	10,15,16 Oct 81		

509	21 May 82 (Na)	9 Aug 81	
		14,16 Oct 81	

Table 2. New Infrared Magnitudes

Galaxy	J[1.2μm]	H[1.6μm]	K[2.2μm]	L[3.5μm]	N[10.6μm]	Aper	Date	Tel[c]
NGC 1068					0.96 ±0.16	9	6 Sep 79	M60
NGC 1275			9.83 ±0.08		4.14 ±0.24	12/9[a]	7 Sep 79	M60
NGC 7469			9.14 ±0.08		4.12 ±0.19	12/9[a]	6 Sep 79	M60
	10.97	10.08	9.34	8.25		11	29 Jun 80	L100
	10.54	9.80	9.14	8.00		18	29 Jun 80	L100
	10.35 ±0.03	9.57 ±0.03	9.00 ±0.03	±0.05[b]		63	1 Aug 80	C36
Mkn 335					5.47 ±0.21	9	7 Sep 79	M60
Mkn 509	11.99 ±0.03	11.14 ±0.03	10.18 ±0.03	8.70 ±0.05		10	3 Jul 80	L100

[a] Larger aperture refers to measurement at shorter wavelength.

[b] Error estimates refer to all three sets of LCO and CTIO observations.

[c] Key: M = Mt. Wilson, L = Las Campanas, C = Cerro Tololo.

Numbers refer to telescope mirror diameter (inches).

Table 3. Coude Spectroscopy -- Equivalent Widths (Angstroms)

Galaxy	Mg I b	Na I D	Ca II 8542 Å
Average spiral	4.5±2.1	3.7±1.6	3.2±0.5
NGC 1068	1.7	2.9	3.0
1275	0.25		
3227	0.75	4.2	
4051	0.8	1.1	
4151	0.2	0.8	1.1
5548	0.2	0.3	
7469	0.3	0.7	
Mkn 335	< 0.1	< 0.2	
509		< 0.25	

Notes:

1) Ca II refers to the width of one component of the triplet, at 8542 Å -- the other two lines (8498, 8662 Å) were more difficult to measure.
2) "<" means line not detected or only marginally detected -- upper limit given.
3) Average spiral: Mg b and Na D from Hartwick and Cowley (1980) and Stauffer (1983). Ca II from Cohen (1978).

Table 4. Fluxes at 5400 Å (mJy)

Galaxy	Within 10" Aperture		Total Starlight Within Aperture of:			
	Stellar	Nonstellar[a]	15"	20"	25"	30"
NGC 1068	65	17	100	140	180	220
1275	5.2	2.9	9.3	13	15	17
3227	7.6	5.2	14	19	25	
4051	7.3	5.7	10	13	16	19
4151	14	21/29[b]	21	28	34	40
5548	3.4	6.9	5.6	7.4	9.0	10
7469	6.8	7.5/12[b]	7.9	10	13	15
Mkn 335	1.5	7.4				
509	1.5	8.6				

[a] The nonstellar flux (f_ν) is approximately a power-law with slope -1.1 to -1.2 in all cases.

[b] The two nonstellar fluxes refer to measurements when the continuum was faint, and when it was bright.

REFERENCES

Aller, L. H. and Walker, M. F. 1970, Ap. J., 161, 917.

Alloin, D., Laques, P., Pelat, D., Despiau, R. 1981, Astr. Ap., 95, 394.

Balzano, V. A. and Weedman, D. W. 1981, Ap. J., 243, 756.

Burbidge, E. M., Burbidge, G. R., and Prendergast, K. H. 1959, Ap. J., 130, 26.

Cohen, J. G. 1978, Ap. J., 221, 788.

Cutri, R. M., et al. 1981, Ap. J., 245, 818.

Danziger, I. J. and Aaronson, M. 1974, Pub. A. S. P., 86, 208.

deBruyn, A.G., Sargent, W.L.W. 1978, A. J., 83, 1257.

Filippenko, A. V. 1982, Pub. A. S. P., 94, 715.

Filippenko, A. V. and Malkan, M. A. 1983, in preparation.

Grandi, S. A. 1975, Ap. J. (Letters), 199, L43.

_____ 1978, Ap. J., 221, 501.

Hartwick, F. J. and Cowley, A. 1980, Ap. J., 235, 755.

Kaler, J. B. 1976, Ap. J. Suppl., 31, 517.

Kent, S. M. 1979, Pub. A. S. P., 91, 394.

Kormendy, J. and Illingworth, G. 1982, Ap. J., 256, 460.

Lebofsky, M. J. and Rieke, G. H. 1980, Nature, 284, 410.

Malkan, M. A. 1983a, Ap. J. (Letters), 264, L1.

_____ 1983b, Ap. J., 268,

Malkan, M. A., Margon, B., Chanan, G., Ap. J., submitted.

Malkan, M. A. and Oke, J. B. 1983, Ap. J., 265, 92.

Malkan, M. A. and Sargent, W. L. W. 1982, Ap. J., 254, 22 (MS).

McAlary, C. W., McGonegal, R. J., and Maza, J. 1983, Ap. J., in press.

McAlary, C. W., McLaren, R. A., and Crabtree, D. R. 1979, Ap. J. 234, 471.

Miller, J. S. 1983, preprint.

Minkowski, R. 1968, A. J., 73, 836.

Oke, J.B. 1969, Pub. A. S. P., 81, 11.

Oke, J. B. and Gunn, J. E. 1983, Ap. J., 266, 713.

Osterbrock, D. E. 1978, Proc. Nat. Acad. Sci., 75, 540.

_____ 1981, Ap. J., 246, 696.

_____ 1983, Pub. A. S. P., 95, 12.

Osterbrock, D. E., Koski, A. T., and Phillips, M. M. 1976, Ap. J., 206, 898.

Pelat, D., Alloin, D. and Fosbury, R. A. E. 1981, M. N. R. A. S., 195, 787.

Penston, M. V. et al. 1974, M. N. R. A. S., 169, 357.

Phillips, M. M. 1977, Ap. J., 215, 740.

_____ 1978, Ap. J. Suppl., 38, 187.

Rieke, G. H. 1976, Ap. J. (Letters), 206, L15.

_____ 1978, Ap. J., 226, 550.

_____ 1981, Ap. J., 250, 87.

Rudy, R. J., Jones, B., Levan, P. D., Smith, H. E., Willner, S. P., and Tokunaga, A. T. 1982, Ap. J. 257, 570.

Schmidt, G. D. and Miller, J. S. 1980, Ap. J., 240, 759.

Shectman, S. and Hiltner, W. A. 1976, Pub. A. S. P., 88, 960.

Stauffer, J. 1983, Ap. J., 264, 14.

Thackeray, A. D. 1953, M. N. R. A. S., 113, 211.

Thuan, T. X., and Gunn, J. E. 1976, Pub. A. S. P., 88, 543.

Visvanathan, N., and Oke, J. B. 1968, Ap. J. (Letters), 152, L165.

Wade, R. A., Hoessel, J. G., Elias, J. H., Huchra, J. P. 1980, Pub. A. S. P., 91, 35.

Yee, H. K. C. 1983, Ap. J., in press.

Yee, H. K. C. and Oke, J. B. 1978, Ap. J., 226, 753.

FIGURE CAPTIONS

Figure 1: Surface brightness profiles of NGC 5548, observed through *v* and *i* filters. The violet and infrared fluxes are comparable in the predominantly nonstellar nucleus. At larger radii, the infrared/violet flux ratio increases, leveling off at the much redder color typical of a galaxy. The dashed line is a seeing profile, scaled to match the center of the *i* brightness distribution in NGC 5548. In other words, it shows the portion of light in NGC 5548 which is unresolved.

Figure 2: The integrated flux as a function of diameter enclosed by a circular aperture centered on the nucleus of NGC 5548. The scale for the violet fluxes is on the right; the infrared fluxes are plotted on a scale which is a factor of five larger. The dotted lines show seeing profiles (derived from images of field stars) normalized to match the galaxy growth curves at the smallest diameters. They correspond to the fraction of the light which is unresolved: 5.4 mJy at 4000 Å, and 10.8 mJy at 7900 Å. The sharp bend in the *v* curve indicates that the nucleus of NGC 5548 dominates at 4000 Å; the image at 7900 Å is more extended because the starlight is much redder than the light from the nucleus.

Figure 3: Coude spectra, shifted to zero redshift, of

NGC 1068 and NGC 4151 near the Mg b, Na D, and Ca II near-infrared absorption lines. The continuum has been normalized to unity in each case, and relative intensities refer to flux per unit frequency interval. Very low and high flux levels are not plotted in order to emphasize the continuum. The emission feature indicated by a question mark is an unidentified line at $\lambda \sim 5120$ Å.

Figure 4: Same as Figure 3, but for NGC 3227, 4051, and 5548 near Mg b and Na D.

Figure 5: Same as Figure 3, but for NGC 1275, NGC 7469, and Mkn 335 near Mg b, and for NGC 7469, Mkn 335, and Mkn 509 near Na D.

Figure 6: The observed violet surface brightness profile of NGC 1068, and its decomposition into an unresolved nonstellar component (hatched region bounded by the dashed line labeled "point source") and a galactic starlight component (hatched region bounded by the dashed line labeled "galaxy"). The sum of the nonstellar and stellar components is equal to the observed profile (solid line). Integrating the galaxy curve and assuming a normal starlight color yields the stellar flux estimates given in Table 4. At the nucleus ($r \sim 0$) stars make up about a third of the light at y, in excellent agreement with the spectroscopic results.

Figure 7: The observed v and i surface brightness profiles of NGC 4151. The starlight component is shown extrapolated into the nucleus by the thin dotted lines. The i seeing profile is shown by the heavy dashed line.

Figure 8: Decomposition of the spectra of NGC 4051, 4151, 5548, and 7469 at optical and infrared wavelengths. Bars represent the total observed fluxes in a 10" aperture. The dashed line shows the amount of flux due to starlight, as given in Table 4, and the solid line is the remaining nonstellar flux found by subtracting the dashed line from the observed fluxes. Arrows indicate the frequency of the Balmer limit. All objects have a marked contribution from blended Balmer lines and continuum which reaches its maximum value at 3650 Å. The spectra on the left side have low-luminosity nonstellar components, which resemble a power-law of slope -1.2, but with slight downward curvature. Those on the right have brighter nonstellar components which are more similar to the spectrum of Mkn 509.

Figure 9: The nonstellar spectra from Figure 8, rescaled for easy comparison with each other. The "faint" spectra fall steadily all the way to the Balmer limit, and are not very different from the $f_\nu \propto \nu^{-1.2}$ power-law shown for comparison. The "bright" nonstellar spectra are almost identical to that of Mkn 509, which has a detectable

flattening in the blue well before the Balmer limit.

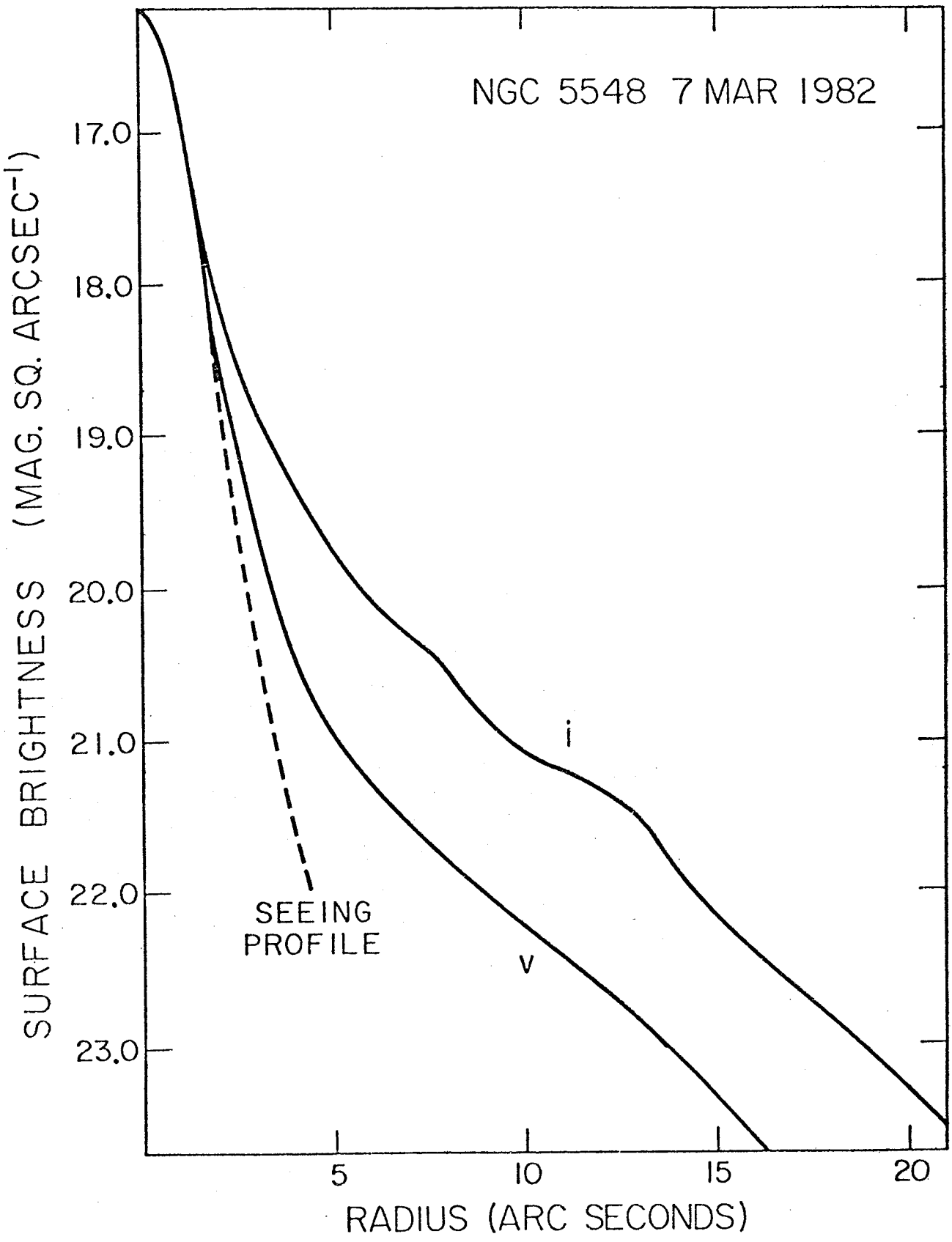
NGC 5548 7 MAR 1982
SURFACE BRIGHTNESS (MAG. SQ. ARCSEC^{-1})
17.0
18.0
19.0
20.0
21.0
22.0
23.0
i
v
SEEING PROFILE
5
10
15
20
RADIUS (ARC SECONDS)

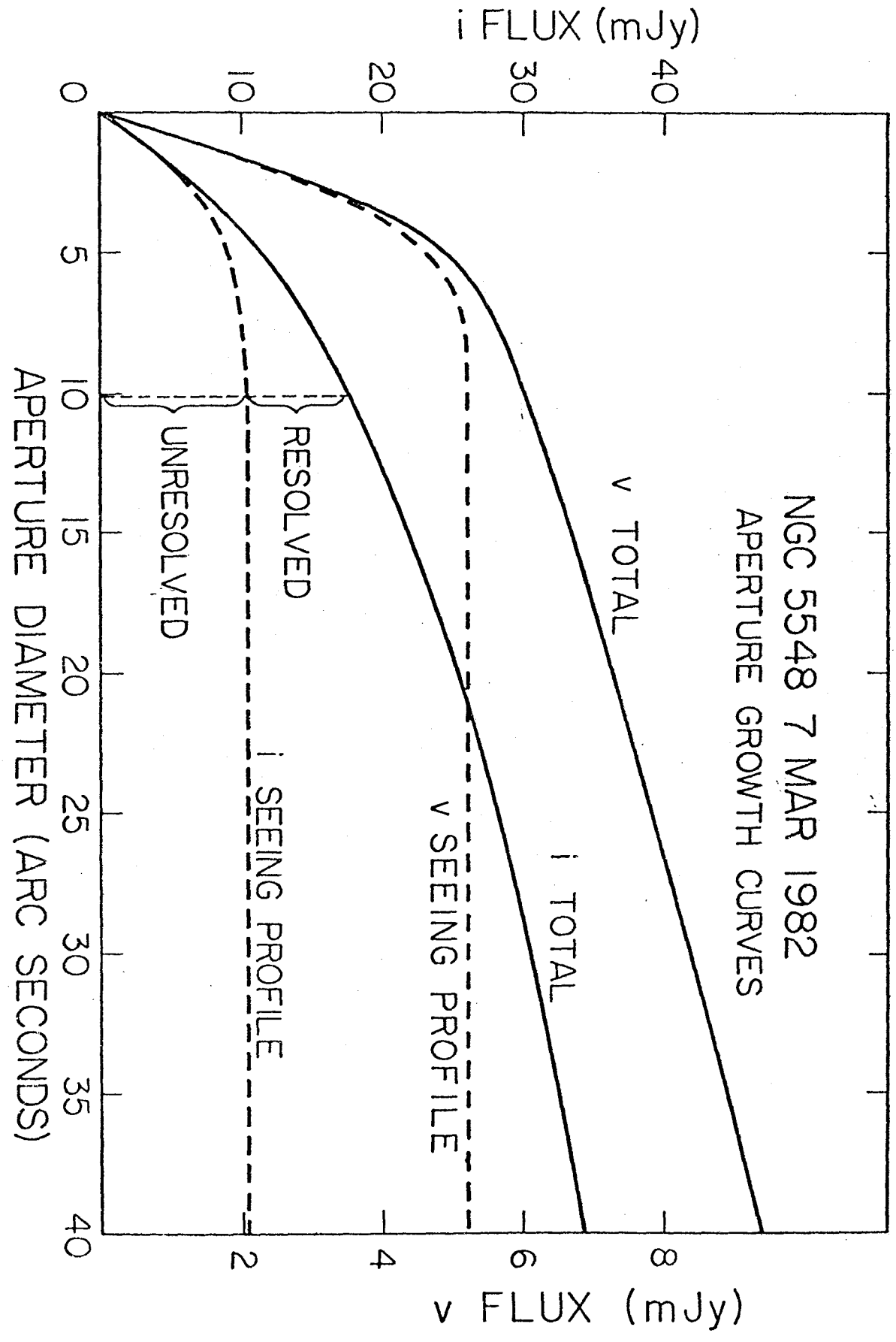
NGC 5548 7 MAR 1982
APERTURE GROWTH CURVES
v TOTAL
i TOTAL
v SEEING PROFILE
i SEEING PROFILE
RESOLVED
UNRESOLVED
APERTURE DIAMETER (ARC SECONDS)
0
5
10
15
20
25
30
35
40
i FLUX (mJy)
10
20
30
40
v FLUX (mJy)
2
4
6
8

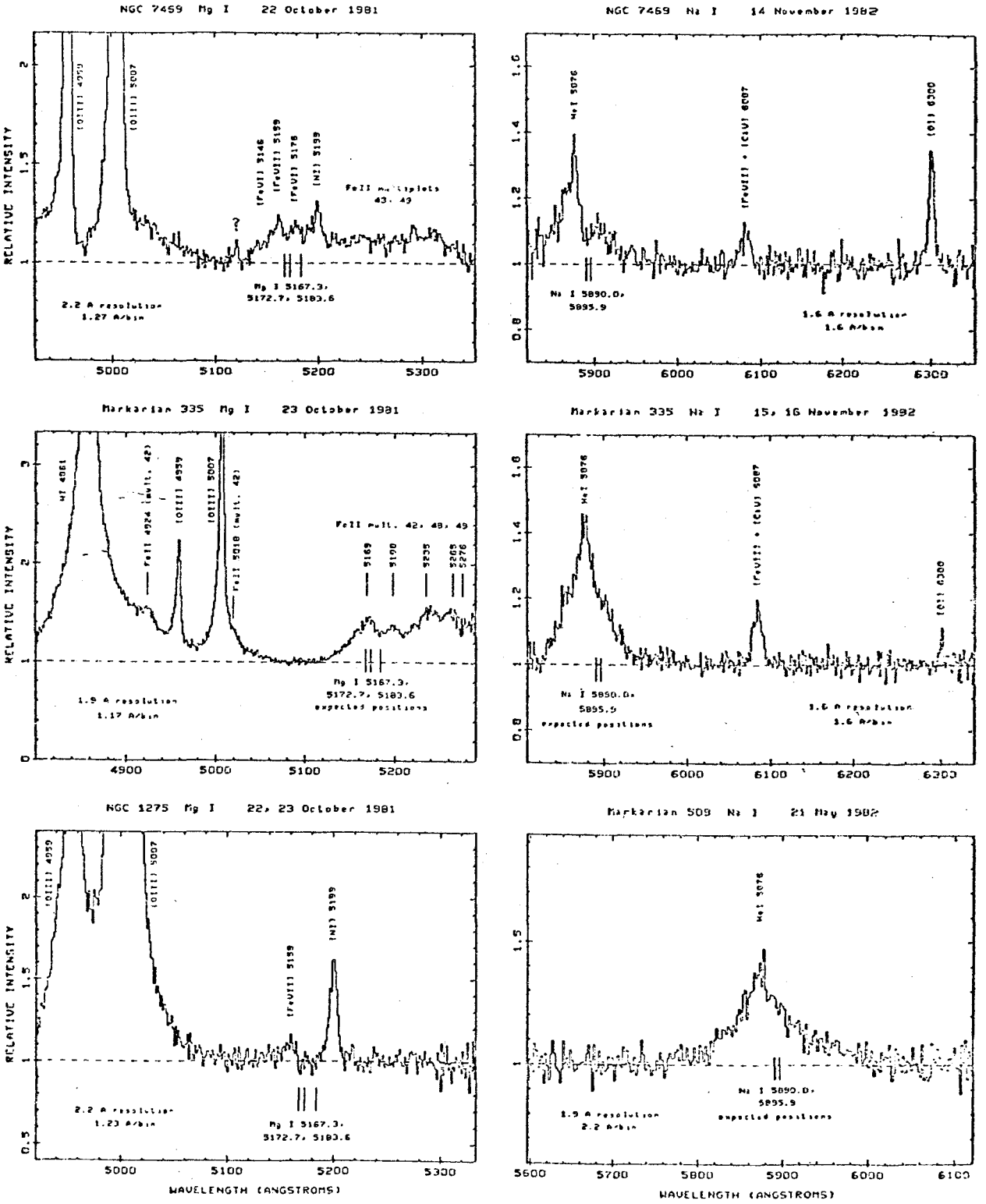
NGC 7469 Mg I 22 October 1981
NGC 7469 Na I 14 November 1982
Markarian 335 Mg I 23 October 1981
Markarian 335 Na I 15, 16 November 1982
NGC 1275 Mg I 22, 23 October 1981
Markarian 509 Na I 21 May 1982
RELATIVE INTENSITY
WAVELENGTH (ANGSTROMS)
Mg I 5167.3, 5172.7, 5183.6
Na I 5890.0, 5895.9
expected positions
2.2 A resolution
1.27 A/bin
1.6 A resolution
1.6 A/bin
1.9 A resolution
1.17 A/bin
2.2 A resolution
1.23 A/bin
1.9 A resolution
2.2 A/bin

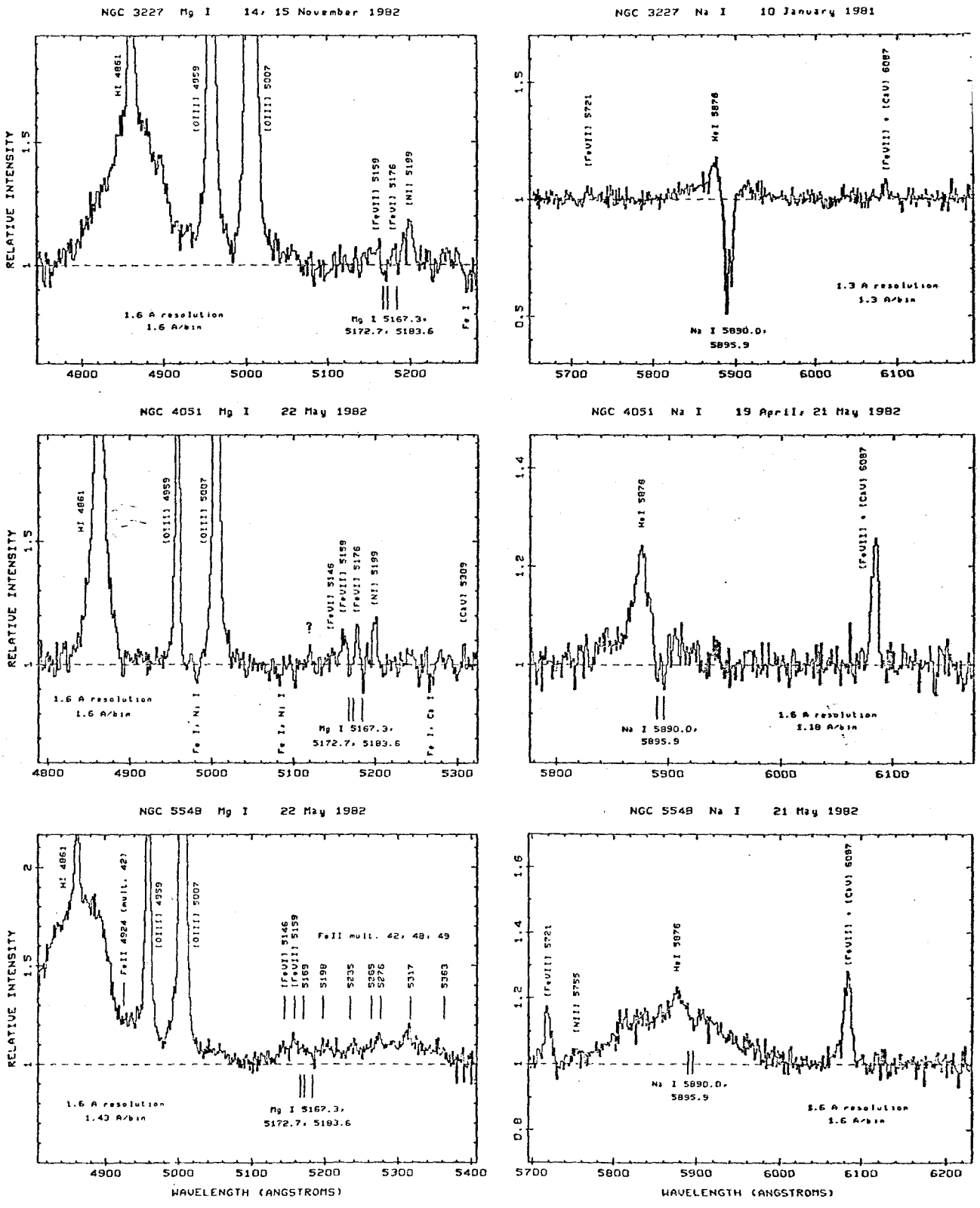
NGC 3227 Mg I 14, 15 November 1982
NGC 3227 Na I 10 January 1981
NGC 4051 Mg I 22 May 1982
NGC 4051 Na I 19 April, 21 May 1982
NGC 5548 Mg I 22 May 1982
NGC 5548 Na I 21 May 1982
RELATIVE INTENSITY
WAVELENGTH (ANGSTROMS)
HI 4861
[OIII] 4959
[OIII] 5007
[FeVII] 5159
[FeVI] 5176
[NII] 5199
[FeVII] 5721
NaI 5876
[FeVII] + [CaV] 6087
[FeVII] 5146
[CaV] 5309
FeII mult. 42, 48, 49
[NII] 5755
1.6 A resolution
1.6 A/bin
1.3 A resolution
1.3 A/bin
1.18 A/bin
1.43 A/bin
Mg I 5167.3, 5172.7, 5183.6
Na I 5890.0, 5895.9
Fe I, Ni I
Fe I, Ca I

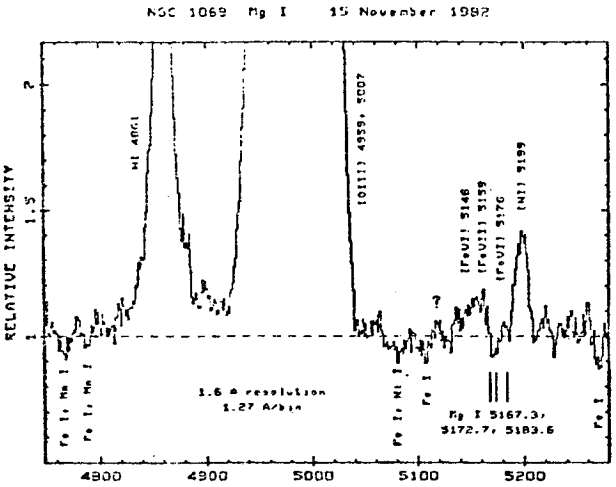
NGC 1068 Mg I 15 November 1982
RELATIVE INTENSITY
[OIII] 4959, 5007
[FeVII] 5146
[FeVII] 5159
[FeVII] 5176
[NI] 5199
1.6 A resolution
1.27 A/bin
Mg I 5167.3, 5172.7, 5183.6
4800
4900
5000
5100
5200

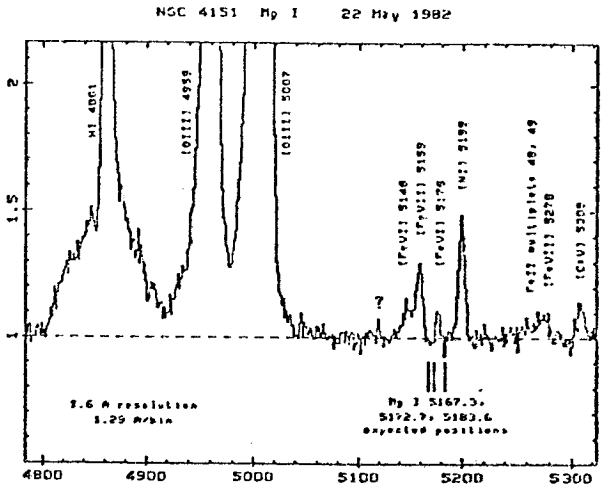
NGC 4151 Mg I 22 May 1982
[OIII] 4959
[OIII] 5007
[FeVII] 5146
[FeVII] 5159
[FeVII] 5176
[NI] 5199
1.6 A resolution
1.29 A/bin
Mg I 5167.3, 5172.7, 5183.6
expected positions
4800
4900
5000
5100
5200
5300

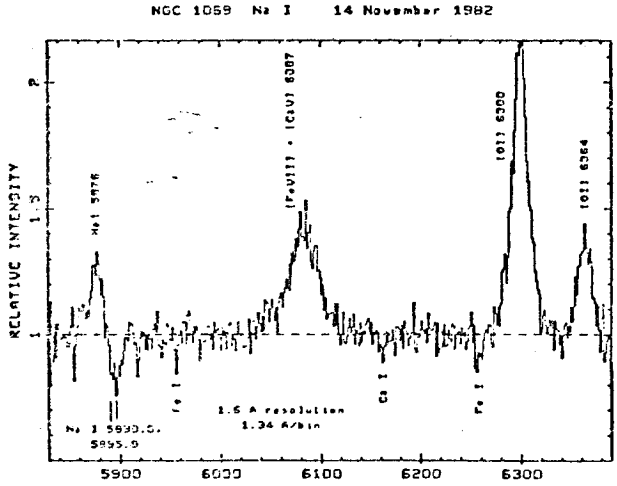
NGC 1068 Na I 14 November 1982
RELATIVE INTENSITY
NaI 5976
[FeVII] + [CaV] 6087
[OI] 6300
[OI] 6364
Na I 5890.0, 5895.9
1.6 A resolution
1.34 A/bin
5900
6000
6100
6200
6300

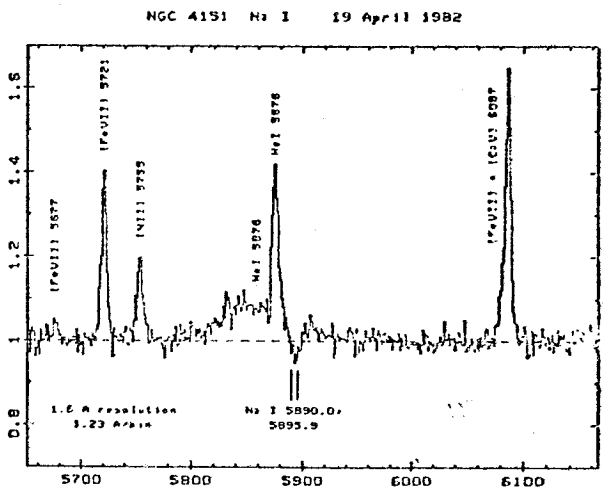
NGC 4151 Na I 19 April 1982
[FeVII] 5721
[NII] 5755
NaI 5976
[FeVII] + [CaV] 6087
1.6 A resolution
1.23 A/bin
Na I 5890.0, 5895.9
5700
5800
5900
6000
6100

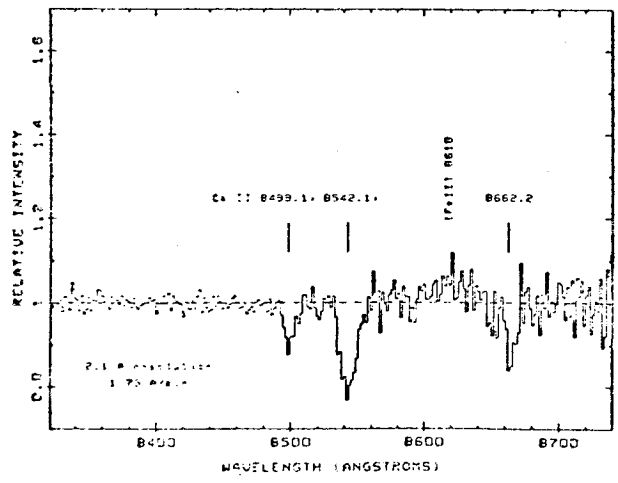
NGC 1068 Ca II 24 October 1981
RELATIVE INTENSITY
Ca II 8498.1, 8542.1
[FeII] 8618
8662.2
8400
8500
8600
8700
WAVELENGTH (ANGSTROMS)

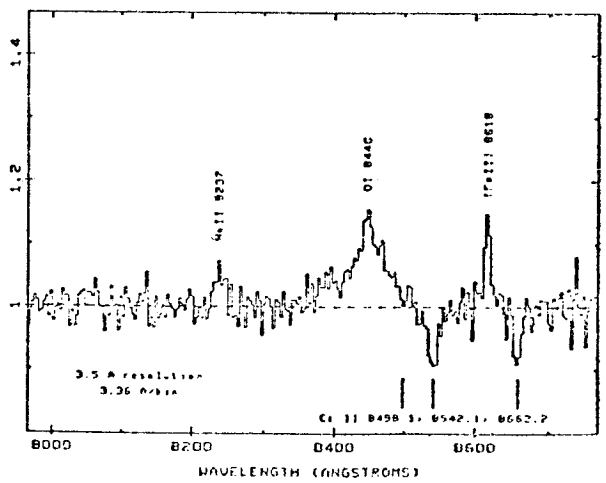
NGC 4151 Ca II 20 April 1982
NaI 8237
OI 8446
[FeII] 8618
3.5 A resolution
3.36 A/bin
Ca II 8498.1, 8542.1, 8662.2
8000
8200
8400
8600
WAVELENGTH (ANGSTROMS)

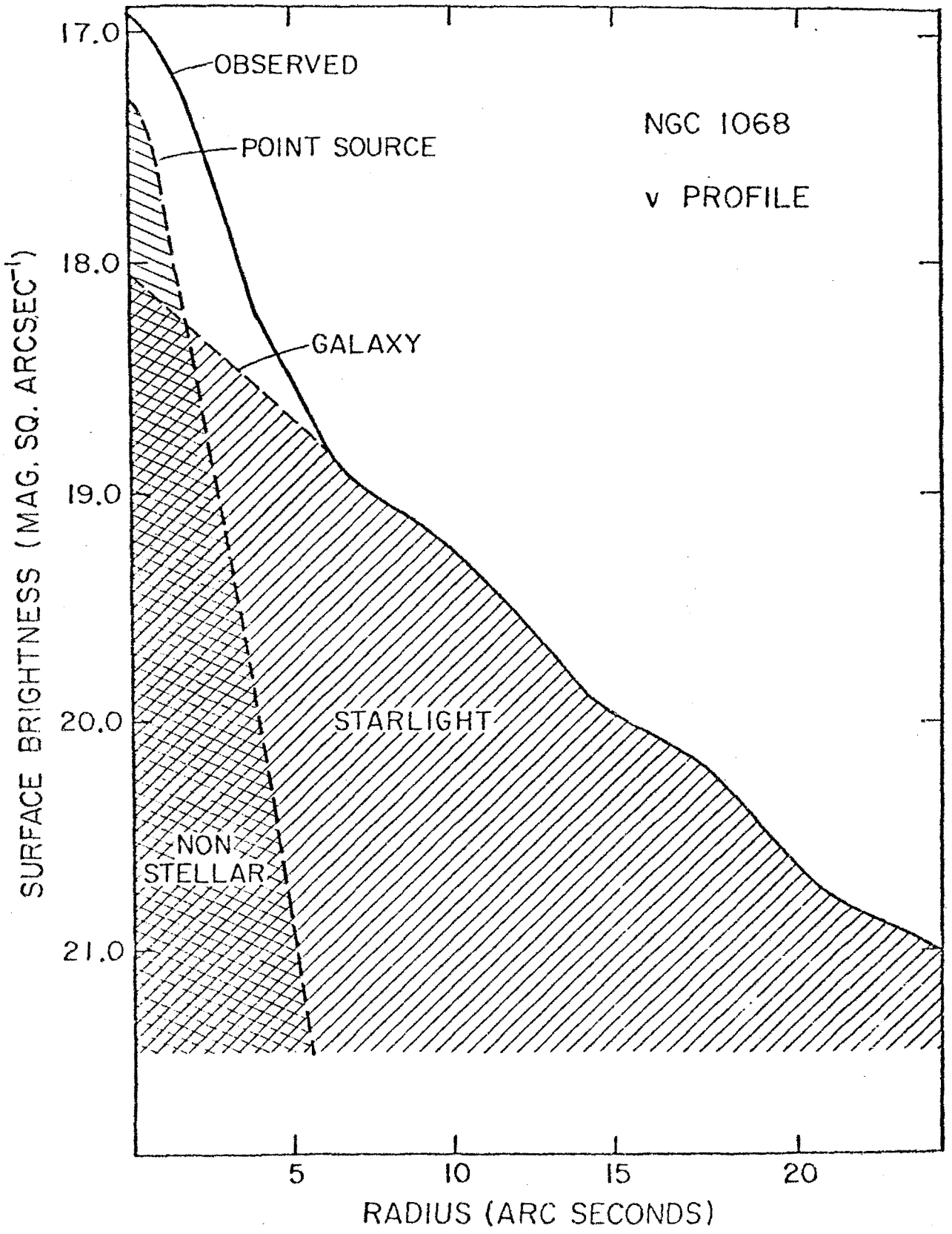
17.0
18.0
19.0
20.0
21.0
SURFACE BRIGHTNESS (MAG. SQ. ARCSEC^{-1})
OBSERVED
POINT SOURCE
GALAXY
STARLIGHT
NON STELLAR
NGC 1068
v PROFILE
5
10
15
20
RADIUS (ARC SECONDS)

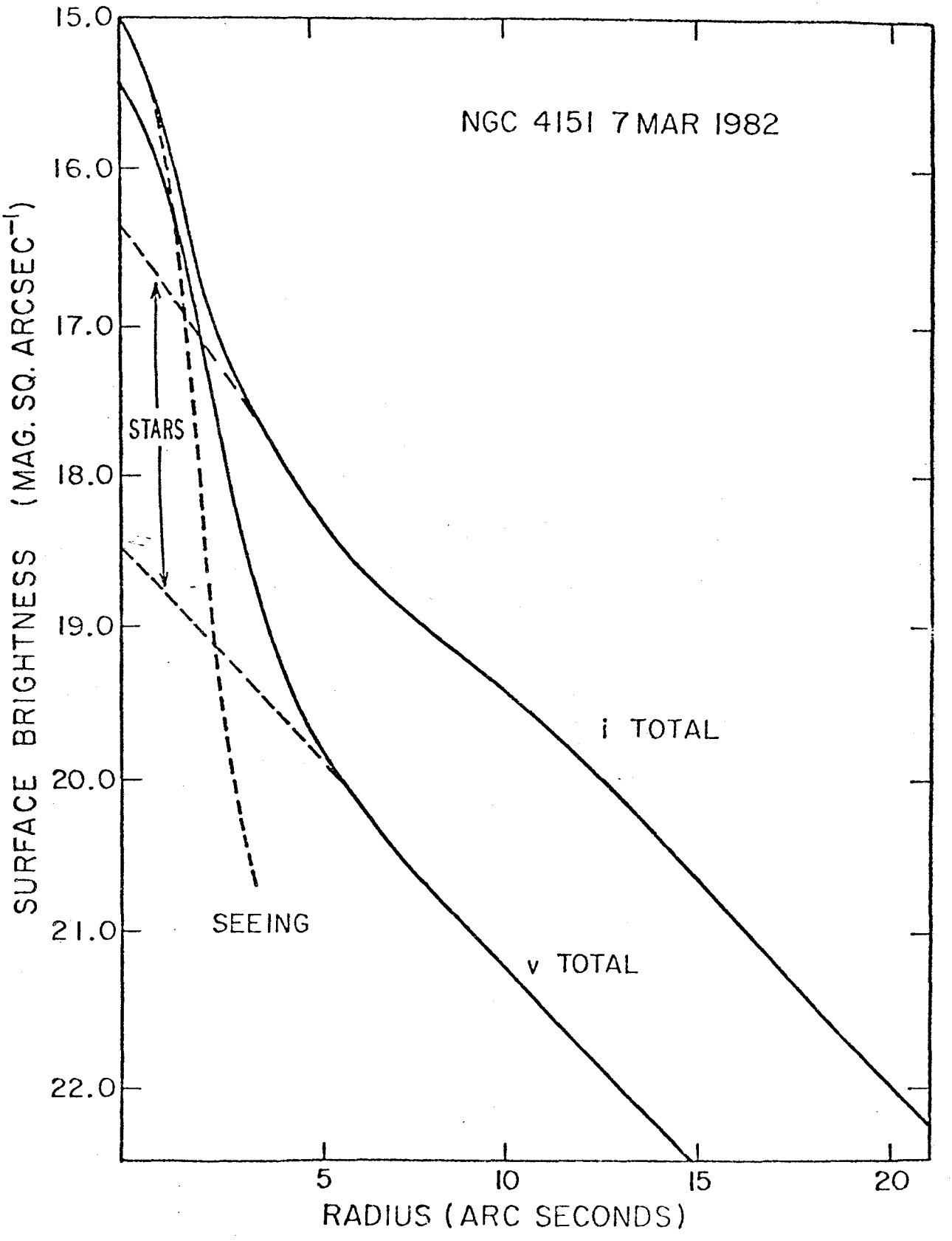
NGC 4151 7 MAR 1982
SURFACE BRIGHTNESS (MAG. SQ. ARCSEC^{-1})
15.0
16.0
17.0
18.0
19.0
20.0
21.0
22.0
STARS
SEEING
i TOTAL
v TOTAL
5
10
15
20
RADIUS (ARC SECONDS)

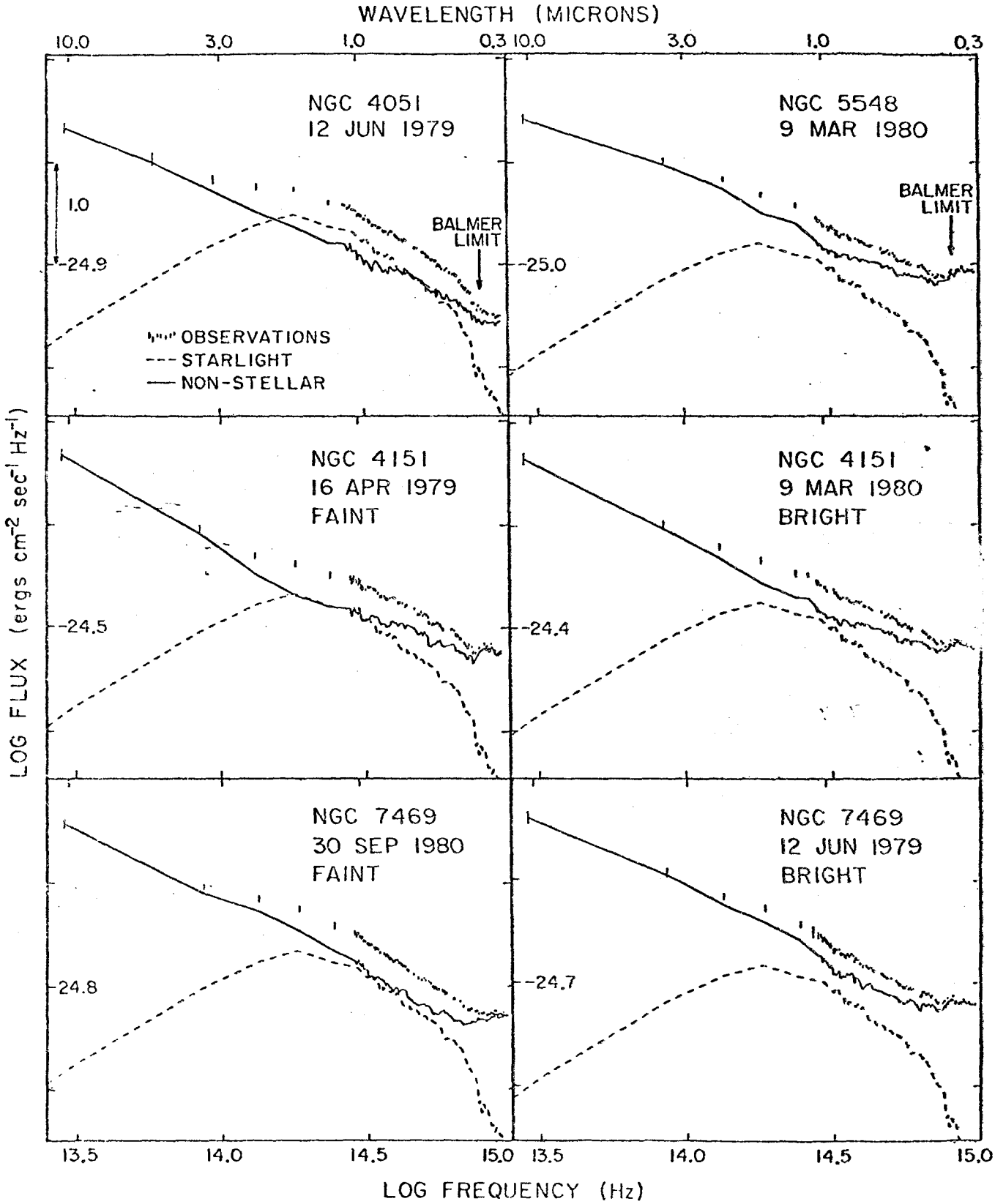
WAVELENGTH (MICRONS)
10.0
3.0
1.0
0.3
NGC 4051
12 JUN 1979
1.0
-24.9
BALMER LIMIT
OBSERVATIONS
STARLIGHT
NON-STELLAR
NGC 5548
9 MAR 1980
BALMER LIMIT
-25.0
NGC 4151
16 APR 1979
FAINT
-24.5
NGC 4151
9 MAR 1980
BRIGHT
-24.4
NGC 7469
30 SEP 1980
FAINT
-24.8
NGC 7469
12 JUN 1979
BRIGHT
-24.7
LOG FLUX (ergs cm^{-2} sec^{-1} Hz^{-1})
13.5
14.0
14.5
15.0
LOG FREQUENCY (Hz)

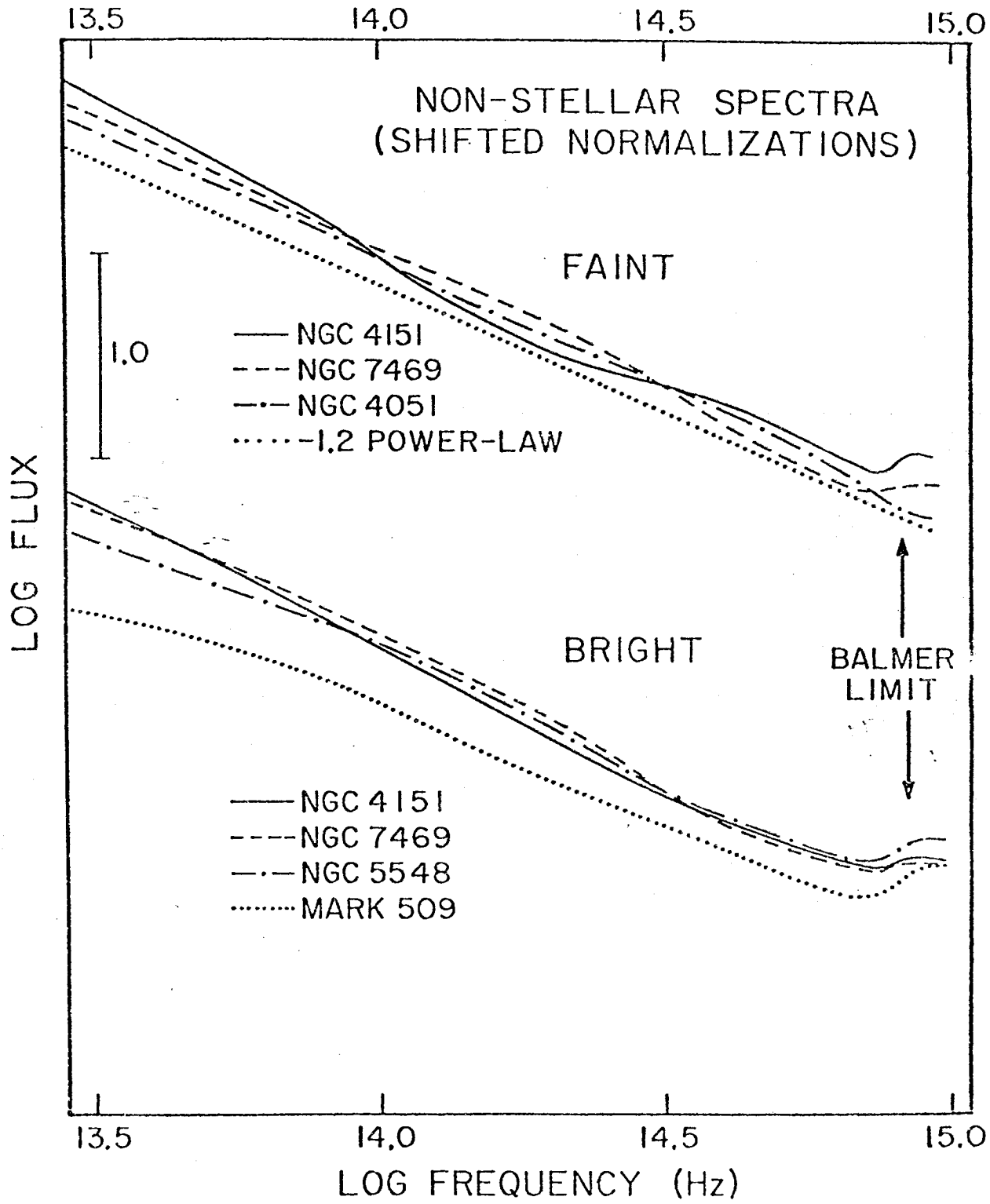
13.5
14.0
14.5
15.0
NON-STELLAR SPECTRA
(SHIFTED NORMALIZATIONS)
FAINT
1.0
NGC 4151
NGC 7469
NGC 4051
1.2 POWER-LAW
BRIGHT
BALMER
LIMIT
NGC 4151
NGC 7469
NGC 5548
MARK 509
LOG FLUX
LOG FREQUENCY (Hz)

The Underlying Galaxies of X-Ray-Selected Quasars

Matthew A. Malkan

Palomar Observatory; California Institute of Technology

Bruce Margon

University of Washington

Gary A. Chanan

Columbia University

Abstract

We have obtained deep red images of 24 X-ray selected quasars, using the SIT Area Photometer on the Palomar 1.5 meter telescope. About half were also imaged through green and violet filters. The images of all 15 of the quasars with redshifts up to 0.4 certainly are extended, the two at z=0.45 probably are, while the rest are too distant to be resolved. The resolved structures are 8 to 30 arc seconds across, symmetric, and centered on the point-like quasar nuclei. For most of the quasars we can roughly separate the nuclear light and the extended emission. The extended emission appears to be starlight from a surrounding galaxy. If so, we can deduce several properties of the host galaxy. Its colors, surface brightness, size, ellipticity, and association with groups of galaxies indicate that it is usually a normal spiral galaxy.

I. Introduction

The historical distinction between "quasars" and "Seyfert 1 galaxies" has been steadily crumbling over the past decade. Since there has never been a reliable photometric or spectroscopic criterion to distinguish them, the definitions are purely morphological. A "quasi-stellar object" is, by definition, unresolved in direct images (as in the Palomar Sky Survey, for example). Unfortunately the degree of resolution depends critically on the distance and luminosity of the object, and the plate scale, limiting magnitude, and image quality of the observations.

New imaging studies with greater sensitivity continue to resolve more and more objects previously known as quasars. Wyckoff, Wehinger, and Gehren (1981) found that 11 of 15 quasars they photographed had noticeably non-stellar images. Observing with slightly better seeing, Hutchings et al. (1982) could resolve all 28 quasars they observed with redshifts up to 0.45. These studies indicate that the historical distinction between "quasars" and "Seyfert 1 galaxies" resulted from insufficient resolution and sensitivity of previous ground-based observations. Thus the same active galaxy which, seen at low redshift would be called a "Seyfert," would be considered a "quasar" when seen at a redshift of more than 0.1--0.2. At this distance, the surrounding galaxy is too small and faint to be easily recognized.

Boroson and Oke (1982) and Boroson *et al.* (1983a, b) have shown that the extended emission ("fuzz") around 3C 48 (z=0.37) and 18 other luminous quasars has a stellar spectrum. Spectroscopy is a key to proving that the resolved light is an underlying host galaxy. Once this is established, it is far more efficient to study the host galaxy through direct imaging, which is two orders of magnitude more sensitive, and allows study of the entire galaxy at once.

Most of the previous imaging has utilized photographic plates, which have yielded little color information. For this application, two-dimensional electronic detectors are better, since:

1) their vastly higher quantum efficiency makes the same observations possible on smaller telescopes,

2) the digitized linear output is much easier to reduce and reliably calibrate, and

3) a large field of view is not required.

In this paper we analyze deep electronic images of a sample of 24 quasars which were first discovered as serendipitous X-ray sources by the Einstein Observatory Imaging Proportional Counter. They were then confirmed as quasars by spectroscopy (Chanan, Margon, and Downes 1981). The X-ray selection technique is free of many of the biases of most quasar searches. It tends to find quasars at lower redshift and lower luminosities, which are ideal

for imaging studies. Some of our preliminary results were presented at the 159th meeting of the AAS (Malkan, Margon, and Chanan 1982).

II. Observations

We observed all but one of the 19 quasars identified by Chanan, Margon and Downes (1981), and 9 more unpublished quasars discovered in the same way. Our only selection was for objects at favorable elevations over Palomar when the observations were made. These objects should be representative of X-ray selected quasars as a whole. Nearly all the quasars in this sample are brighter than 19th magnitude, and 0.01 Einstein IPC counts/second.

The images were obtained on 13 clear nights in 1980--1982 at the Cassegrain focus of the 1.5 meter telescope. The detector, an SIT digital area photometer described by Kent (1979), has a field of 256 x 256 square pixels, each 0.72 arc seconds on a side. A standard set of broad-band filters was used to measure colors on the Gunn photometric system (Thuan and Gunn 1976). The vgr bandpasses are preferable to the corresponding BVR colors because they reject the strongest night-sky emission lines.

The SIT has a limited dynamic range. A single exposure saturates with 2,000 detected photons per pixel, so the maximum signal/noise ratio for an individual pixel is 40. To obtain long integrations without saturating the central parts of the quasar image, we added several consecutive 300--600 second exposures. Four of these were observed only in short exposures, and their magnitudes are included in Table 1. The peak position of the quasars was measured to an accuracy of a few tenths of an arc

second in each frame. Small shifts (up to a few pixels) were then applied to align the frames before they were stacked. The total integrations were 1,500--2,500 seconds for each filter. Each pixel typically detected 1,000--2,000 night-sky photons. The one-sigma photon statistical fluctuations in the night-sky in an individual pixel correspond to brightnesses of 24.7, 25.0, and 24.5 magnitudes per square arc sec with the violet, green, and red filters, respectively.

The erase level was measured each night by averaging about 10 null-exposure images. This average erase frame was then subtracted from all the other frames. They were then flattened by dividing by an average of exposures of the uniformly illuminated dome ceiling, to eliminate variations in the sensitivity over the 3 arc minute field. The images of the quasars were centered in the frames, so that the pincushion distortion from the image tube was unimportant. The average sky level was measured for pixels in an annulus (typically 30 to 50 arc seconds in diameter) surrounding each object.

The observing log in Table 1 gives the total magnitudes measured in a 14 arc second aperture. Repeated observation of quasars and standard stars throughout the night indicates that the photometry is accurate to 0.1--0.2 mag. The agreement with the magnitude estimates in CMD is satisfactory, except for 1059+730, where the CMD value is more than a magnitude brighter than ours. We suspect that much of this discrepancy is due to the soft image

of this low-redshift object on the Sky Survey print which CMD used to estimate its magnitude. Photoelectric photometry (Neugebauer et al. 1982) of 6 quasars agrees with ours, except for 0100+020 and 0318-196, which may have been ~1 mag. fainter when they were imaged. Malkan's (1983) detailed study of the continuous spectrum of 0302-223 agrees with the present magnitude estimate, and he found no variability over the last two years.

A representative sample of three images is shown in Plate 1. Except for 1526+286, most of the quasar images do not show strong departures from circular symmetry. To maximize the signal/noise ratio in the faint outer parts of the image, we summed up the signal in circular annuli each one pixel wide, centered on the peak determined previously. This allows us to measure brightnesses in the outer parts of images at 1% of the sky brightness. In the same way, unsaturated images of bright stars in the same fields were also reduced to radial brightness profiles. Under good seeing conditions the detector produces stellar images with a full-width at half-maximum of 1.5 arc seconds. Observations made when the seeing was worse than 2.0 arc seconds were omitted. Thus all the various seeing profiles used in our analysis were quite similar.

Four objects in our sample were also observed by Hutchings et al (1982) on red-sensitive III-a-F photographs. Our relative red intensity profiles agree very well with theirs.

III. The Extended Emission

All 7 quasars at redshifts greater than 0.5 are unresolved. Figure 1e is a blow-up of the profiles of two high-redshift quasars plotted against seeing profiles determined from stars on the same frames. Down to about 1% of the peak brightness, both quasar profiles agree with the seeing profiles (FWHM=2 arc sec), with no deviations exceeding 10—15%. Below this level error increases due to uncertainties in determining the sky background. The figure also illustrates that the seeing profile did not vary much during the night.

Although the image of 0919+515 is resolved, it lies on the wings of a bright field star 11" away, preventing us from making an accurate sky subtraction. We did not include it in our profile analysis.

The images of the quasars 0844+377 (Figure 1d) and 1526+286, both at z=0.45, appear to be resolved, but they are not much larger than the resolution limit set by the seeing. The image of 1526+286 is asymmetric, partly because of a faint object 7 arc seconds east of the quasar. The image of 0844+377 may also be confused by a faint object 5 arc seconds east-southeast. In any case, it is clear that the following analysis of the resolved images applies only to these two distant quasars in a very approximate way.

All 15 quasars with redshifts less than 0.4 are certainly resolved. Three cases are illustrated in Figures 1a--c. Most of the remaining brightness profiles are even more easily resolved than these examples. The best explanation of the extended emission is that it is the starlight of a galaxy in which the quasar nucleus resides. If these objects were closer, they would probably have been classified as "high-luminosity Seyfert 1 galaxies." At their large distances from us, their nuclear light gives them a stellar appearance on the Palomar Sky Survey. All previous imaging results are also consistent with our hypothesis. Slit spectra of the fuzz around 1059+730 (Balick and Heckman 1983) confirm that it is starlight from a normal galaxy at the quasar redshift. Therefore, in much of what follows, we assume that the extended light comes from a host galaxy, so that we may study it in more detail.

Table 1 also gives the axial ratio (b/a) of each resolved image and its position angle at an isophote of 25.4 red magnitudes per square arc sec. Repeated measurements on different nights show that the ratios are accurate to 0.1, and the position angles to 5 or 10 degrees.

A. Colors

We have images with more than one filter for 9 quasars with prominent resolved emission. In these, we were able to measure the colors of the extended emission in a series of annuli centered on the nucleus. They are plotted in the lower parts of Figures 1a and 1b. The colors change sharply from the nucleus to the halo,

leveling off at radii larger than 7 arc seconds, where the contribution from the nucleus becomes negligible. This constant level is the color of the starlight, uncontaminated by the quasar nucleus.

The observed vgr colors of the host galaxies are plotted with slashes in Figure 2. When only g-r colors are available, they are plotted on the right side of the graph. The lines show the K-corrections which should be applied if the extended light comes from a galaxy at the quasar's emission-line redshift. They were calculated by William Sebok (private communication) using the energy distributions for Sb galaxies from Wells (1972) and the Thuan and Gunn (1976) filter response curves. Thus the X's give the actual zero-redshift colors of the host galaxies. The open circles and squares represent the colors of the disks of Seyfert 1 and 2 galaxies, respectively, measured with the same telescope, detector, and filters by Yee (1983). The small black dots represent the colors of E and S0 galaxies from Thuan and Romanishin (1981). Also shown are the approximate average colors of spiral galaxies, which were estimated from photometry that one of us (MM) also obtained with the same instrument. The host galaxies have the same colors as the nearby Seyfert galaxies, but are on the average bluer than E and S0 galaxies by 0.15 ± 0.05 mag. in g-r, and 0.45 ± 0.15 mag. in v-g. Their colors are the first observational evidence that they are early to intermediate-type spiral galaxies.

The zero point of the vgr colors is defined by an F6 subdwarf. Starburst galaxies, whose light is dominated by A stars, are often observed to have negative v-g and g-r colors. The galaxy around 3C 48 has a continuous spectrum dominated by A stars (Boroson et al. 1982). But our results show that in these less luminous cases the quasar phenomenon is not associated with such an intense burst of star formation throughout the host galaxy. The work of Malkan and Filippenko (1983) and Yee (1983) leads to the same conclusion for the low-luminosity Seyfert 1 galaxies.

B. Ellipticities

Seventy per cent of the resolved quasars have outer isophotes which are detectably non-circular. The histogram of the axial ratios (b/a) is shown in Figure 3. The true ratios could be a little smaller, since there has been some image degradation from the (circularly symmetric) seeing. It is virtually impossible to measure true inclinations for quasar galaxies beyond z=0.35, as the seeing makes them nearly round. Therefore we cross-hatched all objects in Figure 3 with z>0.35, as a reminder that they may well have intrinsic axial ratios considerably less than 0.9. The distribution we observed is very similar to the one Hutchings et al. (1982) found for 26 quasars (also shown in Figure 3). Neither distribution is the same as those of elliptical, S0, or spiral galaxies, as measured by Sandage et al. (1970). (Their axial ratios are shown for comparison). Even without correcting for seeing, there is no excess of round (b/a=1.0--0.8) objects such as

is seen among elliptical galaxies. Many of the quasar galaxies are moderately inclined, like the disk systems. Yet their ellipticity distribution differs from that of spiral galaxies because it lacks any nearly edge-on objects. It seems very unlikely that image degradation from seeing could explain away all of this deficiency.

The histogram of Keel's (1980) axial ratios for Seyfert 1 galaxies, plotted at the bottom of Figure 3, is very similar to those of quasar galaxies. Most of the known Seyfert galaxies are clearly spirals, and no Seyfert nucleus has been conclusively shown to reside in an elliptical galaxy (Adams 1977). Yet there are few highly inclined Seyfert galaxies, probably for the same reason that edge-on quasar galaxies are not found: there is a selection against finding active galactic nuclei viewed through the heavy obscuration of a dusty, edge-on disk. Thus the ellipticities of quasar galaxies are at least consistent with the hypothesis that they are intrinsically flattened, like the disks of spiral galaxies. The lack of highly inclined systems is what we would expect, from a comparison with the ellipticities of nearby Seyfert galaxies, and an allowance for the seeing.

C. Radial Brightness Profiles

We have attempted to separate the resolved light from the quasar nucleus by fitting the radial brightness profiles. The extended light was assumed to have one of two possible shapes: an $r^{1/4}$ law $I(r)=I_b\ 10^{-3.331(r/r_{eff})^{1/4}}$, appropriate for bulge-dominated systems; or an exponential disk $I_e=I_d\ e^{-r/r_d}$, as in spiral

galaxies, These distributions were numerically convolved with the seeing profile, and added to a variable amount of unresolved light. Thus the fits determined two independent parameters: the characteristic length scale of the galaxy, and the ratio of its flux to the point source. The effective radius (r_{eff} encloses half of the light) and I_{eff} (surface brightness at that radius) from the bulge fits are listed in Table 2. The exponential scale length and central surface brightness from the disk fits are listed in Table 3. When green and red images were available, we list the average scale length, since the two images usually gave the same result to within 20%. We note that the colors of the starlight are more accurately determined by the annular measurements above, than from the fits in Table 3.

Some exponential + point source fits to surface brightness profiles of representative quasars are shown by the solid and dashed lines in Figures 1a--d. Table 4 gives the effective surface brightness ($I_{eff}=I_B/2140$), corrected for redshift by $(1+z_{em})^4$, and converted to blue magnitudes by assuming B-r=1.2 and B-g=0.7 mag. (see Section A above). It also lists the scale lengths, transformed to kiloparsecs, again assuming the galaxy is at the emission-line redshift.

(i) Bulges

The formal fitting uncertainties in the bulge parameters in Table 2 are usually less than 20%. The fits with spheroidal components are usually not altered much much by small increases in the effective surface brightness, as long as they are offset by corresponding decreases in r_{eff}. That is, these fitting parameters are highly anti-correlated. However, the product $F_{gal}=22.67\ I_{eff}\ r_{eff}^2$ is quite accurately determined.

We made several numerical simulations to test for systematic errors which could bias the results. We calculated surface brightness profiles for model elliptical galaxies (obeying an $r^{1/4}$ law) with a superimposed point source in their nuclei. The bulge parameters were selected to be similar to those actually observed. After adding an appropriate amount of random noise to the profiles, we convolved them with the seeing. The smeared profiles were then fitted in the same way as the observed quasar profiles. As long as the starlight exceeds that of the point source, and the effective radius is at least as large as the seeing FWHM, the fitting procedure recovers the correct bulge parameters, to 20 or 30%. Table 2 shows that this condition is satisfied by most of the quasar images we resolved. As pointed out by Hutchings et al. (1982), the error is systematic in the sense that the total amount of galactic light as well as I_b are <u>under-estimated</u>. This is because at large distances, the center of the galaxy begins to appear indistinguishable from the seeing profile, and is incorrectly attributed to a point source. Seeing could lead to the

weak correlation of scale length with redshift we find. Or, if the trend is real, it may simply be the result of a selection effect. At low redshift, the underlying galaxy must have a small angular extent so that the quasar is not classified as a Seyfert 1 galaxy; at high redshift, it must be intrinsically large to be resolved at all.

Schneider et al. (1983) made similar numerical simulations of cluster elliptical galaxies (lacking nonthermal nuclei). They found they could very accurately recover r_{eff} and I_{eff} even when r_{eff} was only half the seeing FWHM.

The derived bulge parameters are compared with those of elliptical galaxies in Figure 4, which plots B_{eff} against r_{eff}. The data for normal and compact ellipticals, and cD galaxies are from a summary by Kormendy (1980). The solid line shows the relation he found (adjusted to our choice of Hubble Constant):

$$B_{eff} = 3.28 \log r_{eff} + 19.9 \text{ B mag. arcsec}^{-2}$$

which gives a good fit to virtually all the ellipticals studied. If the galaxies around the quasars we are studying were ellipticals, Figure 4 shows that they would be systematically different from those previously measured. For a given r_{eff}, they tend to be an average of 0.5--1.0 mag. too faint in the center. Alternatively, for a given total magnitude, they tend to be several times too large. Although some of the galaxies could be consistent with the standard elliptical relation, those of 0037+061, 0120+091, 0351+026, 1403+546, 1519+279, 1557+272, and 1704+607 lie well away

from the region defined by elliptical galaxies. The discrepancy in these cases (one to two magnitudes in B_{eff}) is too large to be explained by random or systematic errors.

In many objects, the assumption that the underlying galaxy is spheroidal would require that a substantial portion (e.g. 25--50%) of the light in the center of the image come from stars. Elliptical galaxies have strong stellar absorption lines (such as Ca II H and K, the G band, Mg I b, and Na I D). Even with a 50--75% dilution from nonstellar light, these strong absorption lines would be detectable in spectra with good signal-to-noise ratios. The discovery spectra by CMD did not reveal any obvious absorption lines, but the integrations were usually stopped soon after strong emission lines were detected. Obtaining better spectra, and then following the procedure Malkan and Filippenko (1983) used for nearby Seyfert 1 galaxies would decisively settle the question of whether any of these host galaxies are ellipticals.

(ii) Disks

Since many of the galaxies are not quite circularly symmetric, we corrected the fitted disk parameters to their intrinsic face-on values. We numerically calculated the azimuthally-averaged radial brightness profiles of pure exponential disks viewed at various inclinations. For disks with $b/a>0.5$, the resulting radial brightness profile is still fitted to within a few per cent by an exponential law over 5 magnitudes of brightness. The fitted scale length is approximately /b/a times the true de-projected scale

length (along the major axis). The fitted central surface brightness is a/b times the true (face-on) value. The values in the tables have all been corrected in this way for inclination.

The agreement between the exponential scale lengths determined for different images of the same quasars, confirms that the measured lengths are physically meaningful, and accurate to 15 or 20%. Allowing for the different choice of Hubble Constant, our estimates of the extent, scale height, and absolute magnitude agree with those estimated by Hutchings et al. (1982) in all four cases.

We also made numerical simulations to test for systematic errors when fitting the combination of point source + exponential disk. Since their respective light profiles are very different, they are easier to separate. We found that the true amount of galactic light is underestimated by only 10 or 20%, as long as it exceeds that of the nuclear point source, and its characteristic radius is larger than the seeing FWHM.

There are several ways to compare the structure of these quasar galaxies with that of spiral disks. Figure 5 shows the blue central surface brightness, corrected to face-on, plotted against the exponential scale-length of the disk. The dark circles show the values for the disks of spiral galaxies studied by Boroson (1981), and the open circles represent the disks of S0 galaxies, from Burstein (1979). The distribution of central surface brightness and scale length in the quasar galaxies is <u>identical</u> to

that of ordinary spiral galaxies. We find disk surface brightnesses of 21.95±0.86, remarkably similar to 21.79±0.78, the distribution Boroson (1981) found in spirals. Although our objects are many times more distant than those studied by Boroson, this close agreement supports our view that the estimated galaxy parameters in Table 4 are not seriously flawed by lack of spatial resolution. There is a marginal indication that the quasar galaxies have lower central surface brightnesses than S0 galaxies. There is certainly no tendency for the quasar disks to have unusually luminous disks--several have M_B of -19 or fainter. If the host spirals were sites of massive bursts of star formation (as could be happening in 3C 48), the disks should be much brighter than observed.

Our estimates of disk central surface brightnesses agree reasonably with Yee's (1983) findings for the disks of Seyfert galaxies. His values were, on average, several tenths of a magnitude brighter, but he attributes this small difference to observational and selection effects in his study. The exponential scale lengths we found overlap very well with Yee's.

Figure 6 is the plot of the average radius at a blue isophote of 26.6 mag/sq. arc sec (the Holmberg radius) versus the total blue magnitude of the galaxy within that radius. This diagram is particularly useful because the plotted quantities are more precisely determined than those in Figures 2--4. The Holmberg isophote is reached well outside the central seeing profile, but is

typically a magnitude above the faintest detectable isophote. As discussed above, the total galaxy magnitudes are also better determined than their detailed structural parameters, due to the presence of anti-correlated fitting errors. Within the uncertainties, the quasar galaxies all lie exactly along the sequence defined by spiral galaxies measured in the Hercules cluster by Peterson, Strom, and Strom (1981). This remarkable agreement indicates that the Holmberg radius/absolute magnitude diagram will be a powerful tool in future studies of quasar morphology.

The average ratio of the bulge effective radius r_{eff} to disk scale length r_0 in spiral galaxies is 0.3 ± 0.2 (Boroson 1981). If the host spiral galaxies in our sample also have ordinary spheroidal components, those would be so small that they would be indistinguishable from a point source. Our numerical models confirm that any bulge light superimposed on a disk is entirely attributed to the "point source" by the fitting procedure. Since Boroson (1981) finds $\langle \log \text{Bulge/Disk} \rangle = -0.54\pm0.56$, this effect only leads to substantial under-estimate of the total galactic light in spiral galaxies with unusually large bulge-to-disk ratios.

(iii)Comparison

In most of the well-resolved quasars, the fit with a pure bulge galaxy is too centrally peaked, and the fit with a disk gives a better match with the observed profile. Two thirds (18 of 27) of the brightness profiles are better fitted by the point source +

exponential than the point source + spheroidal. In several cases, such as 0038+071 (illustrated in Figure 1f), and 0318-196 and 1701+610, replacing the exponential with an $r^{1/4}$ law more than doubles the sum of the squared residuals. For the remaining 9, most of the bulge fits are only insignificantly better than the disk fits. In five of these cases, the profile obtained with the other filter gives the opposite result--a better fit with the disk. Although 0351+026 and 1557+272 are somewhat better fitted with the pure bulge, as noted above, their derived bulge parameters would make them unique among elliptical galaxies. (The detection of 21 cm and optical line emission from 0351+026 (Bothun et al. 1983) would also be very unusual). Only for 1526+286 could the brightness profile suggest the underlying galaxy is elliptical. But, as mentioned above, its image is too complex and poorly resolved to take this indication very seriously. Thus the fitting results themselves rule out the possibility that all the host galaxies are elliptical, with no disk component. Among the remaining galaxies which can be fitted well with bulges, several would have structural parameters extremely unlike those of normal elliptical galaxies. It seems likely that many, if not all of the host galaxies have a disk component, and are probably spirals. It this is true, we can further conclude that the structural parameters of their disks are the same as those of ordinary spirals.

Compared to the exponential disk, the bulge distribution is more centrally peaked, like the seeing profile (see Figure 1f). A larger portion of the unresolved light in the center is attributed to stars. Therefore the bulge galactic magnitudes are 0.4--0.7 mag brighter than those made assuming it is a pure disk. Table 5 lists the magnitudes of the point source found from the fits to the brightness profiles of each quasar. As expected, the fits assuming a bulge galaxy always find less point source flux, because the bulge has a strong central brightness peak. We can always set an upper limit to the point source (as Wyckoff et al. 1981 did) by matching the seeing profile to the central peak of the quasar brightness profile. In effect, this is the practical result of our exponential disk fits. When the galaxy is assumed to be a pure exponential disk, the light at the center of the image is almost entirely attributed to the point source. Since the starlight contribution to the flux at the center of the image can never be negative, the point source derived in the exponential fits is within 0.1--0.2 mag. of an absolute upper limit. It is essentially the maximum allowed flux from a point source, on the assumption that it produces essentially all of the light in the center of the image. Since the amount of light from the point source is sometimes only 25--35% of the total, it may be significantly over-estimated by our fitting procedure (and probably any other one as well). The true contribution from a point source cannot be measured with better than ~50% accuracy when it is superposed on a bulge component with a comparable total flux and an

effective radius less than twice the seeing FWHM.

IV. Companion Galaxies

Although the fields imaged in this study were relatively small, we frequently found faint non-stellar images near those of the quasars. The most dramatic example, 0351+026, shares a common luminous envelope with a bluer galaxy with g~18.4, about 13" south. It has already been studied in detail by Bothun et al. (1982).

Our classification is very cautious: we only refer to objects as "galaxies" if their surface brightness distributions are unmistakably resolved. Nonetheless we often find galaxies less than an arc minute away from the program quasars. The most likely cases of physical association are discussed individually:

0100+021: has a galaxy with normal colors and g~17.5 45" west-southwest, and one with g~18.5 60" to the northeast.

0844+377: has at least a dozen faint objects within an arc minute.

0919+515: has two unusually blue galaxies 35" south-southeast (g~19.5) and 45" north-northeast (g~20.5) and a galaxy (r~19) 100" to the southeast.

1059+730: has an unusually blue galaxy with g~20 only 15" west-southwest. Two other galaxies, 70" north-northeast (g~19.5 and normal colors), and 75" south (r~20; colors not measured) could possibly be chance superpositions from the field.

1339+053: has two rather blue galaxies, one with g~18.5 20" south, and one with g~19 50" west-southwest.

1519+279: has a blue galaxy (g~19.5) 60" to the northeast, and four galaxies with normal colors, 50" east-northeast, and 60" north-northwest (both g~20), 45" east (g~19.5), and only 13" east (g~21).

1701+610: has two galaxies (both r~17.5) 25 and 35" to the north-northwest, and one with r~20 only 19" to the northwest (see Plate I).

2344+184: has one galaxy 30" north with g~18 and normal colors, and two galaxies with g~19 and 20 about 100 and 90" to the north-northeast. Several fainter images are also visible on Plate I within about 60" of the quasar.

Green and Yee used the same instrument to study the association of faint galaxies and quasars. In their 108 control fields (each a degree north of a quasar) they found slightly fewer than one galaxy with $17 < r < 19$ in an average 9 square arc minute frame. They point out that their estimated galaxy field density agrees very well with those of Kron (1982) and Sebok (1983). Thus, the higher frequency with which we find galaxies near the quasars indicates they are related in a statistical sense, although we cannot be sure of the association in individual cases.

At a redshift of ~0.13, the field of view of our frames is comparable to the core (D~500 Kpc) of a rich galaxy cluster. Schneider's (1983) luminosity functions for clusters at this redshift indicate that we would see at least 4--10 galaxies with r < 18 and more than twice as many with r < 19 in any frame centered on a rich cluster. Hintzen et al.'s (1982) study of the cluster of galaxies around 3C 275.1 (z=0.557) offers an interesting contrast to our observations. In a six times smaller field of view, they found ~20 galaxies brighter than R=22.66. Our observations could not fail to detect such a cluster at a lower redshift. Yet we do not find nearly such a high density of galaxies in any of our frames. Thus none of the ten quasars in this study with $0.06 \leq z \leq 0.17$ reside in the cores of rich galaxy clusters. The association of quasar galaxies with small groups but not rich clusters (studied in more detail by Yee and Green 1983) is again consistent with the hypothesis that they are primarily spiral, rather than elliptical galaxies.

Conclusions

We imaged a sample of X-ray selected quasars with an SIT detector. Every quasar with a redshift up to 0.4 is resolved, and we analyzed the extended light on the assumption that it comes from a galaxy with the quasar in its nucleus. There are several reasons to believe that most of the galaxies are ordinary early to intermediate-type spirals:

1) Their vgr colors are significantly bluer than those of E and S0 galaxies, but much redder than those of late-type spirals.

2) More of the systems are elongated ($b/a \leq 0.8$) than would be expected if they were elliptical galaxies.

3) They have radial brightness profiles which are best fitted with exponential laws which have central surface brightnesses and scale lengths typical of spiral disks.

4) Although they are sometimes found in small groups of galaxies, they are not located in the cores of rich clusters.

We thank Skip Staples and Bob Griffith for assistance at the telescope, W. L. W. Sargent, D. Schneider, and K. Borne for helpful discussions, C. Santillan for help with some preliminary data analysis, and the Fannie and John Hertz Foundation for financial support. This work could not have been undertaken without the superb image processing package written at Caltech by William Sebok, to whom we are deeply indebted. This work was supported through NSF grant NAG 5-49 to W. L. W. S.

Table 1 Observing Log and Photometry

QUASAR	z	DATES	v	g	r	b/a	Pos.	Angle$_d$
0031-076	.29	18 Oct 80				18.0	0.9	5:
0031-077[a]	.39	17 Oct 80				18.3		
0037+061	.063	18,19 Oct 80	17.6		16.9	16.4	0.75	-20
0100+021	.39	17 Oct 80			17.3	17.2	0.9	20
0120+091	.17	18 Oct 80			17.9	17.5	0.85	35
0121+03[a]	.34	18 Oct 80				18.5		
0240+007	.57	17 Oct 80				16.9	U	
0302-223	1.41	18 Oct 80				16.3	U	
0318-196	.11	18,19 Oct 80	16.8		16.5	16.0	0.8	10
0351+026	.036	8 Mar,19 Oct 80	16.5		16.3	15.9	0.65	-10
0844+377	.45	18 Oct 80			18.2	18.3	0.9	30:
0919+515	.16	17 Oct 80			17.4		.85	50:
1059+730	.089	21 May 82	16.7		16.4	16.1	0.6	70
1339+053	.27	20 May 82	16.7		17.0	16.7	0.7	25
1403+546	.082	27 Nov 80				17.1	0.7	60
1519+279	.23	19 May 82	17.7		17.8	17.9	0.85	65
1526+286	.45	08 Mar 80				16.5	0.9	-80:
1557+272	.065	12 Mar 80					0.7	-25
1640+401	.99	31 Mar 81				17.9	U	
1640+399	.55					18.8	U	
1641+399	.59	25 May 80				19.8	U	
1701+610	.16	25 Apr 80,27 Oct 80			17.6	17.1	0.8	30
1704+607	.080	25 Apr 80,27 Oct 80			17.7	17.2	0.85	-15
1726+499	.81	25 Apr 80				18.0	U	
1847+334	.51	31 Mar 81				17.5	U	
2215-037[a]	.24	27 Oct 80				16.8		

2216-041[a]	.24	27 Oct 80		17.3		
2344+184	.14	17 Oct 80	17.7	17.0	0.85	-50

---

[a] although we lack deep images for these quasars, their magnitudes were measured on short exposures.

[b] photometric uncertainties are one to two tenths of a magnitude

[c] axial ratios are accurate to 0.1. Therefore b/a=0.9 means that the image shows no significant departures from perfectly round.

[d] 0 degrees means the major axis runs north-south; position angle increases as it rotates clockwise.

U unresolved image, indistinguishable from the seeing disk

no information about the shape of any extended emission since it is not detected

Table 2: Bulge Paramters from Surface Brightness Profile Fitti

QUASAR	$r^{1/4}$ Fitting Parameters		
QUASAR	r_{eff} [a]	m_g [b]	m_r [b]
0031−076	2.8		17.9
0037+061	3.3	16.7	16.45
0100+021	2.8	18.0	18.2
0120+091	3.1	18.2	17.85
0318−196	1.5	16.7	15.9
0351+026	3.1	16.4	16.15
0844+377	1.8	18.4	18.9
1059+730	2.0	16.8	16.4
1339+053	4.2	18.0	17.5
1403+546	2.0		17.3
1519+279	1.9	19.5	19.6
1526+286	2.7		17.0
1557+272	3.5		17.05
1701+610	3.8		16.5
1704+607	3.0		17.5
2344+184	2.5	17.5	16.8
Uncertainty	±30%	±0.3	±0.3

[a] the average of the green and red effective radii is given, in arc sec

[b] total bulge magnitude integrated to infinity ($F=22.67\ I_{eff}\ r_{eff}^2$)

Table 3: Disk Parameters from Surface Brightness Profile Fitting

QUASAR	Exponential Fitting Parameters				
	r_o [a]	I_o	m_g [b]	I_o	m_r [b]
0031-076	2.1			22.2	18.6
0037+061	2.8	21.3	17.3	21.0	16.8
0100+021	2.3	22.0	18.7	23.1	19.0
0120+091	2.6	23.0	18.6	22.4	18.2
0318-196	2.0	20.8	17.4	20.2	16.8
0351+026	2.7	21.2	17.1	21.0	16.7
0844+377	1.6	22.0	19.0	23.0	19.3
1059+730	2.6	21.7	17.4	20.0	16.4
1339+053	4.5	23.6	18.5	23.2	18.0
1403+546	2.9			22.1	17.9
1519+279	2.1	23.6:	19.9	23.4:	19.9
1526+286	1.9			20.9	17.6
1557+272	3.2			22.0	17.5
1701+610	3.2			21.5	17.1
1704+607	2.6			22.0	18.0
2344+184	2.3	21.6	17.9	21.3	17.3
Uncertainty	±20%	±0.3	±0.2	±0.3	±0.2

Scale lengths are listed in arc seconds; surface brightnesses are in magntidues per square arc second.

Both are corrected to face-on.

[a] the average value of r_o for the g and r images is given. The actual (slightly different) fitting values were used to calculate total galaxy magnitudes.

[b] the galaxy magnitudes refer to <u>all</u> the light, integrated

out to infinite radius, using $F = 2 \pi r_0^2 I_0$

Table 4: Derived Galaxy Parameters

	If Host Galaxy is a Spheroidal			If it is a Disk			
QUASAR	r_{eff}(Kpc)	B_{eff}	M_B[a]	r_0(Kpc)	B(0)	M_B[c]	Holm. Rad.
0031-076	10	23.5	-21.6	8	22.2	-20.9	26
0037+061	4	23.1	-19.8	3.3	21.7	-19.4	13
0100+021	12	22.7	-22.2	10	21.6	-21.6	29
0120+091	8	23.8	-20.8	7	22.6	-20.4	19
0318-196	2.7	20.9	-21.3	3.7	20.9	-20.5	16
0351+026	2.1	22.4	-19.2	1.9	21.4	-18.6	11:
0844+377	9:	22.0:	-22.8:	8:	21.1:	-22.3:	29
1059+730	3.1	21.8	-20.6	4	21.2	-20.3	19
1339+053	15	23.7	-22.1	16	22.9	-21.5	35
1403+546	2.9	22.9	-19.5	4.1	22.9	-18.8	12
1519+279	6	23.9	-20.0	7	23.2	-19.4	16
1526+286	12	22.0	-23.6	9	20.3	-23.0	36
1557+272	4.2	23.9	-19.1	3.9	22.8	-18.6	11
1701+610	9	23.2	-21.6	8	22.0	-21.0	26
1704+607	4.2	24.1	-19.0	3.7	22.9	-18.5	11
2344+184	5.7	22.8	-21.0	5	21.6	-20.6	18
Uncertainty	±30%	±0.4	±0.3	±20%	±0.3	±0.2	±15%

[a] assuming H_0=70 km/sec/Mpc and q_0=0

[b] surface brightnesses corrected for redshift, K dimming, and interstellar extinction

[c] ignoring possible bulge component

Table 5 Magnitudes of Point Sources

QUASAR	Green		Red	
	Bulge	Disk[a]	Bulge	Disk[a]
0031-076			18.6	18.1
0037+061	—[b]	17.3	17.4	16.7
0100+021	17.4	17.3	17.5	17.2
0120+091	17.8	17.8	17.7	17.4
0318-196	17.7	16.8	16.5	15.8
0351+026	17.1	16.3	17.8	17.4
0844+377	18.8	18.0	18.4	18.1
1059+730	16.7	16.2	16.9	16.3
1339+053	17.0	16.7	16.5	16.4
1403+546			17.8	17.1
1519+279	17.6	17.5	17.8	17.6
1526+286			17.2	16.6
1557+272			—[b]	17.7
1701+610			17.5	17.4
1704+607			17.2	17.1
2344+184	—[b]	19.2	19.0	17.2
Uncertainty	±0.6	±0.4	±0.6	±0.4

[a] Since these magnitudes include any possible bulge component, they are actually absolute upper limits to the possible amount of nuclear light.

[b] Point source not confidently detected, i. e. fit not substantially improved by its addition.

REFERENCES

Adams, T. F. 1977, Ap. J. Suppl., 33, 19.

Balick, B. and Heckman, T. M. 1983, Ap. J. (Letters), 265, L1.

Boroson, T. A. 1981, Ap. J. Suppl., 46, 177.

Boroson, T. A. and Oke, J. B. 1982, Nature, 296, 397.

Boroson, T. A. and Oke, J. B. 1983, preprint.

Boroson, T. A, Oke, J. B., Green, R. F. 1982, Ap. J., 263, 32.

Bothun, G. D., Mould, J., Heckman, T., Balick, B., Schommer, R. A., and Kristian, J. 1982a, Astron. J., 87, 1621.

Bothun, G., Romanishin, W., Margon, B., Schommer, R. A., and Chanan, G. A. 1982b, Ap. J., 257, 40.

Burstein, D. 1979, Ap. J., 234, 435.

Burstein, D. and Heiles, C. 1982, Astron. J., 87, 1165.

Chanan, G. A., Margon, B., Downes, R. A. 1981, Ap. J. (Letters), 243, L5.

Hintzen, P., Boeshaar, G. O., and Scott, J. S. 1981, Ap. J. (Letters), 246, L1.

Hutchings, J., Crampton, D. and Campbell, B. 1982, Ap. J. (Letters), 261, L23.

Hutchings, J. B., Crampton, D., Campbell, B., Gower, A. C., Morris, S. C. 1982b, Ap. J., 262, 48.

Hutchings, J. B., Crampton, D., Campbell, B., and Pritchet, C. 1981, Ap. J., 247, 743.

Keel, W. 1980, Astron. J., 85, 198.

Kent, S. M. 1979, Pub. A. S. P., 91, 394.

Kormendy, J. 1980, in ESO Workshop on Two-Dimensional Photometry, ed. P. Crane and K. Kjar (Geneva: ESO), p. 191.

Kron, R. G. 1980, Ap. J. Suppl., 43, 305.

Malkan, M. A. 1983, Ap. J., 268,

Malkan, M. A. and Filippenko, A. V. 1983, Ap. J., in press.

Malkan, M. A., Margon, B., Chanan, G. 1982, Bull. Amer. Astr. Soc. 14, 958.

Neugebauer, G., Soiffer, T., Matthews, K., Margon, B., Chanan, G. A. 1982, Astron. J., 87, 1639.

Peterson, B. M., Strom, S. E., Strom, K. M. 1979, Astron. J., 84, 735.

Sandage, A. R., Freeman, K., Stokes, N. R. 1970, Ap. J., 160, 831.

Schneider, D. P., Gunn, J. E., and Hoessel, J. G. 1983, Ap. J.

Sebok, W. L. 1982, Ph. D. thesis, California Institute of Technology, Pasadena.

Thuan, T. X., Gunn, J. E. 1976, Pub. A. S. P. 88, 543.

Thuan, T. X. and Romanishin, W. 1981, Ap. J. 248, 439.

Wells, D. C. 1972, Ph. D. thesis, University of Texas, Austin.

Wyckoff, S., Wehinger, P. A., Gehren, T. 1981, Ap. J., 247, 750.

Yee, H. K. 1983, Ap. J., in press.

FIGURE CAPTIONS

Figure 1a. The azimuthally averaged v, g, and r surface brightness profiles of quasar 0037+061. The observations are shown by the dots. The best point source + exponential fits are shown by the lines. The lower panel shows the v-g and g-r annular colors as a function of radius.

Figure 1b. Same as 1a, for quasar 0120+092.

Figure 1c. Same as 1c, for quasar 0100+021. The unresolved nuclear light was too strong to allow a reliable determination of the color in the outer annuli.

Figure 1d. Same as 1c, for quasar 0844+377. The lower solid line shows the point source we derived from brightness profile fitting. The observed quasar profile (solid dots) appears to be marginally resolved.

Figure 1e. Expanded plots of four radial surface brightness profiles of unresolved images. The dots represent two quasars, with redshifts of 0.51 (filled circles) and 0.99 (open circles). The solid and dashed lines are profiles of stars on the same frames. They are indistinguishable from those of the quasars.

Figure 1f. A comparison of the exponential disk and $r^{1/4}$ bulge fits for the red surface brightness profile of 0037+061. The thin lines are the two estimates of the point source. As discussed in the text, 0.4—0.7 mag. more light is attributed to the point source when the remaining light is assumed to follow an

exponential law, which lacks a sharp central peak. The long-dash line shows the exponential disk light; alternately, the short-dash line shows the galaxy light if it is assumed to obey an $r^{1/4}$ law.

Figure 2. The colors of the resolved light, as measured in annuli with diameters of 14" and greater, are indicated by slashes. The X's represent the colors, K-corrected to zero-redshift. The resolved light has similar colors to the outer parts of Seyfert 1 and 2 galaxies measured by Yee (1983), which are shown by the open circles and squares, respectively. These colors are significantly bluer than those of E and S0 galaxies (filled circles) measured by Thuan and Romanishin (1981). Yet they are not nearly as blue as the average colors of later-type spiral galaxies.

Figure 3. Distributions of axial ratio (b/a), in logarithmic bins. The top two histograms are for the quasar host galaxies in this study and that of Hutchings et al. (1982). Objects with high redshifts are shown with cross-hatching, because seeing probably leads us to seriously overestimate their axial ratios. Neither distribution has the peak of round (b/a>0.8) objects seen in elliptical galaxies. Yet there is a deficiency of nearly edge-on quasar galaxies in comparison to S0 and spiral galaxies (also from Sandage et al. 1970). The most similar histogram is that of Seyfert 1 galaxies, measured by Keel (1980), which is shown at the bottom. Obscuration from the galactic disk probably leads to a selection against finding edge-on active galaxies.

Figure 4. Bulge parameters derived assuming an $r^{1/4}$ brightness distribution. The crosses are the values found for the quasar host galaxies in this study. The comparison points are from the compilation of Kormendy (1980): the filled dots represent elliptical galaxies, open circles represent compact galaxies, and the filled squares represent cD galaxies. The steep dashed lines indicate constant absolute magnitudes M_B=−19 and −23. The solid line shows Kormendy's empirical relation for spheroidal systems. About half of the quasar host galaxies lie well above this line, outside the region defined by normal ellipticals.

Figure 5. Disk parameters derived assuming an exponential brightness distribution. The crosses are the values found for the quasar host galaxies in this study. The filled circles represent spiral galaxies from Boroson (1981), and the open circles represent S0 galaxies from Burstein (1979). The spiral and quasar galaxies have identical distributions in this diagram. The Seyfert galaxies also have fairly similar structural parameters. The dashed lines are loci of constant absolute magnitude, M_B=−19 and −22.

Figure 6. The Holmberg radius/absolute magnitude relation for the quasar galaxies, compared with spiral galaxies in the Hercules and Virgo clulsters photometered by Peterson, Strom and Strom (1979). The straight line is their fit to the Hercules spirals. It also happens to fit the quasar galaxies almost perfectly. As they noted, the Virgo spirals appear to be 0.6 mag brighter at a given radius than those in Hercules.

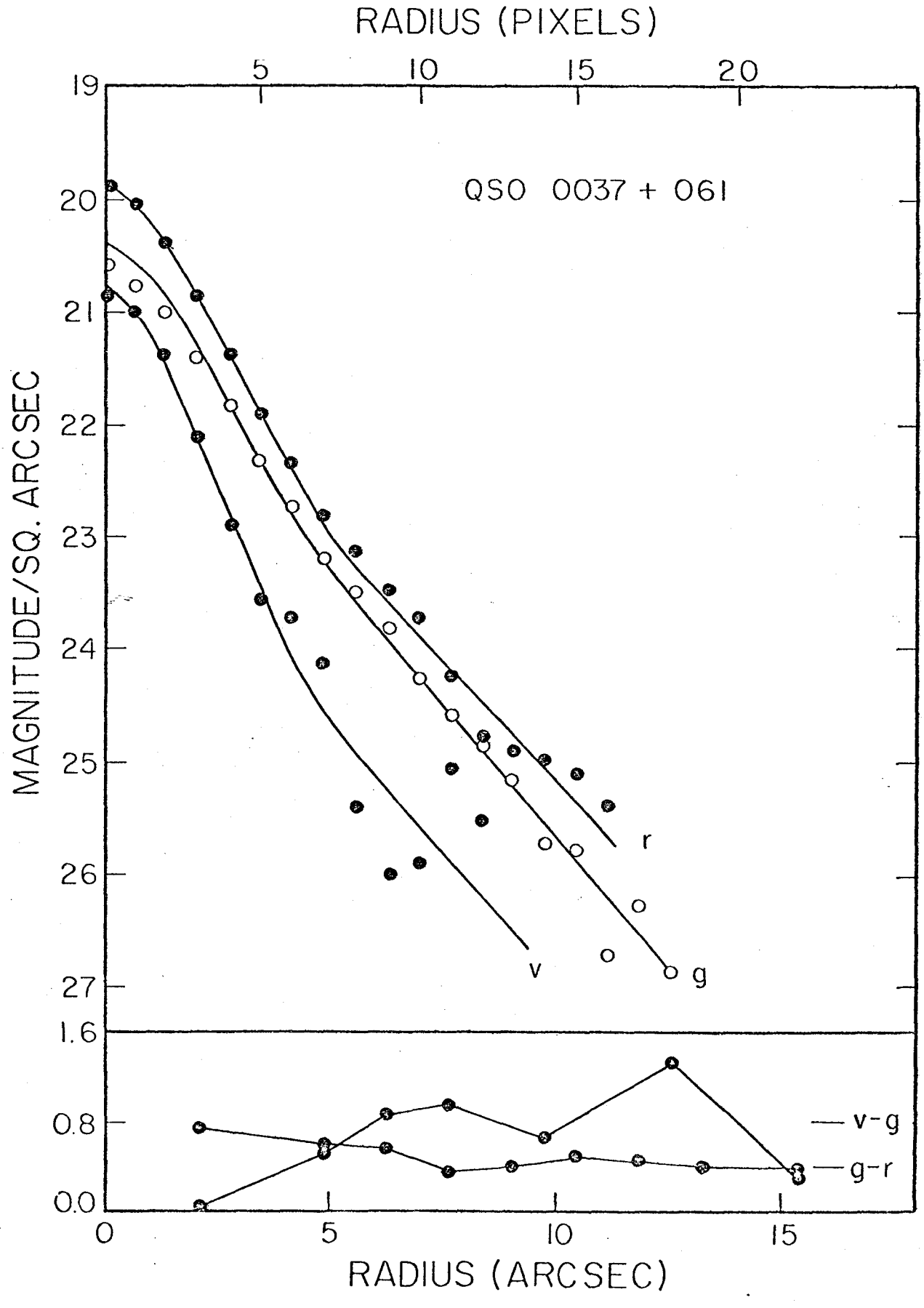
RADIUS (PIXELS)
5
10
15
20
19
20
21
22
23
24
25
26
27
QSO 0037 + 061
r
g
v
MAGNITUDE/SQ. ARCSEC
1.6
0.8
0.0
v-g
g-r
0
5
10
15
RADIUS (ARCSEC)

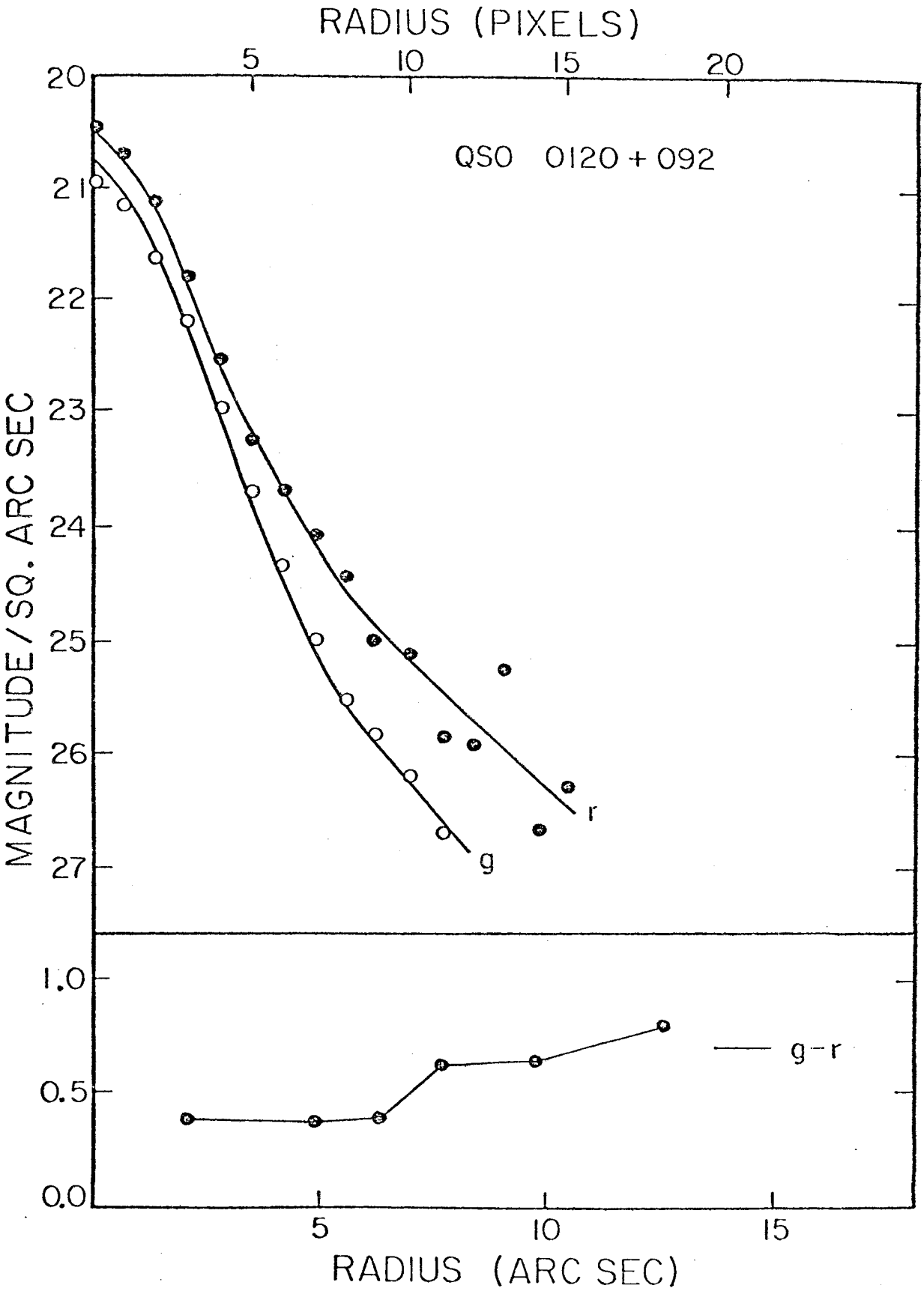
RADIUS (PIXELS)
5
10
15
20
QSO 0120+092
MAGNITUDE/SQ. ARC SEC
20
21
22
23
24
25
26
27
r
g
1.0
0.5
0.0
g-r
5
10
15
RADIUS (ARC SEC)

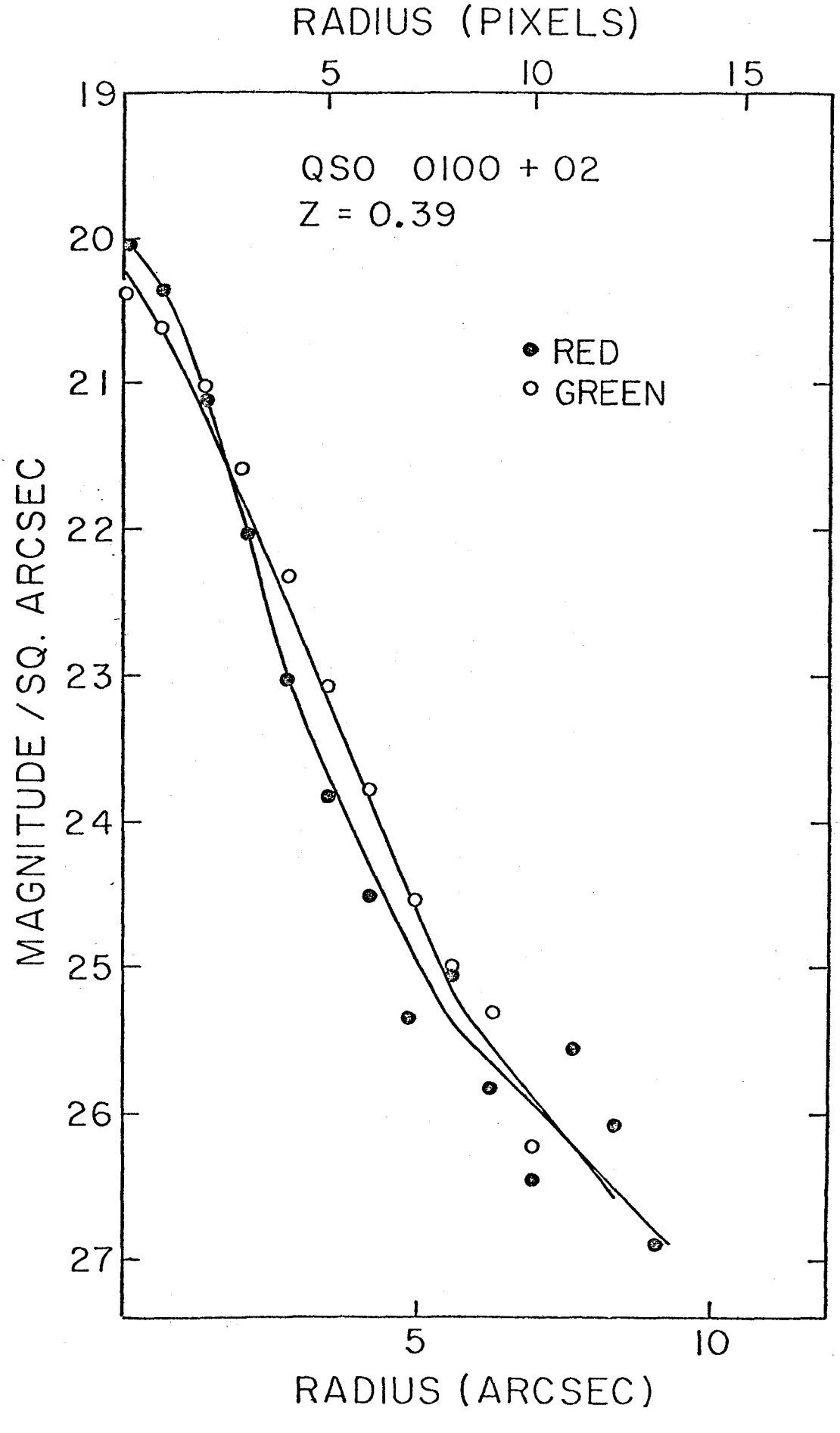
RADIUS (PIXELS)
5
10
15
19
20
21
22
23
24
25
26
27
QSO 0100 + 02
Z = 0.39
RED
GREEN
MAGNITUDE / SQ. ARCSEC
5
10
RADIUS (ARCSEC)

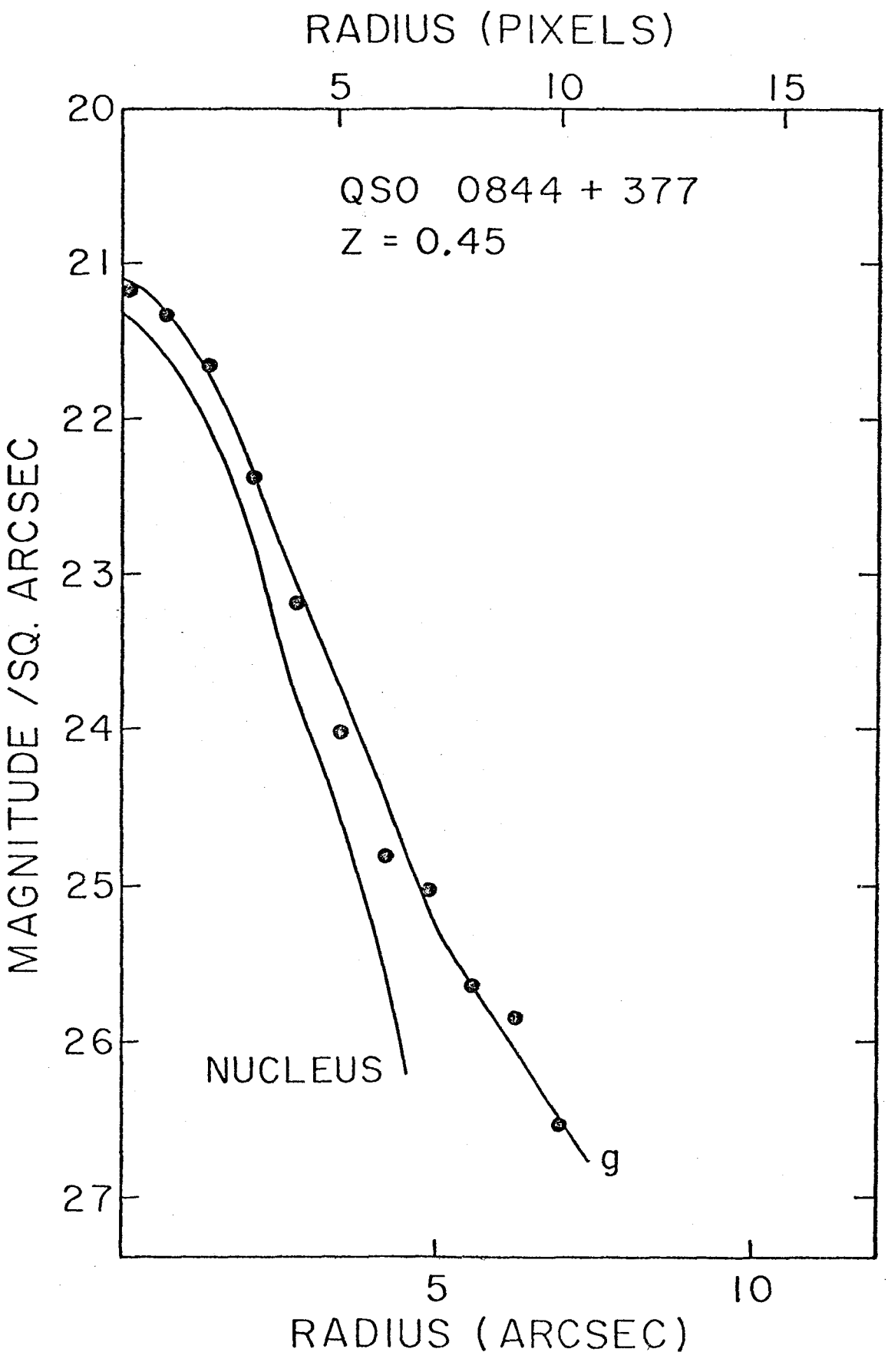
RADIUS (PIXELS)
5
10
15
20
21
22
23
24
25
26
27
QSO 0844 + 377
Z = 0.45
MAGNITUDE /SQ. ARCSEC
NUCLEUS
g
5
10
RADIUS (ARCSEC)

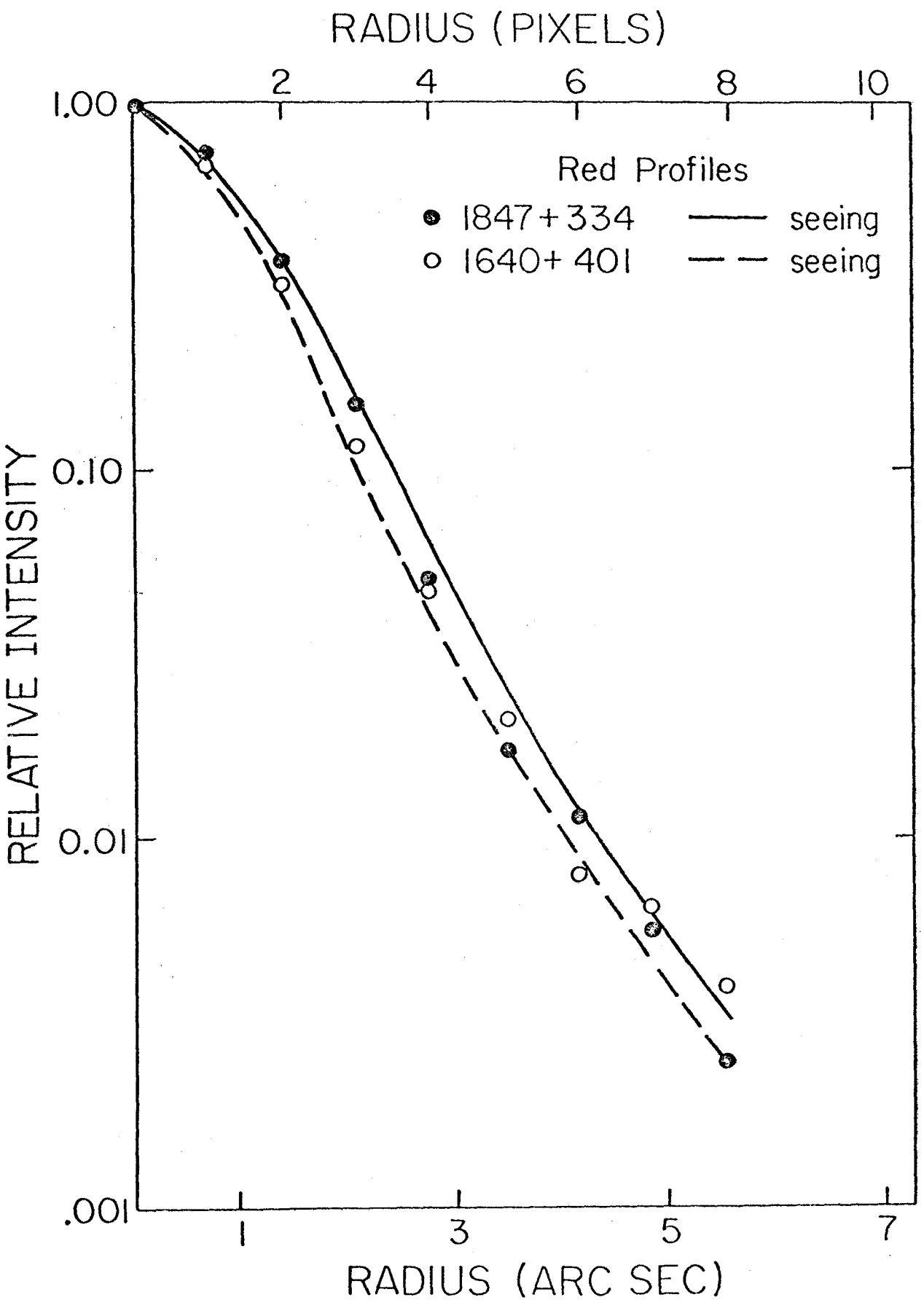
RADIUS (PIXELS)
2
4
6
8
10
1.00
0.10
0.01
.001
RELATIVE INTENSITY
Red Profiles
1847+334
seeing
1640+401
seeing
1
3
5
7
RADIUS (ARC SEC)

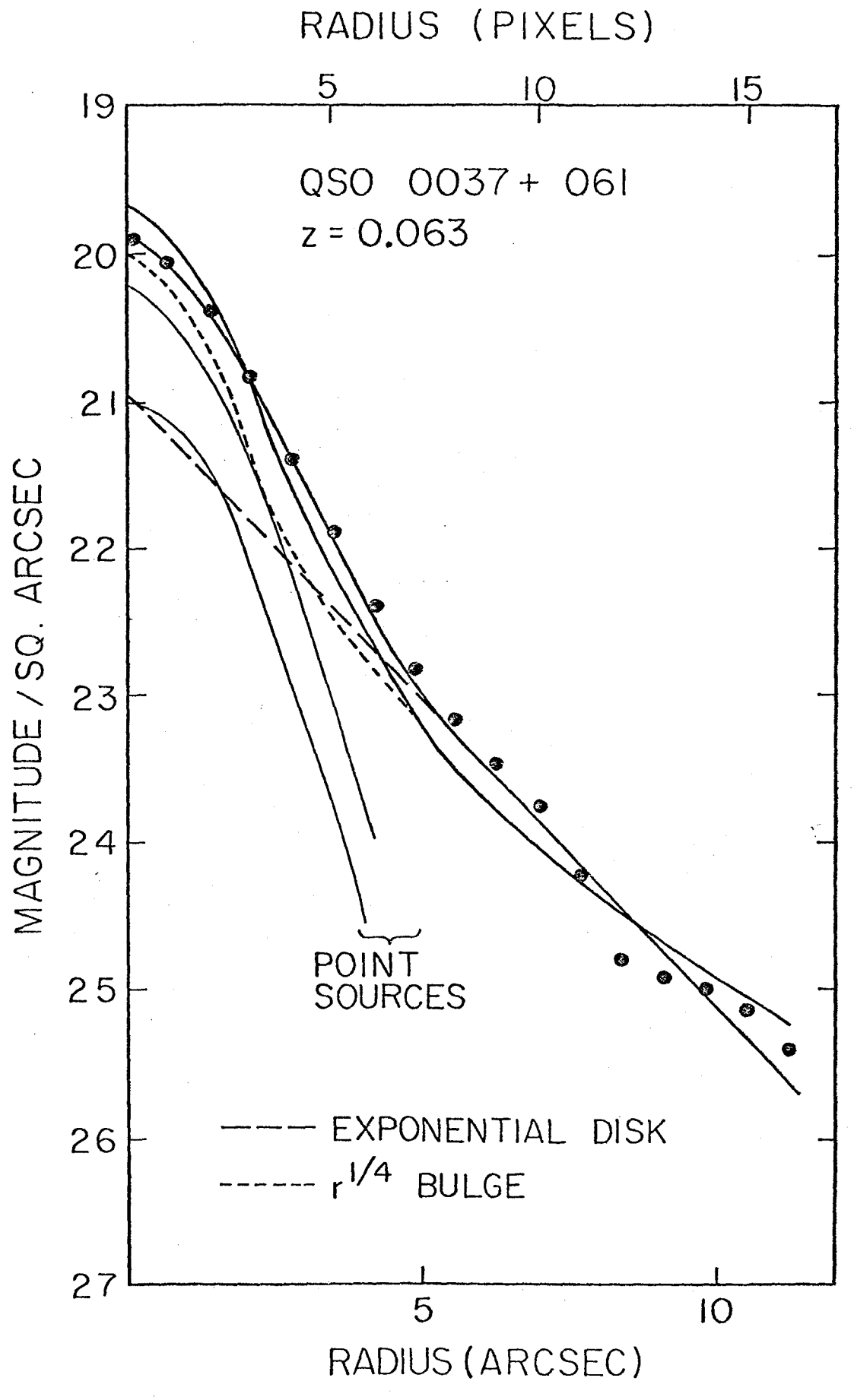
RADIUS (PIXELS)
5
10
15
19
20
21
22
23
24
25
26
27
QSO 0037+061
z = 0.063
MAGNITUDE / SQ. ARCSEC
POINT SOURCES
EXPONENTIAL DISK
r^1/4 BULGE
5
10
RADIUS (ARCSEC)

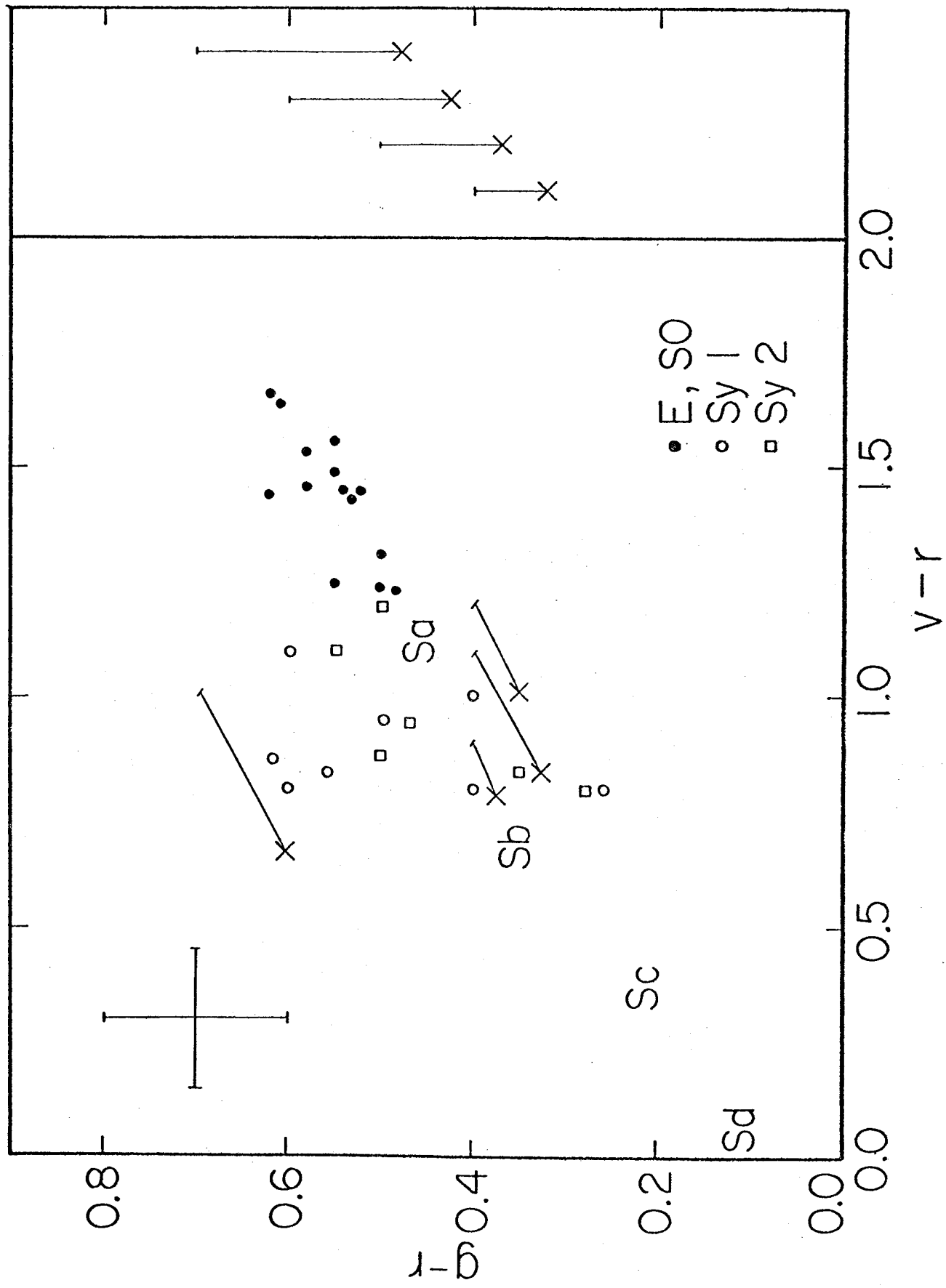
E, SO
Sy 1
Sy 2
Sa
Sb
Sc
Sd
g-r
v-r
0.0
0.2
0.4
0.6
0.8
0.0
0.5
1.0
1.5
2.0

AXIAL RATIOS

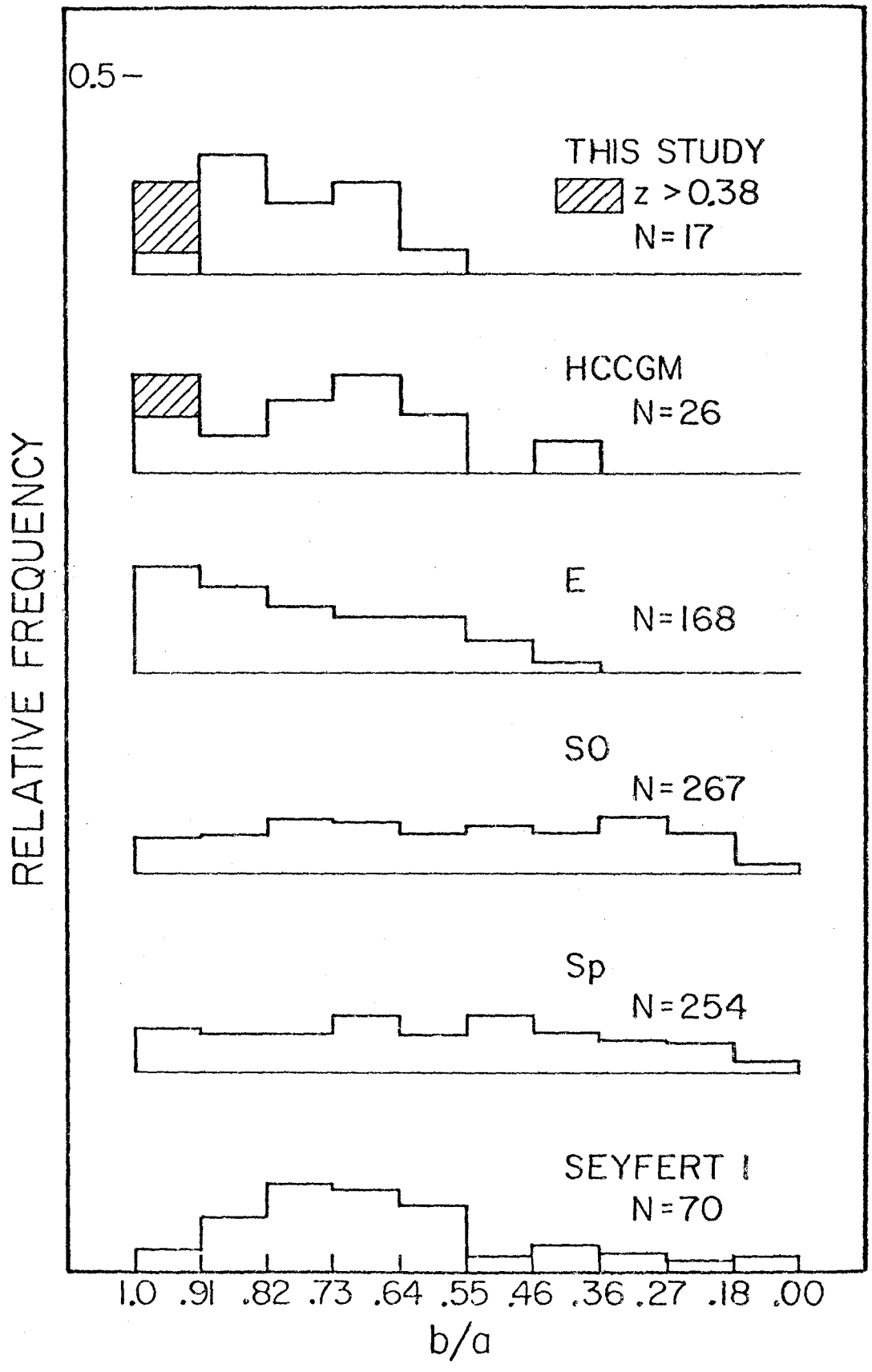

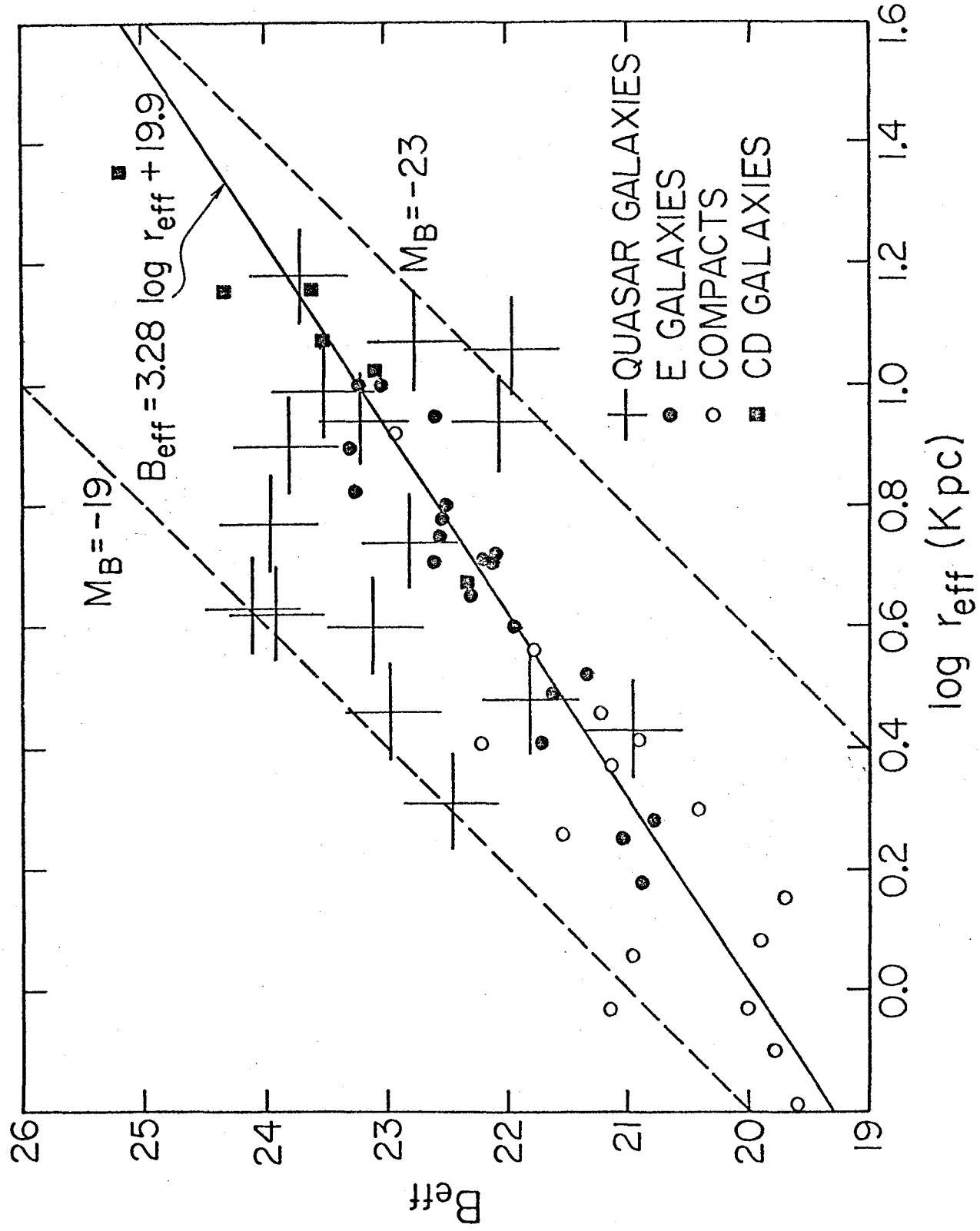
$B_{eff} = 3.28 \log r_{eff} + 19.9$
$M_B = -19$
$M_B = -23$
QUASAR GALAXIES
E GALAXIES
COMPACTS
CD GALAXIES
B_{eff}
log r_{eff} (Kpc)
26
25
24
23
22
21
20
19
0.0
0.2
0.4
0.6
0.8
1.0
1.2
1.4
1.6

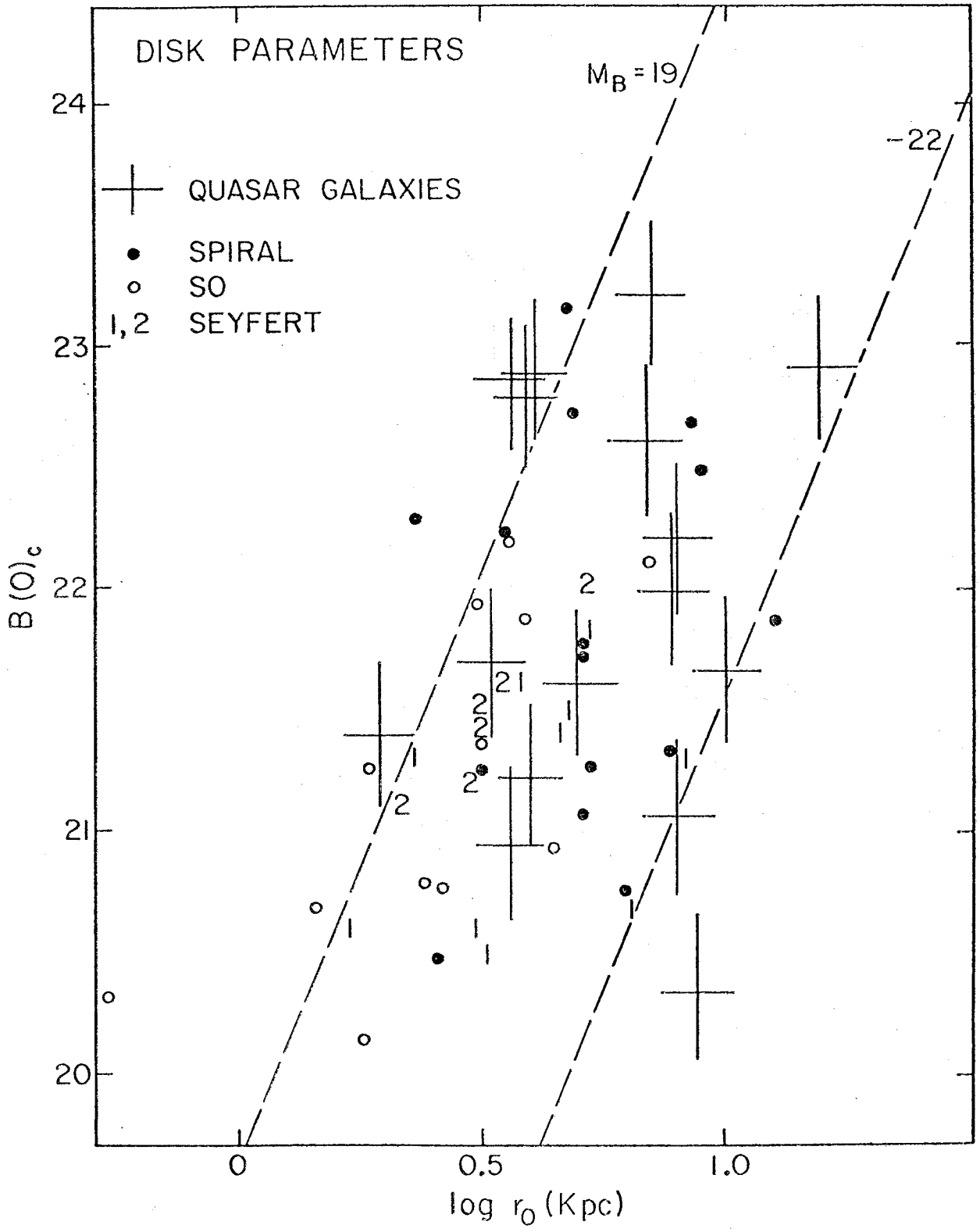
DISK PARAMETERS
$M_B = 19$
-22
QUASAR GALAXIES
SPIRAL
SO
1, 2 SEYFERT
$B(O)_c$
24
23
22
21
20
0
0.5
1.0
log r_0 (Kpc)

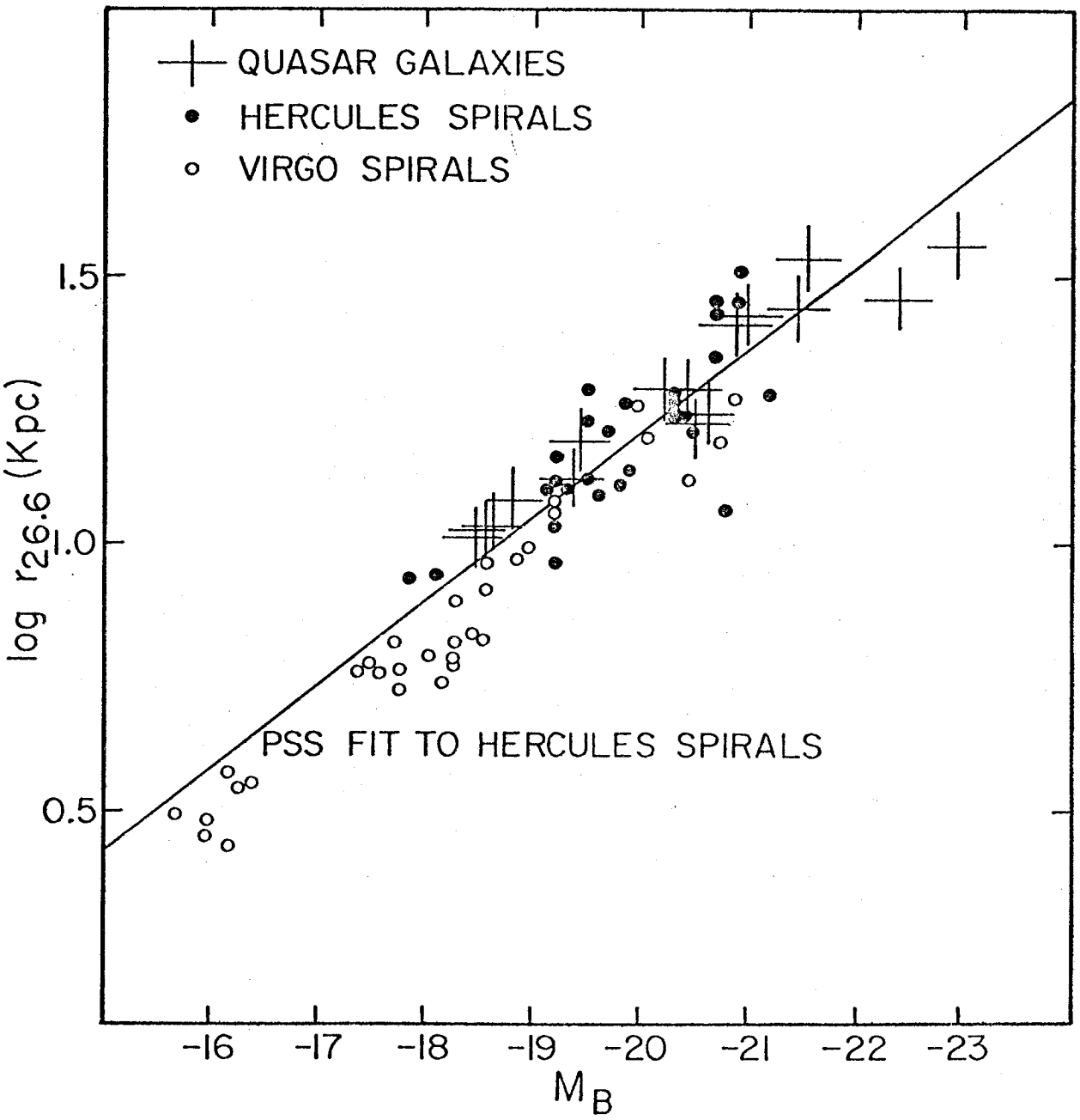
QUASAR GALAXIES
HERCULES SPIRALS
VIRGO SPIRALS
PSS FIT TO HERCULES SPIRALS
log $r_{26.6}$ (Kpc)
1.5
1.0
0.5
-16
-17
-18
-19
-20
-21
-22
-23
M_B

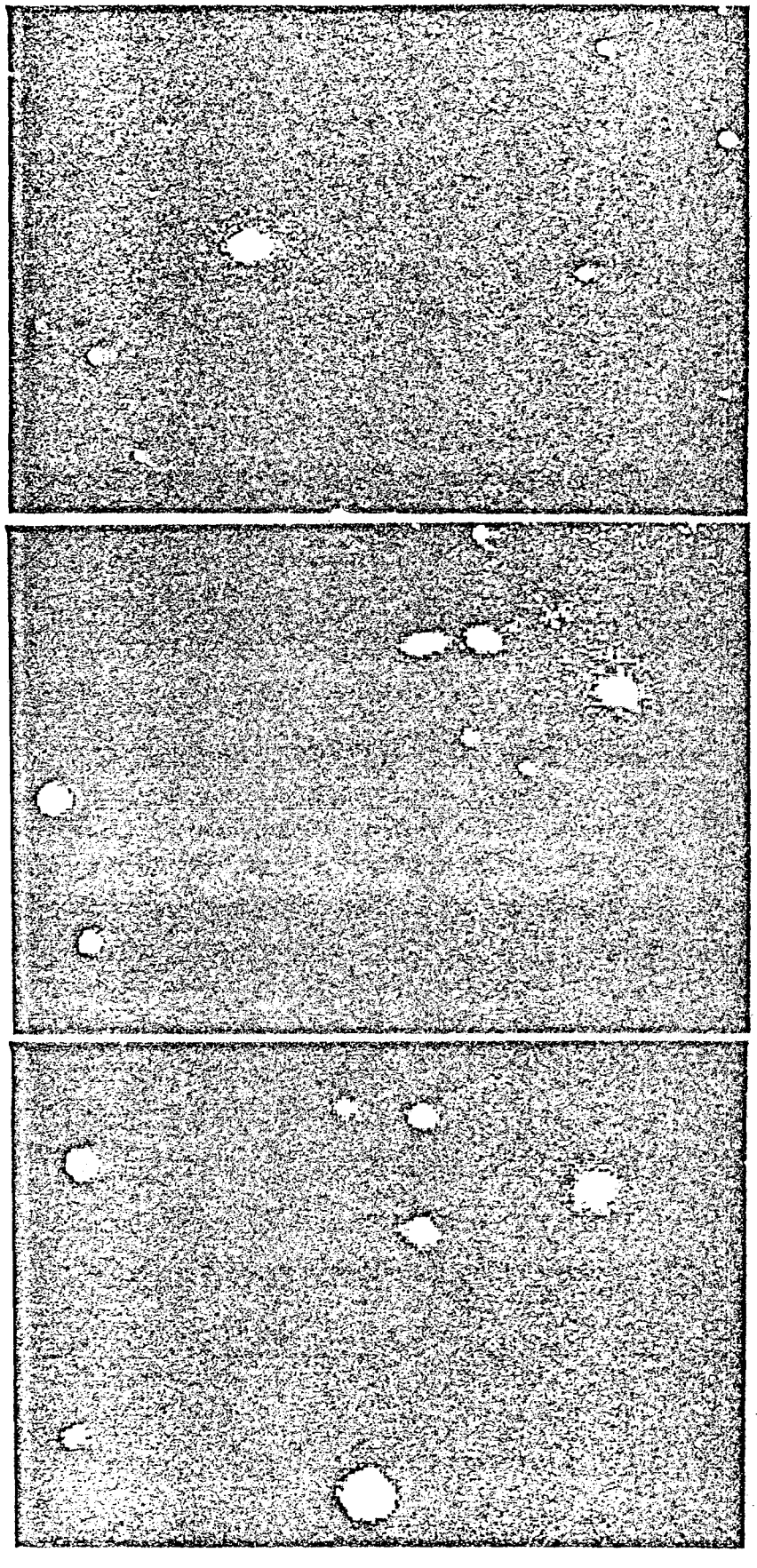

THE ASTROPHYSICAL JOURNAL, 265:92-106, 1983 February 1

IUE OBSERVATIONS OF MARKARIAN 3 AND 6: REDDENING AND THE NONSTELLAR CONTINUUM

MATTHEW A. MALKAN AND J. B. OKE
Palomar Observatory, California Institute of Technology
Received 1982 May 17; accepted 1982 July 21

ABSTRACT

We have used *IUE* visual and infrared observations to study the spectra of the Seyfert 2 galaxies NGC 1068 and Markarian 3, and the Seyfert 1.5 galaxy Markarian 6. The starlight in these galaxies is reddened by 0.01, 0.18, and 0.06 mag in E_{B-V}, respectively; the forbidden lines are reddened by 0.29, 0.27, and 0.27 mag, respectively. Since these reddenings probably also apply to the permitted lines, the intrinsic Lyα/Hα ratios are 3 to 4, and the Hα/Hβ ratios are 3.5 to 4.

A nonstellar component contributes 15, 20, and 30% of the visual flux, respectively, in NGC 1068, Mrk 3, and Mrk 6, in a 14″ aperture. It has a significant flux in the near-infrared and in the far-ultraviolet, and it is well described by a power law with a slope of ~ -1.1 in all three galaxies. Other possible spectral shapes fail by several orders of magnitude to provide enough ionizing photons to produce the observed line emission.

Seyfert 2 galaxies have 50% smaller Balmer continuum/Hα ratios, and 100% larger C III]C IV ratios than Seyfert 1's. The Seyfert 2's have warm dust which emits a large thermal infrared flux. If the central continuum heats this dust, it must be reddened by 0.3 and 0.5 mag or more in NGC 1068 and Mrk 3.

Subject headings: galaxies: Seyfert — interstellar: matter — spectrophotometry — ultraviolet: spectra

I. INTRODUCTION

Malkan and Sargent (1982) used *International Ultraviolet Explorer* satellite data to study the continua of eight Seyfert 1 galaxies and quasars. They showed that very wide wavelength coverage (e.g., the 6 1/2 octaves from 1200 Å to 10 μm) is essential. Smaller portions of the spectrum can often be fitted in several different ways. Observations with the long and short-wavelength cameras of the *IUE*, combined with optical spectrophotometry, are necessary to *uniquely* specify the continuous spectrum. Broad-band optical photometry is less useful, since it does not resolve important features such as the strength of Balmer continuum emission.

IUE has now observed many active galactic nuclei which are bright in the ultraviolet, of which the eight in Malkan and Sargent's sample are typical representatives. But some intermediate Seyfert 1's and all Seyfert 2's are much fainter in the ultraviolet. Of these, only NGC 1068 had been previously observed by *IUE* (Neugebauer *et al.* 1980). We present new observations of the Seyfert 2 galaxy Markarian 3, and the Seyfert 1.5 galaxy Markarian 6. These data are analyzed along with the earlier observations of NGC 1068, to study the nonstellar continuum in these galaxies.

II. OBSERVATIONS

We observed Mrk 3 and Mrk 6 in 1980 with the *IUE* satellite. Each exposure required an entire 8-hour observing shift with low background radiation. The optical spectrophotometry for all the galaxies discussed in this paper was obtained with the multichannel spectrometer (Oke 1969) on the Hale 5.08 meter reflector.

Several slit spectra were taken with cooled SIT and CCD detectors on the 5 and 1.5 m telescopes. We also used the SIT area photometer (Kent 1979) on the Palomar 1.5 m telescope to obtain direct images of Mrk 3, Mrk 6, and NGC 1068. Table 1 lists the observing log, along with aperture and slit sizes, spectral range, and spectral resolution.

a) *Nuclear Emission Lines*

The line equivalent widths and intensities listed in Table 2 were measured from the multichannel and *IUE* spectra. The slit spectra were used to separate Hα, Hγ, and Hδ from nearby forbidden lines. We assumed that the line ratios (e.g., Hγ/[O III] 4363) measured on the slit spectra also applied to the aperture observations. Although the permitted lines of Mrk 6 are broad, they have strong narrow cores which probably arise in the same region as the forbidden lines. Since we could not reliably separate these from the broad wings, the quoted intensities include both. A comparison of our measured absolute emission line intensities with the results of previous studies indicates that they are accurate to $\pm 10\%$ (except for the uncertain values indicated with colons).

The *IUE* spectra of Mrk 6 are very noisy, and no ultraviolet emission lines were detected. The optical line intensities we measured in 1979 October agree with those of DeBruyn and Sargent in 1975 February, Neugebauer

TABLE 1

OBSERVING LOG

TELESCOPE AND INSTRUMENT	WAVELENGTH[1] Range	WAVELENGTH[1] Resolution[2]	APERTURE (Arcsec)	MRK 3 DATES	MRK 6 DATES	NGC 1068 DATES
			Spectroscopic			
1.5 m + SIT	3600–5300	7	3 × 20	79 Aug–80 Mar	79 Mar–81 Mar	79 Aug–81 Aug
1.5 m + SIT	5900–7500	8	4 × 15	81 Nov 1	81 Nov 1	
1.5 m + SIT	3600–7000	16	6 × 20[3]	81 Feb 20		
5.0 m + SIT	3700–6900	15	1 × 10[3]	...	76 Dec 19	
5.0 m + SIT	3200–7000	15	1 × 10	80 Feb 24	80 Feb 24	
5.0 m + CCD	3200–10,800	8	2 × 10	81 Nov 5	81 Nov 5	81 Nov 5
5.0 m + MCSP	3150–10,800	40/80	14 circ	79 Oct 29; 80 Jan 26	79 Oct 29	
IUE: LWR + SWP	1200–3200	6	10 × 20	80 Feb 21	80 Sep 30	
			Direct			
1.5 m + SIT	3800–4200	400	180 × 180	81 Mar 5, 6	81 Mar 5, 6	81 Mar 5, 6
1.5 m + SIT	7000–9000	2000	180 × 180	81 Mar 5, Oct 15	81 Mar 5, Oct 15	81 Mar 5, Oct 15

[1] In angstroms.
[2] Full width at half-maximum.
[3] Slit positioned off nucleus.

TABLE 2

LINE INTENSITIES

LINE λ (Å)	MARKARIAN 3 E.W. (Å)	MARKARIAN 3 $j \times 10^{14}$ ergs s^{-1} cm^{-2} Obs.	MARKARIAN 3 $j \times 10^{14}$ ergs s^{-1} cm^{-2} Dereddened	MARKARIAN 6 E.W. (Å)	MARKARIAN 6 $j \times 10^{14}$ ergs s^{-1} cm^{-2} Obs.	MARKARIAN 6 $j \times 10^{14}$ ergs s^{-1} cm^{-2} Dereddened
Lyα 1216	:3200	64	810			
N v 1241	:150	3	38			
Si IV 1402	20	1	4			
C IV 1550	255	21	163	<200	<6	<46
He II 1640	95	9	69			
C III] 1909	92	9	76	<200	<5	<40
C II] 2325	96	9	84			
[O II] 2470	:40	:3	:22			
Mg II 2838	127	18	82	<100	<16	<73
He II 3203	:8	:2	:8			
[Ne V] 3346	10	3	10	:4	:1	:4
[Ne V] 3425	28	9	32	11	3	11
[O II] 3727	266	93	313	35	13	44
[S II] 4071	14	8	24	6	2	7
Hδ 4100	12	7	20	7	3	8
Hγ 4340	19	13	37	12	5	15
[O III] 4363	9	6	17	5	2	7
He II 4686	5	5	14	2	1	2
Hβ 4861	30	31	79	54	30	75
[O III] 4959 + 5007	487	505	1214	176	100	240
He I 5876	3	4	7	6	4	8
[O I] 6300	24	33	62	10	7	13
[N II] 6548 + 6584	157	236	428	40	26	47
Hα 6563	105	157	285	333	216	392
[S II] 6720	58	83	148	34	22	39
[O II] 7325	12	13	21	:3	:2	:3
[S III] 9069	29	46	64	15	11	15
[S III] 9532	69	105	141	35	23	31
[S II] 10320	:8	:13	:16	<7	<4	<5
He I 10830	:50	:80	:100			

et al. in 1972 February, and Koski (1978). The Neugebauer *et al.* spectrum of 1969 October had the same forbidden line intensities, but the Balmer lines were twice as strong, and the visual continuum was brighter by 0.6 mag. Our slit spectra of Mrk 6 confirm early indications (Adams 1972; Ulrich 1972) that the profile of the broad component of Hβ varies over a time scale of months. The variability will be discussed in a future paper. Nonetheless, there is no indication that the Balmer line fluxes in Mrk 6 have differed from those in Table 2 by more than 20% since 1972.

b) Extra-nuclear Line Emission

We obtained slit spectra 6″ south of the nucleus of Mrk 6, 7″ north, and 7″ south of the nucleus of Mrk 3, and 3″ and 10″ north of the nucleus of NGC 1068. Identical observations of bright stars showed that the off-nuclear spectra had less than 1% scattered light contamination from the Seyfert nucleus. All the off-nucleus spectra of Mrk 3 and Mrk 6 have strong emission from the [O III] doublet, but no detectable Hβ flux. In the Mrk 6 off-nuclear spectrum the 5007 Å line has an equivalent width of about 13 Å and a flux of 1×10^{-14} ergs cm^{-2} s^{-1}. In both Mrk 3 spectra its equivalent width is 15 Å, and its flux is 3×10^{-14}. The Hα + [N II] complex is probably present in all three spectra, with about the same flux as the 5007 Å line. There appears to be [O II] 3727 emission in the three spectra, but it is no stronger than a quarter of the 5007 Å intensity.

In contrast, the spectra taken through a 1″ slit 3″ and 10″ north of the nucleus of NGC 1068 show weak emission lines with typical H II region ratios: [O III] 5007+4959/Hβ is 4, [N II] 6584/Hα is 0.6, and [S II] 6724/[N II] 6584 is 0.25.

c) Continuum

Neugebauer *et al.*'s (1980) spectrum of NGC 1068 in a 10″ aperture is virtually identical to the one in DeBruyn and Sargent (1978). We corrected it to a 14″ aperture, using the growth curves for each wavelength from Wampler (1971) and the ones derived below by direct imaging.

Neugebauer *et al.* found that Mrk 6's visual flux in a 10″ aperture decreased by 0.25 dex from 1969 October to 1972 February. The flux DeBruyn and Sargent measured in 1975 February was halfway between these two values. Our 1979 October spectrum was taken when Mrk 6 was at its relatively faint level of 1972 February. Readhead, Sargent, and DeBruyn (private communication) observed Mrk 6 on 1980 September 28, two days before our *IUE* observations, and found its brightness was the same as when we observed it in 1979. However, the *IUE* spectrum around 3000 Å is systematically lower by 0.1 dex than the optical one. The nearly simultaneous optical observations virtually eliminate the possibility that this discrepancy is explained by variability. Perhaps there were pointing errors (of a few arc seconds) in the *IUE* observations. For the following analysis we have added 0.1 dex to all the ultraviolet points so that they join continuously with the optical spectrum.

We estimated the infrared fluxes from each object in a 14″ aperture from the photometry of Rieke (1978), Neugebauer *et al.* (1976), McAlary, McLaren, and Crabtree (1979), Cutri *et al.* (1981), Penston *et al.* (1974), and Lebofsky and Rieke (1979). The combined ultraviolet/optical/infrared spectra of Mrk 3 and Mrk 6 are shown in Figure 3*a*, and the spectrum of NGC 1068 is in Figure 4*a*.

d) Direct Imaging

Several digitized images of Mrk 3, Mrk 6 and NGC 1068 were taken through a Wratten 88A filter (with a cut-on wavelength of 7400 Å), and a violet ($\delta\lambda = 400$ Å) filter centered on 4000 Å. The first defines the *i* bandpass (Wade *et al.* 1980), at $\lambda_{\rm eff} \sim 0.8$ μm, while the second is the Gunn violet band (Thuan and Gunn 1976). Both filters measure primarily the continuum, and the corrections for line emission are negligible for the *i* filter, and less than 15% for the violet. The photometry, calibrated with measurements of the multichannel standards BD +17 4708 and HD 19445, agreed with the spectrophotometry from the 5 m telescope to within 10%. The growth curves of flux versus aperture size are illustrated in Figure 1 for each galaxy and both filters. They are accurate to better than 15%.

III. REDDENING

a) Starlight

Mrk 3, Mrk 6, and NGC 1068 are at galactic latitudes of +23, +26, and −52°. We estimate that our Galaxy reddens the respective spectra by 0.10, 0.09, and 0.01 mag in E_{B-V}, from the Burstein and Heiles H I column density method (1978). Since the spectra are dominated by starlight from 1.2 to 0.4 μm, we can compare them to the standard galaxy spectrum (described below), to check these reddening estimates. We use a standard reddening law (Code *et al.* 1976) throughout this paper. The reddening of the starlight in Mrk 3, Mrk 6, and NGC 1068 is 0.18 ± 0.04, 0.06 ± 0.03, and 0.00 ± 0.03, in E_{B-V}, respectively, and arises mostly in the Milky Way.

b) Forbidden Lines

The nuclear emission (i.e., emission lines and nonstellar continuum) from the Seyfert galaxies is probably more reddened than the starlight. We can estimate the nuclear reddening by comparing various observed line ratios with their predicted intrinsic values. Allen (1979) and Malkan (1983) showed at $T_e = 14{,}000$ K and $n_e = 2 \times 10^3$ cm^{-3} the double ratio

$$([\text{O II}]\ 7325/3727) \times ([\text{S II}]\ 6724/4072) = 0.41\ .$$

This value changes by less than 20% when the electron temperature is increased or decreased 6000 K, or when the electron density is increased or decreased by an order of magnitude. (Malkan 1983). Since the logs of the observed values from the DeBruyn and Sargent spectra are

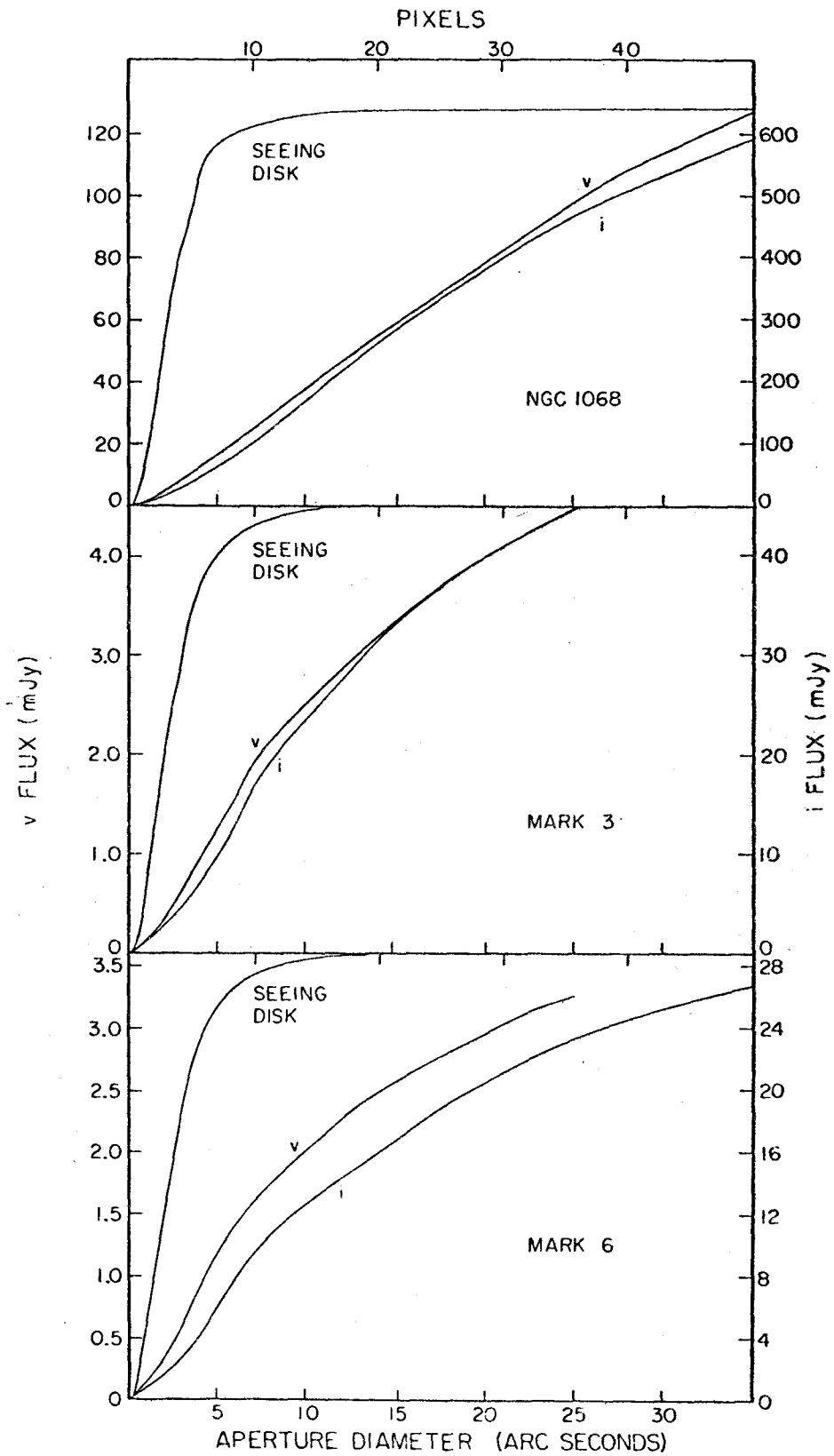

FIG. 1.--The flux growth curves at 4000 Å (v) and 8000 Å (i) for the three galaxies. The absolute flux scale for the v curves is marked on the left; the i scale is on the right, in milliJanskys (10^{-26} ergs cm^{-2} s^{-1} Hz^{-1}). The seeing disks, as determined from stars observed on the same SIT frames, are plotted for comparison, with arbitrary normalizations. The ticks along the bottom of each frame give the aperture diameter in arc seconds; the ticks along the top give it in pixels. Mrk 6's violet flux is more concentrated to the nucleus than is its i flux.

$+0.17 \pm 0.16$ for Mrk 3 and Mrk 6, and $+0.18 \pm 0.16$ for NGC 1068, we deduce that $E_{B-V_{\rm tot}}$ is 0.27 ± 0.08 for Mrk 3 and Mrk 6, and 0.29 ± 0.08 for NGC 1068.

Reddening can also be estimated by observing the (blended) [S II] lines at 10287, 10320, 10336, and 10370 Å. Since they come from the same upper level as the λ4072 doublet, the intrinsic ratio $F(\sum 10300)/F(4072)$ is always near 0.67 for temperatures and electron densities of interest (Malkan 1983). In the Mrk 3 CCD spectrum the infrared [S II] complex is marginally "detected" at the 2 σ level, yielding a reddening of $E(B-V) = 0.25$. The weakness of the infrared lines could also be consistent with no reddening, but rules out $E(B-V)$ of more than 0.35. The spectra of NGC 1068 and Mrk 6 give only upper limits to the [S II] flux, which correspond to $E_{B-V} \leq 0.3$ and 0.35 mag.

In Mrk 3, another check comes from the [O II] 2470/7325 ratio. Since both lines come from the same upper level, the intrinsic ratio is 0.75 over a very wide range of temperatures and electron densities (Malkan 1983). The observed ratio, 0.25, gives a formal $E(B-V)$ of 0.23 mag, but if the λ2470 line was not actually detected, any reddening greater than 0.1 mag would be allowed.

We conclude that the forbidden line reddening is 0.27 mag in Mrk 3 and Mrk 6, and 0.29 in NGC 1068.

c) *Permitted Lines*

We can estimate the reddening in Mrk 3 and NGC 1068 by comparing the observed He II line ratios with those predicted by recombination theory (Brocklehurst 1971; Seaton 1978). In Mrk 3, the observed ratios $I(4686)/I(1640) = 0.57$ and $I(3203)/I(4686) = 0.37$ give reddenings of $E_{B-V} = 0.35 \pm 0.10$ and 0.13 ± 0.16 mag. In NGC 1068 the observed ratios, $I(4686)/I(1640) = 0.43$, $I(4686)/I(10123) = 2.4$, and $I(3203)/I(4686) = 0.5$–0.25, give reddenings of 0.28 ± 0.07, 0.21 ± 0.10, and 0.00–0.44. Within these large uncertainties, the permitted lines in these Seyfert 2 galaxies have the same reddening as the forbidden lines.

The reddening-corrected line intensities are given in Table 2. Mrk 6's intrinsic Balmer line ratios are similar to those in other Seyfert 1 galaxies (Malkan and Sargent 1982; Lacy *et al.* 1982). The narrow cores of the Balmer lines, measured by Koski (1978), also have a large Hα/Hβ ratio.

Our continuum fits in § 5 to show that nearly half of the observed 1200 Å continuum in NGC 1068 comes from stars. We did not assume, as did Neugebauer *et al.* (1980) that the equivalent width of Lyα is independent of observing aperture. We recalculated NGC 1068's Lyα flux assuming that it is spatially unresolved by *IUE* (i.e., its FWHM is less than 5″), and that the efficiency of *IUE*'s small aperture is 50% (Bohlin *et al.* 1980). Both SWP 1921 and 6311 then give a total Lyα flux for NGC 1068 of $5 \pm 1 \times 10^{-12}$ ergs cm^{-2} s^{-1}, 30% less than Neugebauer *et al.*'s estimate.

Our measurements, combined with previous ones by Koski (1978), show that the narrow emission lines in all three galaxies have intrinsic Hα/Hβ ratios of 3.5 to 4, and intrinsic Lyα/Hα ratios of 3 to 4. These are quite different from the respective case B values of 2.8 and 13. The assumption of the case B calculation, that the Balmer lines are all optically thin, must not apply to the bulk of the gas in the narrow-line region. Calculations (Canfield and Puetter 1981; Kwan and Krolik 1981) show that the Hα/Hβ and Hα/Lyα ratios increase in clouds with Lyman limit optical depths greater than 100. Evidently the typical narrow-line clouds in these Seyfert galaxies are larger than $10^{20}/n_{\rm H}$ cm.

NGC 1068's dereddened Paα/Hα ratio (Neugebauer *et al.* 1980) is 0.1, the case B value. But its Paα/Hβ ratio is 0.42 ± 0.07, a little larger than the case B value of 0.28. Similarly, its dereddened Brγ/Hα ratio (Hall *et al.* 1981; Thompson, Lebofsky, and Rieke 1978) is 0.01, the case B value. But its Brγ/Hβ ratio is 0.05 ± 0.01, slightly larger than the case B value of 0.03.

We observe a He I $\lambda\lambda$10830/5876 ratio in Mrk 3 of 22 ± 8, not appreciably different from the value LeVan *et al.* (1981) measured for NGC 1068. The reddening correction derived above cuts this ratio almost in half. In the low-density (pure recombination) limit of $n_e \ll n_{\rm crit} = 3700$ cm^{-3}, it should be 1.6. If the electron density greatly exceeds the critical density, the λ10830 emission is completely dominated by collisional excitation from the metastable 2^3S level (Osterbrock 1974). This collisional enhancement produces a $\lambda\lambda$10830/5876 ratio of 21 in an optically thin 10^4 K gas. Our observations strengthen the suggestion of LeVan *et al.* that substantial He I emission in Seyfert 2 galaxies comes from regions where the electron density is comparable to or less than 3700.

The C III]/C IV ratio in Mrk 3 is 0.45, about the same as in the other observed type 2 Seyfert, NGC 1068. This is roughly twice as large as the ratio observed in several Seyfert 1 galaxies. The difference is probably due to lower electron density or ionization parameter (ratio of ionizing photons to nucleons) in the Seyfert 2 emission-line regions.

d) *Ultraviolet Continuum*

We may also estimate the reddening of the ultraviolet continuum by searching for the interstellar absorption at $\lambda = 2175$ Å. Unfortunately the data for Mrk 3 and Mrk 6 are so noisy that any reddening up to 0.6 mag in E_{B-V} would be consistent with them. NGC 1068's brighter ultraviolet spectrum, however, shows no absorption at 2175 Å. If the standard extinction law applies, the ultraviolet continuum cannot be reddened by more than 0.1 in E_{B-V}. Even if we adopted the most extreme galactic reddening law known (for θ Orionis, Bless and Savage 1972), E_{B-V} would still have to be less than 0.2.

In the following analysis we assume the reddening of the starlight in Mrk 3, Mrk 6, and NGC 1068 is 0.18, 0.06, and 0.01, and that the reddening of the emission lines is 0.27, 0.27, and 0.29 mag. We further assume that the reddening of the nonstellar continuum in Mrk 6 is the same as that of its emission lines. In our

analysis of the Seyfert 2 galaxies, we test several possible continuum reddenings and find that E_{B-V}'s of several tenths of a magnitude are most likely.

IV. THE STARLIGHT COMPONENT

a) Direct Imaging

We have combined our imaging data with measurements of stellar absorption line strengths to estimate the stellar and nonstellar contributions in each of the galaxies. The nonstellar component is assumed to be spatially unresolved. The starlight is extended but can also produce part of the nuclear (unresolved) flux. Like other Seyfert 1 galaxies, Mrk 6 is redder in larger apertures. This is simply the effect of mixing in a greater proportion of starlight with a nuclear continuum which is bluer. This color gradient is much less pronounced in the Seyfert 2 galaxies.

We matched seeing disk profiles (from stars on the same SIT frames) to the central few pixels of the three galaxies. This gave us estimates that the nucleus (i.e., the seeing disk with a FWHM of 2″) contributes 20, 25, and 20% of the 8000 Å light in a 14″ aperture in Mrk 3, Mrk 6, and NGC 1068, respectively. At 4000 Å, the nucleus contributes 40, 60, and 30%. We then used slit spectroscopy to estimate what fraction of this nuclear light is nonstellar. The relative weakness of the stellar absorption lines in the slit spectra, compared to those in normal galaxies (Table 3), indicates that 60–70% of the visual (5200 Å) nuclear light is featureless nonstellar continuum. We then find that the total nonstellar fraction of the visual light in a 14″ aperture in Mrk 3, Mrk 6, and NGC 1068 is 20, 30, and 15% (Table 3).

There are two possible sources of systematic error in these estimates:

1) Poor guiding or bad seeing could shift off-nucleus starlight into the spectrograph slit. This additional contamination would strengthen the observed absorption lines. The effect does not seem serious, since equivalent widths measured with the 3″ slit are not significantly stronger than those obtained with the 1″ slit.

2) The K and D lines could have contributions from the interstellar medium in Mrk 3, Mrk 6, and NGC 1068. The actual equivalent widths of the stellar K and D absorption lines could be less than those quoted in Table 3.

These effects could make the stellar fraction estimates in Table 3 5–10% too large, but we have almost certainly not *underestimated* the contribution from stars.

In § V we compare our direct estimates of the nonstellar contributions with the predictions from continuum fitting.

b) Young Stars

Much of the following analysis uses a standard galaxy spectrum. It is that of Yee and Oke's (1978) average elliptical galaxy, extended into the ultraviolet with Johnson's (1979) observations of M31 and M32, and Oke, Bertola, and Capacciola's observations of NGC

TABLE 3

ABSORPTION LINE EQUIVALENT WIDTHS AND FRACTIONS OF NONSTELLAR LIGHT

Object	3934 Å Ca II K	4304 Å G band	5175 Å Mg I *b*	5892 Å Na I D	8542 Å Ca II
Equivalent widths (Å) in:					
Normal galaxies	9–14	3–7	4–8	2–6	2.5–5
Narrow-line radio galaxies[1]	9.2 ± 1.6	...	7.8 ± 1.5	4.7 ± 0.7	
Mrk 3–7″ N and S	11 ± 2	...	5 ± 0.5	3.1 ± 0.5	
Mrk 3–nucleus	5 ± 1	1.6 ± 0.4	2.0 ± 0.4	1.5 ± 0.5	1 ± 1
Mrk 6–6″ south	11 ± 2	7 ± 3	6 ± 1	5 ± 1.5	
Mrk 6–nucleus	3.5 ± 1.5	1.4 ± 0.3	1.8 ± 0.4	3 ± 0.6	1 ± 1
NGC 1068–nucleus	4 ± 1	1.5 ± 0.3	1.4 ± 0.4	1.3 ± 0.5	2 ± 0.5
Fractions of nonstellar light in the Nucleus of: 5					
Mrk 6	0.7 ± 0.15	0.65 ± 0.2	0.65 ± 0.2	0.4 ± 0.3	0.6 ± 0.4
Mrk 3	0.65 ± 0.15	0.6 ± 0.2	0.6 ± 0.2	0.55 ± 0.3	0.6 ± 0.4
NGC 1068	0.7 ± 0.15	0.65 ± 0.2	0.75 ± 0.2	0.65 ± 0.3	0.4 ± 0.3
In a 14″ aperture:					
Mrk 6	0.5 ± 0.1	0.45 ± 0.1	0.3 ± 0.1	0.2 ± 0.1	0.2 ± 0.15
Mrk 3	0.3 ± 0.1	0.25 ± 0.1	0.2 ± 0.1	0.15 ± 0.1	0.1 ± 0.1
NGC 1068	0.2 ± 0.1	0.2 ± 0.1	0.15 ± 0.05	0.15 ± 0.1	0.1 ± 0.1
Fractions of nonstellar light in 14″ aperture, as predicted from continuum fitting:[2]					
Mrk 6, if nonstellar component is a:					
Power-law	0.52	0.43	0.31	0.28	0.27
Blackbody	0.18	0.12	0.08	0.06	0.03
Mrk 3, if nonstellar component is a:					
Power-law	0.25	0.15	0.12	0.10	0.08
Blackbody	0.10	0.04	0.03	0.01	0.00
NGC 1068, if nonstellar component is a:					
Power-law	0.34	0.28	0.24	0.22	0.20
Blackbody	0.22	0.15	0.08	0.06	0.03

[1] Average of the five radio galaxies in Costero and Osterbrock 1976.
[2] Uncertainties in predicted nonstellar fractions do not exceed 2%.

TABLE 4

FITS TO THE CONTINUUM IN A 14" APERTURE

OBJECT	POWER-LAW FIT			BLACKBODY FIT			EXPONENTIAL FIT		
E_{B-V} (Nucleus)	f_{Stars}[1]	f_{P-L}[1]	α	f_{Stars}[1]	f_{BB}[1]	T (K)	f_{Stars}[1]	f_{Exp}[1]	T (K)
Mrk 6 (0.27)	5.7	3.9	−1.2	7.9	0.4	23,000	7.2	1.6	30,000
Mrk 3 (0.27)	19.0	1.0	−1.3	19.0	0.3	18,000	19.0	2.0	20,000
Mrk 3 (0.50)	19.0	2.7	−1.0	19.0	0.9	23,000	19.0	5.1	30,000
NGC 1068 (0.10)	104.0	25.0	−1.1	120.0	7.0	19,000	107.0	26.0	36,000
NGC 1068 (0.29)	94.0	62.0	−0.9	115.0	20.0	21,000	No fit possible		
Uncertainties	2%	10%	0.2	2%	15%	4000	2%	15%	5000

[1] All fluxes are given for 5500 Å, dereddened, in units of 10^{-26} ergs cm^{-2} s^{-1} Hz^{-1} (milliJanskys).

3379 and NGC 4372, and into the infrared with photometry from Frogel *et al.* (1978) and Glass (1976). The standard galaxy spectrum is shown by the solid line in Figure 2. It is a good match to the Seyfert 2 Mrk 270 (DeBruyn and Sargent 1978) which is plotted with the vertical bars. Also plotted with circles is Turnrose's (1976) spectrum of M100, a typical Sc galaxy, corrected for galactic absorption. Even though the standard galaxy is early type, it is also a reasonable match to a late-type spiral.

There are some non-Seyfert "hot spot" galaxies such as NGC 1073 (Turnrose 1976) which are as blue as Mrk 6. Their extra ultraviolet light comes from a large population of young, early-type stars. But there are several reasons to believe the ultraviolet excess observed in all three Seyfert galaxies is nonstellar:

1) Mrk 3 and Mrk 6 are both early-type spirals with smooth light distributions (Adams 1977). The equivalent widths of Ca II H and K, G band, Mg *b*, and Na I D in their off-nucleus spectra are quite similar to those observed in normal galaxies whose light is dominated by red giants (Table 3). Since $I(5007+4959)/I(H\beta)$ is at least 10, the off-nucleus emission lines are probably photoionized by a hard continuum such as a power law, rather than radiation from young stars in normal H II regions. There is certainly no substantial population of young stars more than 500 parsecs from the center of these galaxies.

NGC 1068 is an Sa galaxy (de Vaucouleurs and de Vaucouleurs 1968). Its off-nucleus H II region emission lines show that it has a modest proportion of young stars in its central kiloparsec. The slit spectra north of NGC 1068's nucleus all show Na D, Mg *b*, and G absorption features present at their normal strengths. There are also weak Balmer absorption lines. Hβ is filled in by emission, but Hδ, which is nearly undiluted, has an absorption equivalent width of about 2 Å. These young stars make a relatively minor contribution to the spectrum and could not produce the bulk of the observed ultraviolet excess. In fact the young stars probably influence the observed colors very little, since a multichannel spectrum taken with a 7" aperture, 10" southwest of NGC 1068's nucleus looks indistinguishable from the standard galaxy, as shown in Figure 2. Thus our standard galaxy spectrum is probably a good description of the starlight in all three galaxies.

2) We found that the continuum observations could be approximately reproduced if A0 stars [with spectra given by Hayes and Latham (1975) and Wu, Boggess, and Gull (1980)] contributed 10% of the visual light in Mrk 6, and 20% in NGC 1068. This would correspond to contributions of 45 and 60% at 4000 Å. (Stars cooler than A5 were ruled out since they produce virtually no flux at wavelengths shorter than 1800 Å.) Since A stars have Balmer absorption line equivalent widths of 17 Å or more (Kurucz 1979), they would produce 8 and 10 Å absorption equivalent widths in the large aperture spectra. Although Hα and Hβ would be filled in by nuclear emission, the emission at Hδ and the higher Balmer lines is very weak, and would be overwhelmed by the absorption. Yet the required Balmer line absorption is not present in any of our spectra.

3) The absorption line strengths observed in the nuclear spectra are inconsistent with dilution by young star light. The strength of the K line and G band would require that A stars produce two thirds of the violet ($\lambda = 4000$ Å) continuum. They would then produce only 20% of the visual flux, so that the Mg I *b*, Na I D, and Ca II 8542 lines would be seen at nearly full strength. Their observed weakness cannot be explained by dilution from a young stellar continuum. A featureless continuum must be present at least from 3900 to 8600 Å.

4) The ultraviolet continuum from young stars alone could not account for the observed strength of high-ionization emission lines such as [Ne V] and [Fe VII], which are seen in all three spectra.

All three Seyfert galaxies show an ultraviolet excess with respect to our standard galaxy spectrum which must be nonstellar. We measure this nonstellar component by continuum fitting in the next section.

V. CONTINUUM FITTING: MEASUREMENT OF THE NONSTELLAR COMPONENT

a) Procedure

We have fitted the continuous spectra with combinations of starlight, recombination emission, and one of three possible nonstellar components:

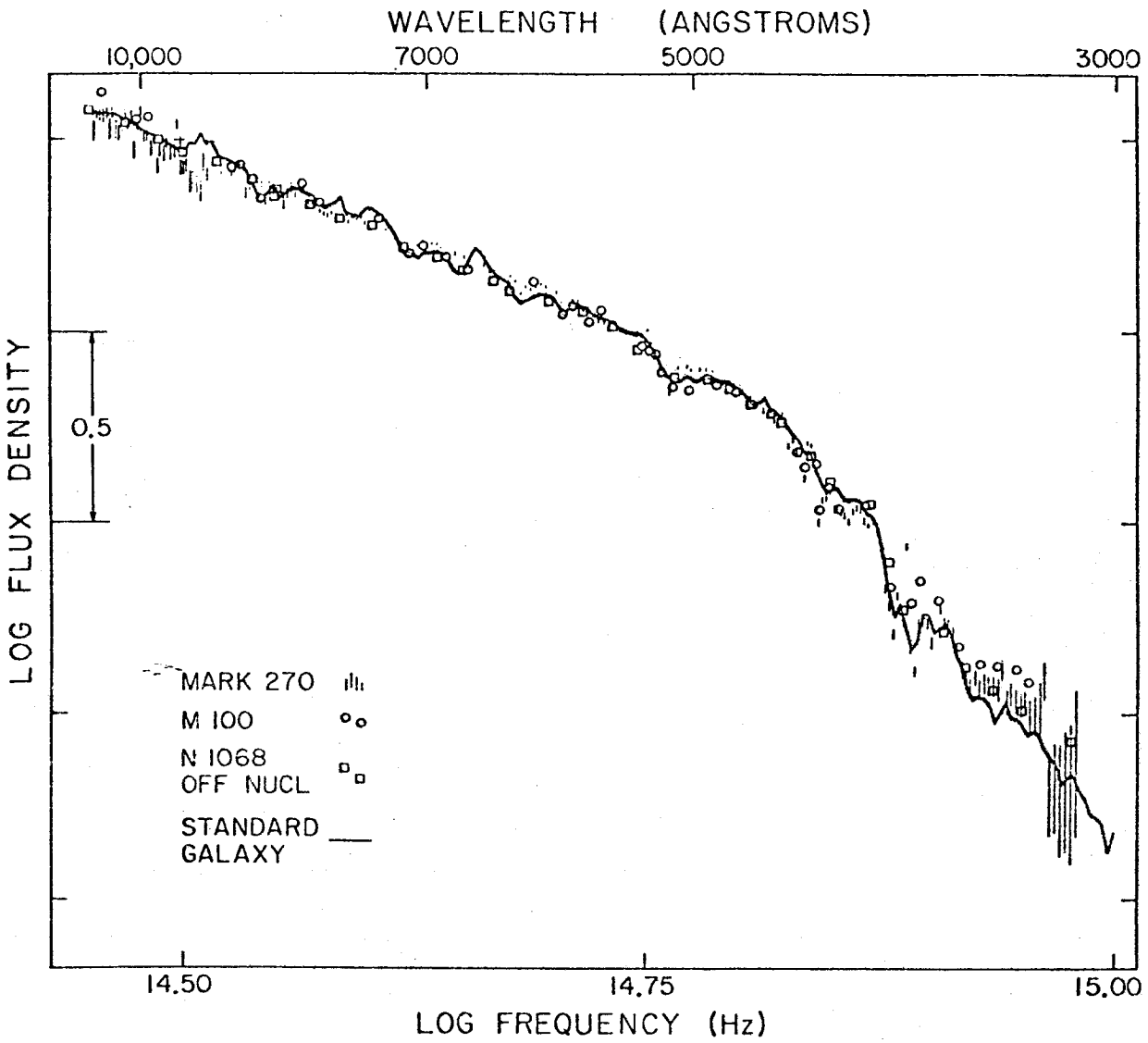

FIG. 2.—The solid line represents the optical portion of the standard galaxy spectrum, which is used in the continuum fitting. DeBruyn and Sargent's (1978) spectrum of Mrk 270 is plotted with vertical bars, and Turnrose's (1976) spectrum of M100's nucleus is shown by the open circles. The open squares represent the spectrum of NGC 1068 taken 10" southwest of the nucleus. All four spectra were obtained with the multichannel spectrometer on the Hale telescope. They are quite similar and are dominated by light from red giants.

1) a power law, $f_\nu = C\nu^\alpha$. The strength C and slope α were free parameters;

2) optically thick emission from a blackbody. Its strength and temperature were free parameters;

3) an exponential component with

$$f = C \exp(-h\nu/kT).$$

Its strength and temperature were free parameters. It was chosen to illustrate an intermediate case which has less red flux than the power law, but more than the blackbody.

The proportion of starlight was also a free parameter, but we checked the results for consistency with our independent estimates from direct imaging in § IV. The free-free and Paschen continuum contributions were scaled to the Hβ flux, while the strength of the Balmer continuum (assumed to be optically thin) was a free parameter.

A nonlinear least-squares computer program fitted the continuous spectra by varying these parameters, as in Malkan and Sargent. We ignored the wavelengths longer than 1.6 μm ($\nu = 1.8 \times 10^{14}$ Hz) in all three galaxies because of possible contamination from thermal dust emission.

For Mrk 3 and NGC 1068, we used two different reddenings for the nuclear continuum. One was the reddening derived from the forbidden lines in § III. The other is discussed below.

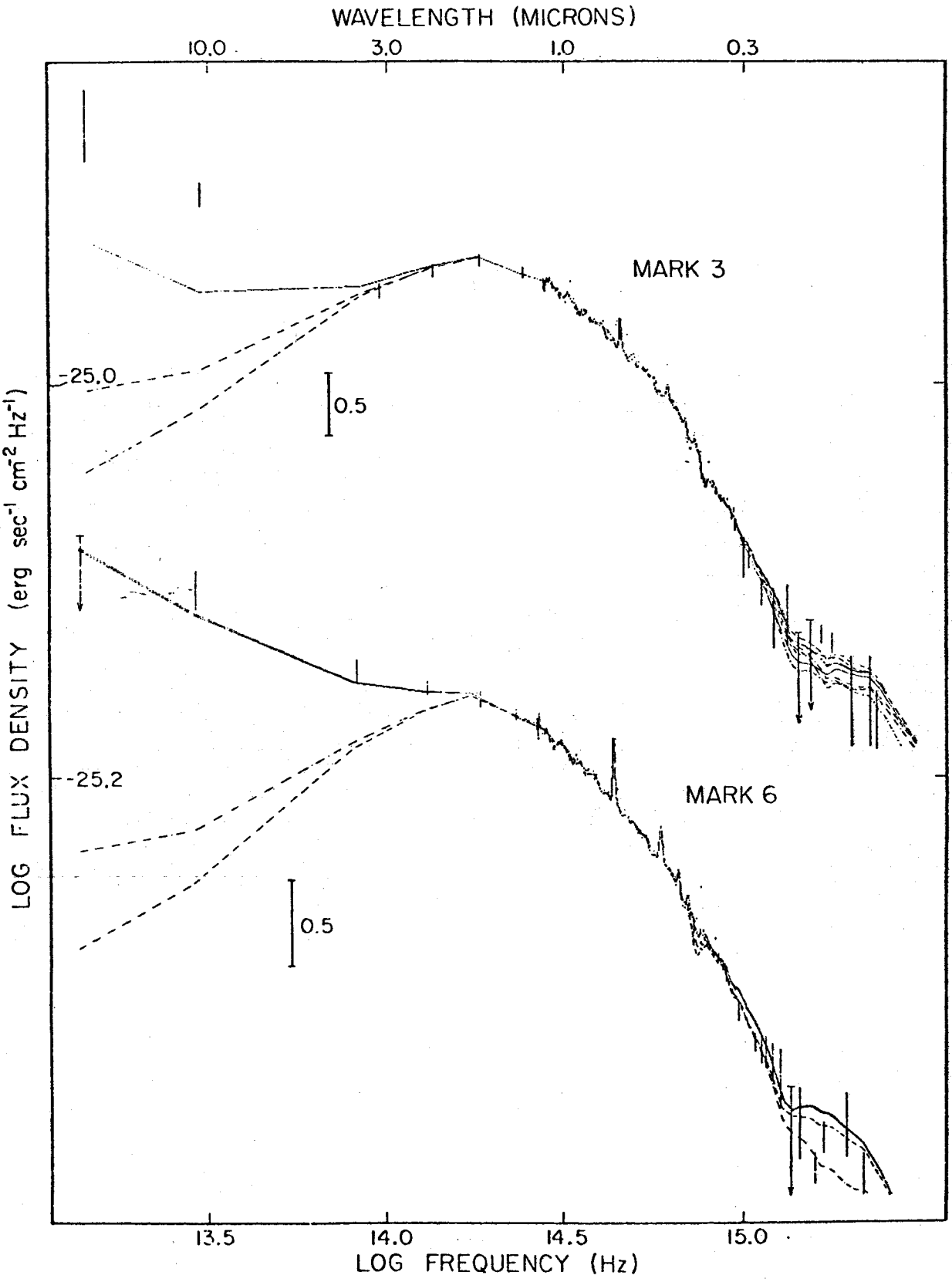
WAVELENGTH (MICRONS)
10.0
3.0
1.0
0.3
MARK 3
-25.0
0.5
MARK 6
-25.2
0.5
LOG FLUX DENSITY (erg sec^{-1} cm^{-2} Hz^{-1})
13.5
14.0
14.5
15.0
LOG FREQUENCY (Hz)

FIG. 3a

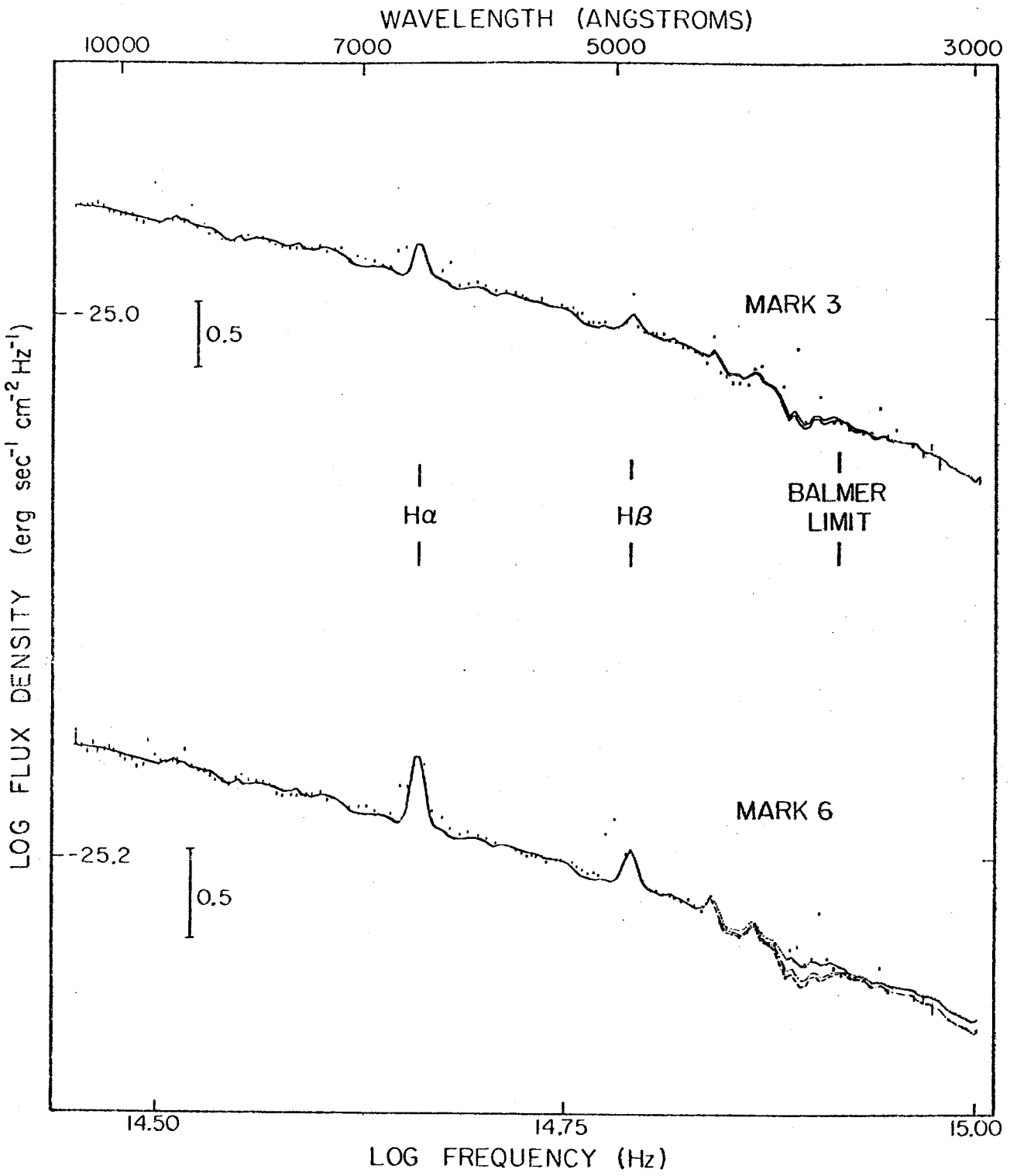

FIG. 3*b*

FIG. 3*a*.—The infrared/optical/ultraviolet spectra of Mrk 3 and 6 in a 14″ aperture is shown by the vertical bars. The lines are fits to the data, described in § V. The solid lines have a power law, the dashed lines a blackbody, and the dot-dash lines an exponential component. Mrk 3 has two sets of lines, for the two different assumed continuum reddenings. The various fits diverge in the infrared and the ultraviolet. However, they are all acceptable, since the additional contribution from thermal infrared emission is not known a priori, and the ultraviolet continuum observations are quite noisy.

FIG. 3*b*.—The blowup of the optical portion of the spectra in Fig. 3*a*. The various fits to the data coincide closely over this wavelength range.

b) Results

The fits for Mrk 3 and Mrk 6 are shown in Figures 3*a* and *b*; the fits to the spectrum of NGC 1068 are in Figures 4*a* and *b*. The solid curves represent fits with a power law, the dashed curves have a blackbody, and the dot-dash curves have an exponential nonstellar component. Figures 3*b* and 4*b* are blowups of the optical portion of Figures 3*a* and 4*a*. In this region all of the curves are nearly indistinguishable. The parameters for each fit are listed in Table 4.

The ultraviolet excess of Mrk 3 in the 14" aperture is so weak that it could be reproduced by recombination emission and starlight, without any additional components. This case is shown by the lower solid line in Figure 3*a*. In the other two Seyfert galaxies, the continuum fitting itself is sufficient to demonstrate the presence of another nonstellar component. In the best observed case, NGC 1068, the exponential component gives either a poor fit or no fit at all to the observed spectrum. Unfortunately, the data do not allow a unique choice between the other two nonstellar components: either a power law or a blackbody added to starlight and recombination emission can be adjusted to give a good match to any of the spectra.

Although these different functional forms for the nonstellar light (power law, blackbody, and in some cases the exponential) can reproduce the observed spectra, they lead to different estimates of the ionizing flux, the total nonstellar flux, and the proportion of starlight in the nucleus.

The final part of Table 3 lists the proportions of nonstellar continuum in the spectra predicted by the fits from Table 4. Just below 3500 Å the Balmer continuum contributes as much as 40% (in Mrk 6) of the total observed flux. However, on the red side of the Balmer jump, the recombination continuum falls to only a few per cent of the total. So the proportions of light from stars at each of the five wavelengths are almost 1.00 minus the fractions given in Table 3.

The nonstellar light in these galaxies cannot be attributed to a blackbody or exponential component, for several reasons:

1) In Table 5 we list the total reddening-corrected permitted line and Balmer continuum fluxes, and the total ionizing fluxes available in the various nonstellar components fitted above. The blackbody and exponential components produce 4–1000 times less ionizing flux than is present in Hα alone. If photoionization accounts for the line emission, the spectrum must have some harder ultraviolet component such as a power law.

2) The [Ne v] and [Fe vii] emission lines require the absorption of 100 eV photons, which are not present in the blackbody and exponential components.

3) Since the exponential and especially the blackbody are weak in the red, they would require that starlight produce nearly all of the green and red continuum in all three spectra. Yet the Mg *b*, Na D and Ca infrared absorption lines in the nuclear spectra are weak, indicating a significant contamination in the red from a featureless nonstellar continuum. Thus § IV's direct imaging estimates of the nonstellar flux also indicate that it is best described by a power law.

TABLE 5

REDDENING-CORRECTED FLUXES (in units of 10^{-14} ergs cm^{-2} s^{-1})

OBJECT	MRK 3	MRK 6	NGC 1068
Balmer Contin.	380	680	2100
Permitted Emission Lines[1]	1900	500[2]	22,000
Ionizing Flux from:			
Power law with:			
Small E_{B-V}	1100	7400	90,000
Large E_{B-V}	10,000		350,000
Blackbody with:			
Small E_{B-V}	0	1.8	3.0
Large E_{B-V}	4.0		40
Exponential with:			
Small E_{B-V}	0.9	11	440
Large E_{B-V}	33		–[3]
Minimum thermal infrared flux	20,000	...	1,000,000

[1] Lyα + Balmer lines + C IV + C III] + Mg II.
[2] Ultraviolet lines not included.
[3] Dash indicates flux could not be measured.

c) Covering Factor

Assuming the power law is present in all three galaxies, it contains enough ionizing energy to power all the nuclear line emission. In Mrk 6, the ratio of line to ionizing flux is slightly larger than 1/10, as Malkan and Sargent found for other Seyfert 1 galaxies and quasars. The covering factor could be larger since some ionizing energy may go into other processes, such as cloud acceleration. NGC 1068 has at least as small a covering factor as Mrk 6. Mrk 3 would have a comparable covering factor if we adopt the larger continuum reddening. But if Mrk 3's power law is only reddened as much as its lines, it would have a covering factor of 100%.

d) Balmer Continuum

The estimated Balmer continuum flux at 3646 Å is insensitive to the exact shape of the other components, since they are very broad, and smooth around 3646 Å. Although the temperature of the Balmer continuum was a free parameter, it was poorly constrained by the data. Satisfactory fits could usually be obtained with any temperature from 5000 to 40,000 K. In the calculation of the total integrated Balmer continuum energy, we assumed a temperature of 14,000 K (Malkan and Sargent 1982; Canfield and Puetter 1981; Kwan and Krolik 1981). The reddening-corrected integrated Balmer continuum/Hα ratio in Seyfert 2 galaxies is 1.3 ± 0.4, a value consistent with the case B prediction (1.4 at $T_e = 10{,}000$), but lower than Malkan and Sargent found in any Seyfert 1 galaxy or quasar. The Balmer continuum energy in Mrk 6 is 1.7 ± 0.5 times Hα, but is a sum over the narrow and broad-line regions. Thus it is possible that the narrow-line region could have a case B ratio, while the broad-line region has the larger ratio

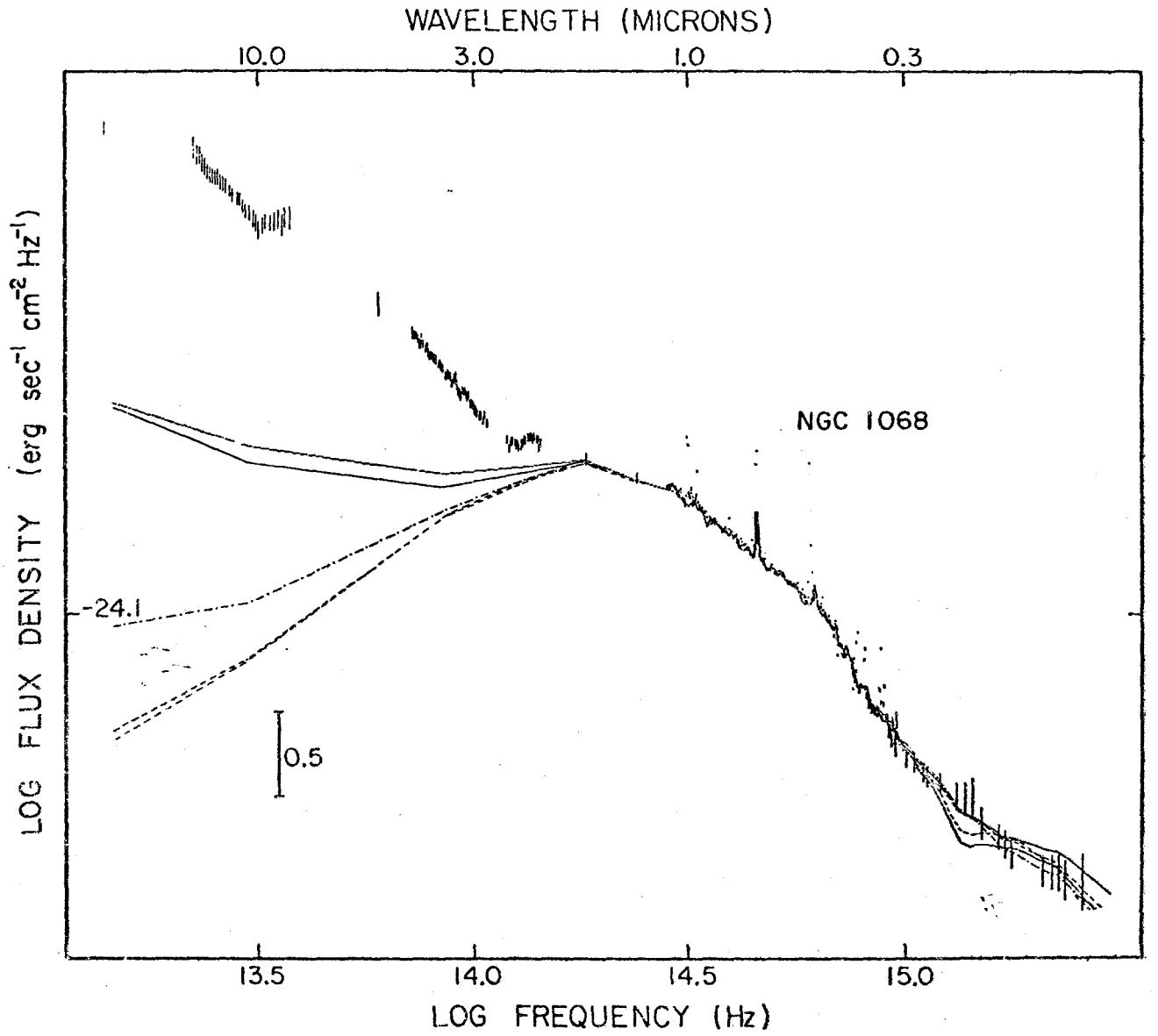

FIG. 4*a*.—The infrared/optical/ultraviolet spectrum of NGC 1068, in a 14" aperture is shown by the vertical error bars. The lines are fits to the data, with the same meanings as in Fig. 3*a*. The power-law (*solid line*) fits, and the blackbody (*dashed line*) fits are acceptable for either assumed reddening. The exponential (*dot-dash*) fit is noticeably less good.

typical of Seyfert 1 galaxies. The simplest explanation, discussed by Malkan and Sargent, is that the broad-line clouds have larger optical depths.

e) Thermal Infrared Emission

We showed above that Mrk 6 has a red nonstellar component which is well described by a power law with a -1.2 slope. Although this component was found by fitting the fluxes at wavelengths less than 2 μm, its extension to longer wavelengths matches the observed fluxes. If, as we argued above, the red nonstellar flux is a power law, the majority of the mid-infrared flux cannot be attributed to a thermal excess from warm dust.

Both Seyfert 2 galaxies, however, have a large infrared excess rising steeply to longer wavelengths, regardless of whether a power law is present. In NGC 1068, the excess flux starts around 2 μm; in Mrk 3 it does not dominate the spectrum until 10 μm. The infrared excess has a steep spectrum, and, at least in NGC 1068, silicate absorption features (Lebofsky and Rieke 1979) indicating that it is thermal emission from warm dust. There is no indication that Mrk 3 has any dust warmer than 300 K, and its infrared excess looks very similar to those observed in M82 and NGC 253. The excess flux up to 30 μm is 3×10^{-10} ergs cm^{-2} s^{-1}, and extrapolation to 100 μm (the turnover wavelength in NGC 1068) would roughly double this. NGC 1068, however, must also have some dust warmer than 600 K

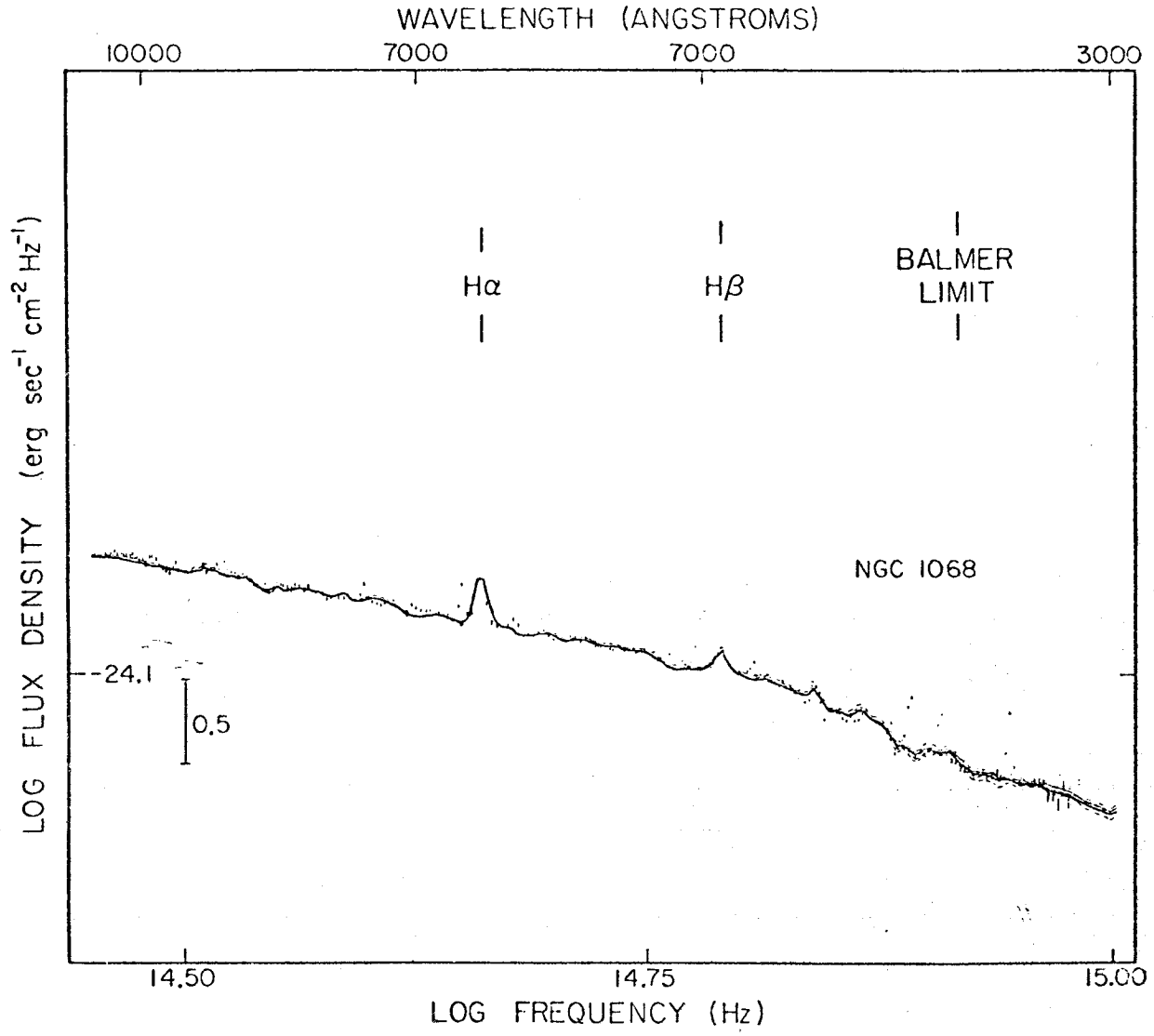

FIG. 4*b*.—The blowup of the optical portion of the spectra in Fig. 4*a*. As with Mrk 3 and 6, all the fits overlap closely over optical wavelengths.

(Cutri *et al.* 1981), to produce its strong 3 μm excess. Its mid-infrared flux is at least 10^{-8}, and up to three times this if all the far-infrared to submillimeter energy is added (Telesco, Harper, and Loewenstein 1976).

The dust which dominates the 10 μm emission is warmed to 300 K. If the grains have a typical infrared emissivity/ultraviolet abstoptivity ratio of 1/100 (Whitcomb *et al.* 1981), they will reach this temperature 20–40 parsecs from the central energy source which heats them. The cooler dust radiating at 20 μm, which absorbs more of the energy, must be about eight times farther out. Therefore no appreciable extinction occurs within the relatively dense, compact Balmer-emitting region. Some extinction may be mixed in with the much larger low-density region where the [O II] and [S II] emission arise. But it is unlikely that the dust/gas ratio increases toward the center of the Seyfert galaxies. (We might expect just the reverse.) Thus the Balmer-emitting region should show the same reddening as the forbidden-line region. The central continuum, however, is presumed to be far smaller. Its line of sight to the Earth passes through a very narrow column of the nuclear dust. On the average, the central continuum should have the same reddening as the permitted lines. But if the reddening is patchy, the nonstellar continuum in any individual Seyfert galaxy could easily have more or less reddening than the average of the emission lines.

Perhaps a large mass of cooler dust could survive in the Balmer-emitting region if it is in the back portions of the emission-line clouds, facing away from the central ionizing source. The dust would be shielded from the ultraviolet radiation, but it would also have little or no

effect on the line emission. This is because the emission we see comes predominantly from the fronts of the clouds which face the ionizing continuum (see, for example, the discussion in Kwan and Krolik 1981). Nor would the continuum be affected, unless its line of sight to the Earth happened to pass through one of these emission-line clouds.

Our first estimate of nuclear reddening for NGC 1068 was 0.1 mag, the largest value consistent with the absence of 2175 Å absorption. And we assumed the reddening in Mrk 3 was 0.27, based on its forbidden lines. Then the total nonstellar ionizing flux available is at least 10 times less than the observed infrared flux. If the infrared emission is really thermal reradiation of the nonstellar continuum by warm dust, then our first estimates of the continuum reddening must have been too small.

We repeated the continuum fitting with larger adopted reddenings for both Seyfert 2 galaxies. For Mrk 3, we took $E_{B-V} = 0.5$, which is larger than the emission-line reddening, but still consistent with the ultraviolet continuum shape. For NGC 1068, we used the emission-line reddening, $E_{B-V} = 0.29$, although it is too large to be consistent with the absence of 2175 Å absorption.

With the larger adopted reddenings, our fitted power laws have four to nine times more ionizing flux. A large proportion of nonionizing ultraviolet and optical flux would also be absorbed by the dust, so the total flux available is about three times the ionizing flux. The estimates in Table 5 show that, with the larger reddenings, there is just enough flux present to produce the observed thermal infrared emission by reradiation.

Although the larger reddenings provide a consistent explanation of the infrared emission, they imply that NGC 1068 has an extremely unusual reddening law, with uniquely weak absorption at 2175 Å. Neugebauer *et al.* (1980) also recognized this problem. As they pointed out, the only way to avoid it is by invoking the existence of some very heavily reddened continuum, which contains the bulk of NGC 1068's luminosity and powers the dust emission. This entirely ad hoc nuclear component would have to be very intrinsically blue and heavily reddened, but it could not extend up to the soft X-rays. This explanation, which invokes a special component designed to have no observable consequences except its reradiation as thermal infrared emission, is highly contrived, although almost impossible to rule out.

f) *X-ray Emission*

Malkan and Sargent (1982) found that the extrapolation of their power law fits gave good predictions of the observed 2 keV flux. NGC 1068 and Mrk 3 have both been detected with good signal-to-noise ratio by the *Einstein Observatory*. Their observed fluxes are 12 μJy (Helfand, private communication) and 0.08 μJy (Kriss, private communication). The extrapolation to 2 keV of the power-law fluxes (with the smaller reddenings assumed) are 14 and 0.14 μJy. The power-law extrapolations are about 10 times larger if the bigger continuum reddenings are adopted. Mrk 6's extrapolated flux at 2 keV is 1 μJy, which is half of the best current observational upper limit, set by *HEAO 1* (Tennant, private communication). It is premature to classify these galaxies as underluminous in X-rays. Their optical flux has a large contribution from starlight, but the ratio of nonstellar optical to X-ray flux could be the same as in other Seyfert 1 galaxies.

VI. CONCLUSIONS

The nonstellar continuum in the Seyfert 1.5 galaxy Mrk 6 has the same features as Malkan and Sargent found in three other low-luminosity Seyfert 1 galaxies: Mrk 10, NGC 4151, and NGC 5548. Each has strong Balmer continuum emission. The remaining nonstellar light is best described by a power law with slope -1.1 ± 0.1.

In both of the Seyfert 2 galaxies studied, we find evidence that the nonstellar continuum must be substantially reddened (by several tenths of a magnitude in E_{B-V}), if it powers the large thermal infrared emission observed. In NGC 1068 this requires an unusual reddening law with a weaker 2175 Å absorption than has yet been observed anywhere else. In Mrk 3, the ultraviolet continuum is more reddened than the emission lines.

The nonstellar continuum in Seyfert 2 galaxies is usually more reddened than in Seyfert 1's, but it can have a comparable intrinsic luminosity. For example, the nonstellar luminosities of Mrk 3 and NGC 1068 are about equal to that of NGC 4151 in its *bright* state (Malkan and Sargent 1982). This strengthens continuity arguments which have been made earlier (Yee 1980), linking the activity in the nuclei of Seyfert 1 and 2 galaxies.

We thank Skip Staples, Bob Griffith, Juan Carrasco, and the *IUE* staff for expert assistance with the observing, and W. Sargent, A. Readhead, A. G. DeBruyn, I. Thompson, and C. McAlary for making available their unpublished data.

REFERENCES

Adams, T. F. 1972, *Ap. J.* (*Letters*), **172**, L101.
———. 1977, *Ap. J. Suppl.*, **33**, 19.
Allen, D. A. 1979, *M.N.R.A.S.*, **189**, 1P.
Bless, R. C., and Savage, B. D. 1972, *Ap. J.*, **171**, 293.
Bohlin, R. C., *et al.* 1980, *Astr. Ap.*, **85**, 1.
Brocklehurst, M. 1971, *M.N.R.A.S.*, **153**, 471.
Burstein, D., and Heiles, C. 1978, *Ap. J.*, **225**, 40.
Canfield, R. C., and Puetter, R. 1981, *Ap. J.*, **243**, 390.
Code, A. D., Davis, J., Bless, R. C., and Hanbury-Brown, R. 1976, *Ap. J.*, **203**, 417.
Costero, R., and Osterbrock, D. E. 1977, *Ap. J.*, **211**, 675.
Cutri, R. M., *et al.* 1981, *Ap. J.*, **245**, 818.
DeBruyn, A. G., and Sargent, W. L. W. 1978, *A.J.*, **83**, 1257.
de Vaucouleurs, G., and de Vaucouleurs, A. 1968, *A.J.*, **73**, 858.
Frogel, J. A., Persson, S. E., Aaronson, M., and Matthews, K. 1978, *Ap. J.*, **220**, 75.

Glass, I. 1976, *M.N.R.A.S.*, **175**, 191.
Hall, D. N., Kleinmann, S. G., Scoville, N. Z., and Ridgway, S. T. 1981, *Ap. J.*, **248**, 898.
Hayes, D., and Latham, D. 1975, *Ap. J.*, **197**, 593.
Johnson, H. M. 1979, *Ap. J.* (*Letters*), **230**, L137.
Kent, S. M. 1979, *Pub. A.S.P.*, **91**, 394.
Koski, A. T. 1978, *Ap. J.*, **223**, 56.
Kurucz, R. L. 1979, *Ap. J. Suppl.*, **40**, 1.
Kwan, J., and Krolik, J. H. 1981, *Ap. J.*, **250**, 478.
Lacy, J. H., *et al.* 1982, *Ap. J.*, **256**, 75.
Lebofsky, M. J., and Rieke, G. H. 1979, *Ap. J.*, **229**, 111.
LeVan, P. D., Puetter, R. C., Rudy, R. J., Smith, H. E., and Willner, S. P. 1981, *Ap. J.*, **251**, 10.
Malkan, M. A. 1983, *Ap. J.* (*Letters*), **263**, in press.
Malkan, M. A., and Sargent, W. L. W. 1982, *Ap. J.*, **254**, 22.
McAlary, C. W., McLaren, R. A., and Crabtree, D. R. 1979, *Ap. J.*, **234**, 471.
Neugebauer, G., Becklin, E. E., Oke, J. B., and Sargent, W. L. W. 1976, *Ap. J.*, **205**, 29.
Neugebauer, G., *et al.* 1980, *Ap. J.*, **238**, 502.
Oke, J. B. 1969, *Pub. A.S.P.*, **81**, 11.
Oke, J. B., Bertola, F., and Capaccioli, M. 1981, *Ap. J.*, **243**, 453.
Osterbrock, D. E. 1974, *Astrophysics of Gaseous Nebulae* (San Francisco: Freeman).
Penston, M. V., Penston, M. J., Selmes, R. A., Becklin, E. E., and Neugebauer, G. 1974, *M.N.R.A.S.*, **169**, 357.
Rieke, G. H. 1978, *Ap. J.*, **226**, 550.
Seaton, M. J. 1978, *M.N.R.A.S.*, **185**, 5P.
Telesco, C. M., Harper, D. A., and Loewenstein, R. F. 1976, *Ap. J.* (*Letters*), **203**, L53.
Thompson, R. I., Lebofsky, M. J., and Rieke, G. H. 1978, *Ap. J.* (*Letters*), **222**, L49.
Thuan, T. X., and Gunn, J. E. 1976, *Pub. A.S.P.*, **88**, 543.
Turnrose, B. T. 1976, *Ap. J.*, **210**, 33.
Ulrich, M. H. 1972, *Ap. J.* (*Letters*), **171**, L35.
Wade, R. A., Hoessel, J. G., Elias, J. H., and Huchra, J. P. 1980, *Pub. A.S.P.*, **91**, 35.
Wampler, J. 1971, *Ap. J.*, **164**, 1.
Whitcomb, S. E., Gatley, I., Hildebrand, R. H., Keene, J., Sellgren, K., and Werner, M. W. 1981, *Ap. J.*, **246**, 416.
Wu, C., Boggess, A., and Gull, T. 1980, *Ap. J.*, **242**, 14.
Yee, H. K. 1980, *Ap. J.*, **241**, 894.
Yee, H. K., and Oke, J. B. 1978, *Ap. J.*, **226**, 753.

MATTHEW A. MALKAN and J. B. OKE: Astronomy Dept., 105-24, California Institute of Technology, Pasadena, CA 91125

THE ASTROPHYSICAL JOURNAL, 264:L1–L6, 1983 January 1

THE REDDENING OF ACTIVE GALACTIC NUCLEI

MATTHEW A. MALKAN
California Institute of Technology
Received 1982 June 14; accepted 1982 September 9

ABSTRACT

We present new calculations of the O^+ and S^+ level populations in order to use the [O II] (λ7320 + λ7330)/(λ3726 + λ3729) and [S II] (λ4069 + λ4076)/(λ6716 + λ6731) ratios as reddening indicators, as suggested by Allen. Using new spectrophotometry obtained at Palomar together with previously published data, we estimate reddenings for forty-seven active galactic nuclei. The resulting values of E_{B-V} are usually only several tenths of a magnitude, with uncertainties of about a tenth. If the permitted emission lines have the same reddening as the forbidden lines, the intrinsic Hα/Hβ ratio in most Seyfert 1 and many Seyfert 2 galaxies is significantly larger than 2.86, the prediction of case B recombination.

Subject headings: galaxies: nuclei — galaxies: Seyfert

I. INTRODUCTION

One of the largest uncertainties in the interpretation of observations of active galactic nuclei comes from the applied corrections for reddening. When the intrinsic continuum shape is unknown, the continuum reddening can only be estimated from the relatively narrow absorption maximum around 2175 Å. However, the origin of the 2175 Å absorption is not well understood, and it can vary by a factor of 2 along different, equally reddened lines of sight (Savage 1975). Even if the 2175 Å feature gives a reliable continuum reddening, the emission-line reddening need not be the same (Malkan and Oke 1983).

Useful emission-line reddening indicators are ratios of lines from the same ion which span a wide wavelength baseline. The observed ratio is then compared with the predicted intrinsic value to estimate the reddening. The most commonly used lines are those of the hydrogen Balmer series. However, the intrinsic Balmer-line ratios are difficult to predict since they may be altered by the effects of large optical depths and electron densities. In this *Letter*, we use the [S II] (λ4069 + λ4076)/(λ6716 + λ6731) and [O II] (λ7320 + λ7330)/(λ3726 + λ3729) ratios, as suggested by Allen (1979). Both are sensitive to electron density, which is why they have not been used previously as reddening indicators.

II. CALCULATED LEVEL POPULATIONS FOR O^+ AND S^+

O^+ and S^+ are both p^3 ions, with very similar lower energy levels. The ground state is a ^4S, and the ^2D and ^2P levels are populated by collisions, with relative populations which are sensitive functions of electron density.

All the calculated atomic parameters for O^+ and most of those for S^+ are probably accurate to better than 15% (Pradhan 1976; Pradhan 1978; Zeippen 1982; Mendoza and Zeippen 1982). Some of the S^+ collision strengths are sensitive to the approximations adopted in the calculations. By far the most extreme example is the collision strength for $^2D_{5/2}$–$^2D_{3/2}$, where the new calculation disagrees with the old by 40%. Nonetheless, the new value is more accurate, and we believe that uncertainties in the calculated level populations are smaller than the observational errors in the line ratio measurements.

We solved the five-level atom equilibrium equations analytically, assuming that collisional de-excitation of the λ7320 + λ7360 and λ4069 + λ4076 lines was negligible. In other words, the analytic solution assumes that $x \ll 500$ and $x \ll 100$ for O^+ and S^+ respectively $\left(\text{where } x \equiv n_e/100 \text{ cm}^{-3} \sqrt{T_e}\right)$. The analytic calculation also ignored the weak temperature dependence of some of the collision strengths, adopting the appropriate values for an electron temperature of 14,000 K. This is a minor source of error since only two collision strengths change by as much as 10% while the temperature runs from 10,000 to 20,000 K. The relative level populations for O^+ are:

$$P\left(^4S_{3/2}\right) = 1 + 9.8x(1 + 1.35\varepsilon) + 10x^2(1 + 2.85\varepsilon + 0.65\varepsilon^2), \quad (1a)$$

$$P\left(^2D_{5/2}\right) = 4.6x\left[1 + 0.229\varepsilon + 3.2x(1 + 0.50\varepsilon + 0.062\varepsilon^2)\right] \times \exp\left(-38,610/T_e\right), \quad (1b)$$

$$P(^2D_{3/2}) = 0.71x[1 + 0.270\varepsilon + 14.0x(1 + 0.55\varepsilon + 0.074\varepsilon^2)] \times \exp(-38,610/T_e), \quad (1c)$$

$$P(^2P_{3/2}) = 0.000249x[1 + 18.9x(1 + 0.80\varepsilon) + 49.8x^2(1 + 1.21\varepsilon + 0.271\varepsilon^2)] \times \exp(-58,250/T_e), \quad (1d)$$

$$P(^2P_{1/2}) = 0.000162x[1 + 17.9x(1 + 0.83\varepsilon) + 51x^2(1 + 1.25\varepsilon + 0.259\varepsilon^2)] \times \exp(-58,250/T_e), \quad (1e)$$

where $\varepsilon \equiv \exp(19,640/T_e)$. The relative S^+ populations are:

$$P(^4S_{3/2}) = 1 + 10.7x(1 + 0.35\varepsilon) + 12.7x^2(1 + 0.90\varepsilon + 0.15\varepsilon^2), \quad (2a)$$

$$P(^2D_{3/2}) = 0.73x[1 + 0.35\varepsilon + 15.7x(1 + 0.59\varepsilon + 0.092\varepsilon^2)] \times \exp(-21,400/T_e), \quad (2b)$$

$$P(^2D_{5/2}) = 3.72x[1 + 0.214\varepsilon + 4.53x(1 + 0.58\varepsilon + 0.056\varepsilon^2)] \times \exp(-21,400/T_e), \quad (2c)$$

$$P(^2P_{1/2}) = 0.000687x[1 + 18.1x(1 + 0.292\varepsilon) + 59.1x^2(1 + 0.589\varepsilon + 0.086\varepsilon^2)] \times \exp(-35,340/T_e), \quad (2d)$$

$$P(^2P_{3/2}) = 0.000839x[1 + 17.9x(1 + 0.377\varepsilon) + 60.3x^2(1 + 0.609\varepsilon + 0.087\varepsilon^2)] \times \exp(-35,340/T_e), \quad (2e)$$

where $\varepsilon \equiv \exp(13,930/T_e)$.

We also solved the equilibrium equations numerically, for a grid of electron temperatures and densities. These computer calculations included all collisional and radiative transitions and are exact for each density. We interpolated Pradhan's (1976, 1978) collision strengths for each temperature. The analytic formulae above agree with the exact results to within a few percent for electron temperatures of 10,000–20,000 K and densities of up to 10^4. The (λ7320 + λ7330)/(λ3726 + λ3729) ratios derived from the above formulae agree with the approximations given by Allen (1979) to within 10%. However, Allen's (λ4069 + λ4076)/(λ6716 + λ6731) ratios are too low for electron densities above a few thousand, since he did not use the newer transition probabilities.

III. REDDENING

The best reddening indicators are pairs of emission lines which come from the same upper level. If the lines are optically thin, their ratios will be a constant, independent of density and temperature. An example, used by Wampler (1971), is the [S II] Σ λ10320/(λ4069 + λ4076) ratio. Both sets of lines come from the ^2P upper level, and our calculations show their ratio is always 0.67. The analogous line ratio for O^+ is (λ7320 + λ7330)/λ2470, which is always 1.33, independent of n_e and T_e. Unfortunately, neither the infrared [S II] lines nor the ultraviolet [O II] line are easy to measure.

The [O II] (λ7320 + λ7330)/(λ3726 + λ3729) and [S II] (λ4069 + λ4076)/(λ6716 + λ6731) ratios are both quite similar functions of electron density. Increasing n_e strengthens [O II] (λ7320 + λ7330) and [S II] (λ4069 + λ4076), which come from the P level, relative to [O II] (λ3726 + λ3729) and [S II] (λ6716 + λ6731), which come from the D level. Allen (1979) has pointed out that, if the [O II] and [S II] emissions are characterized by the same values of n_e and T_e, their line ratios are a powerful reddening indicator. Reddening increases the observed [O II] (λ7320 + λ7330)/(λ3726 + λ3729) ratio, simulating the effect of increased density. At the same time, it decreases the observed [S II] (λ4069 + λ4076)/(λ6716 + λ6731) ratio, lowering the apparent density. Once the reddening law is specified, the condition that the [O II] and [S II] line ratios both give the same value of n_e also uniquely determines the reddening.

The [O II] λ3726/λ3729 and λ7320/λ7330 and [S II] λ4069/λ4076 and λ6716/λ6731 doublet ratios are not sensitive to temperature and are independent of reddening—they are good density indicators. The violet [O II] and [S II] doublets cannot be resolved in most active galactic nuclei. It is relatively easy, however, to measure the [S II] λ6716/λ6731 ratio. Thus another reddening estimate can be made just from observations of the [S II] emission lines. The λ6716/λ6731 ratio gives the electron density, and therefore the intrinsic (λ4069 + λ4076)/(λ6716 + λ6731) ratio, which can then be compared with the observed ratio to find the reddening.

Both techniques assume the emission lines come from a single homogeneous region. This simplification can

lead to systematic errors when reddenings are estimated for inhomogeneous emission-line regions. When gas with a range of electron densities is observed, the denser regions contribute the bulk of the [S II] (λ4069 + λ4076) emission; the thinner regions will produce most of the (λ6716 + λ6731) flux. Thus the electron density derived from the λ6716/λ6731 ratio will be systematically *smaller* than the density derived from the (λ4069 + λ4076)/(λ6716 + λ6731) ratio. That is, for a given λ6716/λ6731 value, the (λ4069 + λ4076)/(λ6716 + λ6731) ratio is intrinsically too large. To make the artificial requirement that these two densities agree requires lowering the reddening below its true value.

The [O II]/[S II] technique can still be approximately valid when a wide range of electron densities and temperatures is present, as long as the intrinsic [O II] and [S II] ratios fall near the unreddened track on the right side of Figure 1. Some photoionization calculations have predicted these line ratios for realistic inhomogeneous gas clouds (Kirkpatrick 1970, 1972; Ferland and Mushotzky 1982, and private communication; Henry and MacAlpine 1982, and private communication). Significant [S II] emission can arise in the H I zones where oxygen is predominantly neutral. Thus, the [S II] emission should be characterized by a somewhat lower electron density and temperature than the [O II] emission. The models predict somewhat smaller [S II] (λ4069 + λ4076)/(λ6716 + λ6731) and larger [O II] (λ7320 + λ7330)/(λ3726 + λ3729) ratios than the single temperature and density case. Our insistence that the [O II] and [S II] ratios give the same electron density leads to an *overestimate* of the reddening of 0.05–0.15 mag.

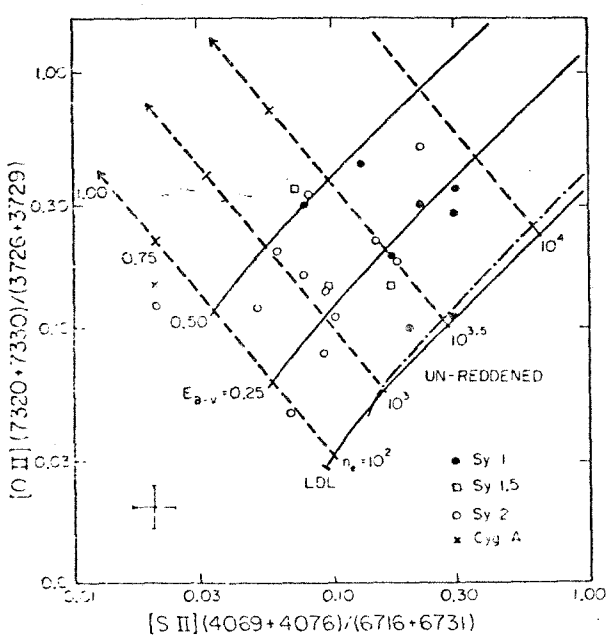

FIG. 1.—The [O II]/[S II] diagram. The solid lines are loci of constant reddening for E_{B-V} = 0, 0.25, and 0.5, with electron density increasing up to the right. The low-density limit is indicated by the circle at the bottom end of the track. The solid lines are for an electron temperature of 14,000 K; the dot-dash line is the unreddened track for 20,000 K. The dashed lines are reddening vectors for electron densities of 10^2, 10^3, $10^{3.5}$, and 10^4. Ticks indicate E_{B-V} = 0, 0.25, 0.5, and 0.75. The tips of the arrows correspond to E_{B-V} = 1.0 mag. Increased reddening and electron density both increase the [O II] (λ7320 + λ7330)/(λ3726 + λ3729) ratio. However, reddening decreases the [S II] (λ4069 + λ4076)/(λ6716 + λ6731) ratio, while higher density increases it. The two ratios are sufficient to specify unique values of E_{B-V} and n_e.

Data from Table 1 are plotted with the symbols indicated on the lower right. All 24 observed active galactic nuclei have line ratios which lie within the physically allowed region. The cross in the lower left corner shows a representative error bar of ±25% in each line ratio.

The systematic biases in these techniques are comparable to the random measuring errors. The reddenings derived in the next section are as accurate as any currently available for active galactic nuclei. It will be difficult to improve them until photoionization models can describe in detail the complex temperature and density distributions in individual galaxies.

IV. OBSERVATIONS

On the nights of 1981 August 29 and 30 and November 1, and 1982 February 21, we used the Palomar 1.5 m telescope with the SIT spectrograph to measure [O II] and [S II] line fluxes in 12 Seyfert galaxies indicated in Table 1. The spectra covered the regions from 3500–5300 Å and 5800–7600 Å at 7 Å (FWHM) resolution. The 4″ × 15″ slit was centered on the nucleus with an integrating television guider, and included most of the nuclear light. The nights were photometric, and small flux corrections to the slit spectra were made by requiring them to give the same intensities of strong forbidden lines as the absolute spectrophotometric scans of DeBruyn and Sargent (1978). The adopted (λ7320 + λ7330)/(λ3726 + λ3729) and (λ4069 + λ4076)/(λ6716 + λ6731) ratios are given in Table 1, along with the reddening determined by both techniques described above. Line ratios were also taken from Anderson (1970), Boksenberg *et al.* (1976), Cohen and Osterbrock (1981), Grandi (1977), Koski (1978), Kunth and Sargent (1979), Malkan and Oke (1983), Oke and Lauer (1979), Oke and Sargent (1968), Osterbrock (1977, 1982), Osterbrock and Koski (1976), Phillips (1978), Phillips and Malin (1982), Shields and Oke (1975), Shuder (1980), Shuder and Osterbrock (1981), Wilson and Penston (1979), and Wampler (1971). When an electron temperature was not available, we assumed it was 14,000 K (Koski 1978). Had we used 20,000 K, the reddenings from the [O II]/[S II] method would have been unchanged, since the unreddened track just shifts along itself (Figure 1). Reddenings from the [S II] doublet method would have been 0.10 mag larger.

TABLE 1

LINE RATIOS AND REDDENINGS FOR ACTIVE GALACTIC NUCLEI

GALAXY	$\frac{7320+30}{3726+29}$	$\frac{4069+76}{6716+31}$	E_{B-V}[a] FROM:		DEREDDENED	
			O II/S II	S II dblt	Hα/Hβ	Hγ/Hβ
(1)	(2)	(3)	(4)	(5)	(6)	(7)
Seyfert 1						
Mrk 464	0.1:	0.2:	0.05:	...	...	...
MCG 8-11-11[b]	0.19	0.17	0.21	0.10	4.1	0.29
IC 4329A	...	0.051	...	0.8:	3.8	0.30
NGC 1275[b]	0.42	0.13	0.43	0.08	5.6	0.39
3227[b]	0.30	0.077	0.47	0.29	3.0	0.38
4051[b]	0.3:	0.22	0.2:	−0.20	3.1	0.47
5548[b]	0.35:	0.30	0.2:	−0.18	3.6	0.41
7469[b]	0.28	0.30	0.17	−0.18	3.0	0.45
I Zw 92	0.11	0.30	0.00	−0.09	3.7	0.46
Seyfert 1.5[c] (Narrow-Line Components Only)						
Mrk 6[b]	0.145	0.095	0.28	0.18	3.6	0.39
79[d]	...	0.042:	...	0.2:	6.8:	0.30:
315[b]	0.35:	0.07	0.5:	0.39	3.7	0.49
NGC 4151[b]	0.145	0.166	0.16	0.10	3.5	0.43
Seyfert 2						
Mrk 1	0.50	0.22	0.38	−0.06	3.4	0.38
3[b]	0.14	0.094	0.27	0.20	3.6	0.45
34	0.045:	0.066	0.2:	0.29	3.3	0.46
42	...	0.19:	...	0.0:	3.5	0.42
78	0.12	0.05	0.40	0.39	3.4	0.33
176	0.182	0.176	0.22	0.01	5.1	0.10:
198	0.2:	0.06	0.4:	0.26	2.4	0.56
268	0.33	0.08	0.51	0.27	2.9	0.66
270	0.08	0.091	0.21	0.20	3.1	0.54
273	0.12:	0.02:	0.7:	0.8:	4.5	0.35
298	...	0.071	...	0.18	3.0	0.40
348[b]	0.16:	0.075	0.4:	0.31	2.9	0.44
463E	0.11	0.10	0.22	0.14	2.9	0.35
533	...	0.086	...	0.23	3.3	0.38
573	...	0.064	...	0.35	2.7	0.51
612	...	0.014	...	0.86	2.0	0.55
NGC 1068[b]	0.22	0.145	0.29	0.30	3.4	0.39
4388	...	0.04:	...	0.5:	2.5	0.49
6764		0.042:	...	0.5:	3.0	0.43
III Zw 55	...	0.063:	...	0.4:	4.6	...
UMCS 16	...	0.073	...	0.26	3.2	0.44
3C 33	...	0.069	...	0.25	2.7	0.45
184.1	...	0.047:	...	0.5:	2.3	0.54
223	...	0.066	...	0.27	2.9	0.46
327	...	0.122	...	0.02	4.2	0.46
433	...	0.046:	...	0.4:	3.7	0.55
452	...	0.042:	...	0.4:	3.2	0.48
5C 3.100	...	0.214	...	−0.16	4.7	0.30
PKS 1345+12	...	0.173	...	−0.09	4.3	0.49
PKS 2322−12	...	0.044	...	0.37	2.7	0.41

TABLE 1—*Continued*

Galaxy (1)	$\frac{7320+30}{3726+29}$ (2)	$\frac{4069+76}{6716+31}$ (3)	E_{B-V}[a] from: O II/S II (4)	E_{B-V}[a] from: S II dblt (5)	Dereddened Hα/Hβ (6)	Dereddened Hγ/Hβ (7)
Narrow-Line X-Ray						
Cyg A = 3C 405	0.144	0.020	0.70	0.83	3.1	0.45
NGC 2110	...	0.041	...	0.58	2.9	0.44
2992	...	0.0092	...	1.3	3.0	0.36
5506	...	0.017	...	1.0	2.5	0.53

[a]The formal errors from uncertainties in observations and atomic parameters are 0.09 mag in E_{B-V} for the [O II]/[S II] technique and 0.16 for the [S II] doublet technique, except for values marked with colons. However, emission-line region inhomogeneities lead to reddening estimates from [O II]/[S II] which are systematically high and ones from the [S II] doublet which are systematically low. As discussed in the text, these systematic errors are 0.05–0.15 mag.

[b]Observed with the SIT spectrograph on the Palomar 1.5 m telescope.

[c]These Seyfert 1 galaxies are listed separately. Their narrow-line and broad-line components have been deblended, and their dereddened Balmer-line ratios refer only to the narrow emission line region.

[d]A 40% correction applied to [S II] λ4069 + λ4076 flux for contamination from [Fe V].

Osterbrock (1981) has pointed out that much of the 4071 Å emission in the unusual high-excitation Seyfert 1 galaxy III Zwicky 77 may actually be from [Fe V]. All the forbidden lines from highly ionized iron are uniquely strong in this galaxy. If the Seyfert galaxies in our study have the same [Fe V]/[Fe VII] ratios as III Zw 77, then [Fe V] makes only a minor (10% or less) contribution to their λ4071 emission, except in Mrk 79.

Unfortunately, the spectrophotometry of many active galactic nuclei does not extend to wavelengths longer than 7000 Å. For these objects, a reddening estimate can only be made from the [S II] ratios. Twenty-three galaxies in Table 1 have reddenings determined by both the [O II]/[S II] and [S II] doublet methods. Reddenings from [O II]/[S II] are systematically larger than those from the [S II] doublet by 0.14 mag. As discussed in § III, the systematic difference probably arises from inhomogeneities in the emission-line regions. Our comparison with photoionization calculations indicated the [O II]/[S II] reddenings are systematically too large by 0.05–0.15 mag, and the results in Table 1 tend to confirm this estimate.

There are also random disagreements between the two techniques, with an individual scatter in E_{B-V} of 0.16 mag. We attribute most of this to observational uncertainties in the [S II] doublet technique. The reddening from the [O II]/[S II] method is less sensitive to measuring uncertainties, since it changes by only 0.09 mag for typical errors of 25% in both line ratios.

V. DISCUSSION

Fourteen reddening estimates have been made from Paα observations (Lacy *et al.* 1982) and ultraviolet continuum observations (summarized by Malkan and Sargent 1982) for Seyfert galaxies in Table 1. In 13 cases, these independent estimates agree with ours. The exception is NGC 1068 (Malkan and Oke 1983), which has a Paα flux consistent with our forbidden-line reddening estimate, but no detectable 2175 Å continuum absorption. However, in the great majority of Seyfert galaxy nuclei, the reddenings of the forbidden and permitted lines and the ultraviolet continuum are about the same.

Nine of the galactic nuclei have reddenings exceeding 0.5 mag. Four of them are in narrow-line X-ray galaxies, and several are found in edge-on spirals with thick central dust lanes. Many heavily reddened narrow emission line galaxies may still remain undiscovered. Unlike the others in Table 1, they are not found by ultraviolet excess or radio emission searches.

Most of the Seyfert galaxies in Table 1 have reddenings of only several tenths or less in E_{B-V}. There is a marginally significant tendency for the Seyfert 1 galaxies to have smaller reddenings and larger electron densities in their forbidden-line regions than the Seyfert 2 galaxies. Some previous workers have over-corrected forbidden-line ratios for reddening by half a magnitude. For example, by assuming the intrinsic Balmer decrements are described by case B recombination, Koski (1978) found reddenings for many of the Seyfert 2 galaxies in Table 1 of nearly 1 mag in E_{B-V}.

Columns (6) and (7) of Table 1 give the Hα/Hβ and Hγ/Hβ ratios for each galaxy, corrected by the forbidden-line reddening in columns (4) and (5). To ensure that we did not underestimate the reddenings based solely on the [S II] doublet, we increased them by 0.1

mag, which should more than compensate for the bias from density inhomogeneities discussed above.

Assuming the broad emission lines have the same reddening as the forbidden lines, the average intrinsic $H\alpha/H\beta$ and $H\gamma/H\beta$ ratios in the Seyfert 1 galaxies are 3.6 ± 0.3 and 0.39 ± 0.02, similar to the ratios Malkan and Sargent (1982) found in several other Seyfert 1 galaxies and quasars.

The average dereddened $H\gamma/H\beta$ ratio in the Seyfert 2 spectra and in the narrow components of the Seyfert 1.5 emission lines is 0.45, not appreciably different from the case B prediction of 0.47. The scatter is $\pm 18\%$ and is mostly attributable to observational uncertainties in the $H\gamma$ flux. However, most of the $H\alpha/H\beta$ ratios are larger than 3.1, and a third of them exceed 3.4. Either the Balmer-line emission in many Seyfert 2 galaxies has systematically more reddening than the forbidden lines, or the intrinsic $H\alpha/H\beta$ ratios are often significantly larger than 2.86, the case B value. Malkan and Oke (1983) came to the same conclusion in their study of NGC 1068 and Markarian 3. They also found that the permitted He II lines had the same reddening as the forbidden lines. Thus the $H\alpha/H\beta$ ratio in many Seyfert 2 galaxies is probably intrinsically larger than 2.86. Malkan and Oke attributed this to moderate optical depths. For example, Netzer (1982) showed that, for $\tau_{H\alpha} > 1$, self-absorption effects can raise $H\alpha/H\beta$ to 3.6, while $H\gamma/H\beta$ is hardly changed. Collisional excitation of $H\alpha$ from the ground state may also be important, even in low-density gas. Ferland and Mushotzky (1981) found this can produce $H\alpha/H\beta$ ratios of 3.1 to 4.1 in typical narrow-line regions. The common practice of deriving reddenings in active galactic nuclei by assuming an intrinsic $H\alpha/H\beta$ ratio of 2.86 must therefore be abandoned.

It is a pleasure to thank Skip Staples and Bob Griffith for assistance at the telescope, W. L. W. Sargent and D. E. Osterbrock for helpful discussions, and the Fannie and John Hertz Foundation for financial support. This work was supported by NSF grant AST 80-22279.

REFERENCES

Allen, D. A. 1979, *M.N.R.A.S.*, **186**, 1P.
Anderson, K. 1970, *Ap. J.*, **162**, 743.
Boksenberg, A., *et al.* 1976, *M.N.R.A.S.*, **173**, 381.
Cohen, R. D., and Osterbrock, D. E. 1981, *Ap. J.*, **243**, 81.
DeBruyn, A. G., and Sargent, W. L. 1978, *A.J.*, **83**, 1257.
Ferland, G. J., and Mushotzky, R. F. 1982, *Ap. J.*, **262**, 564.
Grandi, S. 1977, *Ap. J.*, **215**, 446.
Henry, R. B., and MacAlpine, G. M. 1982, *Ap. J.*, **258**, 11.
Kirkpatrick, R. C. 1970, *Ap. J.*, **162**, 33.
_____. 1972, *Ap. J.*, **176**, 381.
Koski, A. T. 1978, *Ap. J.*, **223**, 56.
Kunth, D., and Sargent, W. L. 1979, *Astr. Ap.*, **76**, 50.
Lacy, J. H., *et al.* 1982, *Ap. J.*, **256**, 75.
Malkan, M. A., and Oke, J. B. 1983, *Ap. J.*, **265**, in press.
Malkan, M. A., and Sargent, W. L. W. 1982, *Ap. J.*, **254**, 22.
Mendoza, C., and Zeippen, C. J. 1982, *M.N.R.A.S.*, **198**, 127.
Netzer, H. 1982, *M.N.R.A.S.*, **198**, 589.
Oke, J. B., and Lauer, T. R. 1979, *Ap. J.*, **230**, 360.
Oke, J. B., and Sargent, W. L. 1968, *Ap. J.*, **151**, 807.
Osterbrock, D. E. 1977, *Ap. J.*, **215**, 733.
_____. 1981, *Ap. J.*, **246**, 696.
_____. 1982, preprint.
Osterbrock, D. E., and Koski, A. T. 1976, *M.N.R.A.S.*, **176**, 61P.
Pradhan, A. K. 1976, *M.N.R.A.S.*, **177**, 31.
_____. 1978, *M.N.R.A.S.*, **183**, 89P.
Phillips, M. M. 1978, *Ap. J. Suppl.*, **38**, 187.
Phillips, M. M., and Malin, D. F. 1982, preprint.
Savage, B. D. 1975, *Ap. J.*, **199**, 92.
Shields, G. A., and Oke, J. B. 1975, *Ap. J.*, **197**, 5.
Shuder, J. M. 1980, *Ap. J.*, **240**, 32.
Shuder, J. M., and Osterbrock, D. E. 1981, *Ap. J.*, **250**, 55.
Wampler, J. 1971, *Ap. J.*, **164**, 1.
Wilson, A. S., and Penston, M. V. 1979, *Ap. J.*, **232**, 389.
Zeippen, C. J. 1982, *M.N.R.A.S.*, **198**, 111.

MATTHEW MALKAN: Astronomy Department, California Institute of Technology, 105-24, Pasadena, CA 91125